VLÁKNA A TEXTIL

FIBRES AND TEXTILES

4

Volume 29
December
2022

TECHNICAL UNIVERSITY OF LIBEREC

STU FCHPT

Trenčianska univerzita Alexandra Dubčeka v Trenčíne
Fakulta priemyselných technológií v Púchove

VÚCHV

VÚTCH CHEMITEX

Spoločnosť pre myselnej chémie

CHEMOSVIT FIBROCHEM

Indexed in:

SCOPUS
Chemical Abstract
World Textile Abstracts
EBSCO Essentials

ISSN 1335-0617
print version

ISSN 2585-8890
online version

VLÁKNA A TEXTIL

http://www.vat.ft.tul.cz

PUBLISHED BY
Technical University of Liberec, Faculty of Textile Engineering
Slovak University of Technology in Bratislava, Faculty of Chemical and Food Technology
Alexander Dubček University of Trenčín, Faculty of Industrial Technologies
Slovak Society of Industrial Chemistry, Bratislava
Research Institute of Man-Made Fibres, JSC, Svit
VÚTCH – CHEMITEX, Ltd., Žilina
Chemosvit Fibrochem, JSC, Svit

PUBLISHER
Technical University of Liberec
Studentska 1402/2, 461 17 Liberec 1, CZ
Tel: +420 485 353615
e-mail: vat@tul.cz
IČO: 46747885

ORDER AND ADVERTISEMENT OF THE JOURNAL
Technical University of Liberec
Faculty of Textile Engineering
Studentska 1402/2, 461 17 Liberec 1, CZ
Tel: +420 485 353615
e-mail: vat@tul.cz

TYPESET AND PRINT
Vysokoškolský podnik, s.r.o., Voroněžská 1329/13, 460 01 Liberec 1, CZ

DATE OF ISSUE
February 2023

APPROVED BY
Rector's Office of Technical University of Liberec
Ref. no. RE 14/23, 20th February 2023

EDITION
First

PUBLICATION NUMBER
55-014-23

PUBLICATION
Quarterly

SUBSCRIPTION
60 EUR

REG. NO. MK ČR E 24338

VLÁKNA A TEXTIL

Volume 29, Issue 4, December 2022

CONTENT

RESOURCE-SAVING TECHNOLOGY OF PRODUCING TEXTILE MATERIALS WITH ANTIMICROBIAL PROPERTIES

MARTIROSYAN IRINA[1*], PAKHOLIUK OLENA[2], DZIUBYNSKYI ANDRII[2], NIKOLAICHUK LARISA[3], LUTSKOVA VIKTORIA[1], LUBENETS VIRA[4] AND PEREDRIY OKSANA[2]

[1] Odessa National Academy of Food Technologies, Kanatna st, 112, Odessa, 65023, Ukraine
[2] Lutsk National Technical University, S.Kovalevska ave., 29, Lutsk, 43008, Ukraine
[3] Hetman Petro Sahaidachnyi National Ground Forces Academy, Heroiv Maidanu street, 32, Lviv, 79026, Ukraine
[4] National University, Lviv Polytechnic, St. Yura Square, 2, Lviv, 79013, Ukraine

ABSTRACT

This work is devoted to the study of antimicrobial properties of cellulose-containing textile materials treated with new safe biocidal products of thiosulfonate structure. A resource-saving method of providing antimicrobial properties to cellulose-containing textile materials is presented. High antimicrobial activity of biocidal products after washing was established. The duration of action and expediency of their use in the textile industry are proved. It is shown that after 10 washes the treated tissues lose only 14-15% of antimicrobial properties.

KEYWORDS

Antimicrobial properties; Cotton; Biocidal treatment; Thiosulfonates.

INTRODUCTION

Today in the textile industry of Ukraine there is an active search for better ways to improve the quality and safety of cellulose-containing textile materials and products with the help of special treatments. Taking into account that one of the criteria for the wear of textiles is biodegradation, their biocidal treatment remains relevant today, as microorganisms not only degrade the appearance, reduce the reliability of textile materials, but also pose a threat to human health. Of course, the process of creating new technologies and decisions on how to provide antimicrobial properties to textiles continues, but this question remains open, as many of these treatments are unable to ensure the stability of the effect, and during a certain period of operation these properties are lost [1-3]. Therefore, the issue of search and development of new antimicrobial substances and technologies, including environmental and resource-saving ones, aimed at protecting textile materials from biodegradation remains very important. It is known that textile materials made of natural fibers provide excellent conditions for the development and growth of microorganisms due to their ability to retain moisture and microbial enzymes. Cellulose is known worldwide as the most common, renewable and almost inexhaustible raw material with an exciting chemical structure and properties. Given these facts, the provision of textile materials with antimicrobial properties is associated with the need to protect tissues from the action of microorganisms and protect the human body from the action of pathogenic microflora. Molds, yeasts and bacteria live and thrive where there are suitable conditions for them - moisture, nutrient medium, the required temperature. The process of decomposition of fiber of plant fibers occurs as a result of exoenzyme action secreted by microorganisms. Hyphae of mycelium of fungi penetrate into the fiber and destroy it from the inside and outside [2,4].

METHODS

Analysis of the literature [2-8] suggests that biocidal substances not only provide antimicrobial protection, but also help to improve the consumer properties of textile materials and increase their wear resistance. After all, antimicrobial textiles due to their properties become a protective barrier to the penetration of microorganisms into the human body. Under such conditions, the use of biocidal substances in the textile industry becomes practical importance.

[*] **Corresponding author:** Martirosyan I., e-mail: *miaviva@ukr.net*
Received October 3, 2022; accepted November 21, 2022

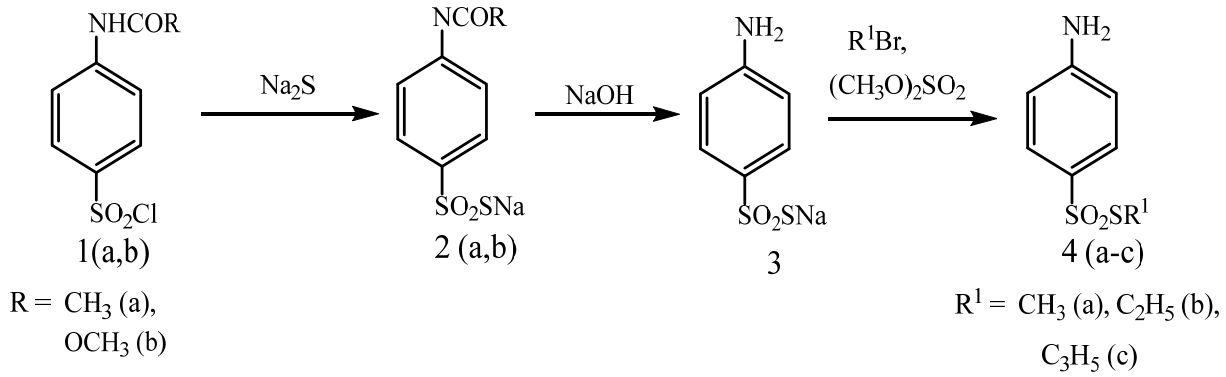

Figure 1. Scheme of obtaining biocidal products of thiosulfonate structure.

The global biocides market is expected to reach $ 11,787.3 million in 2022, according to a new study by Grand View Research, Inc[9]. Nanotechnology also plays an important role in the development of antibacterial textiles. As a promising tool for creating highly stable, effective and environmentally friendly antibacterial textile coatings, sonochemistry was first used by applying inorganic nanoparticles (CuO, ZnO, MgO) to tissues without damaging the structure of textile materials [10-12]. The bactericidal properties of such textile coatings have been preserved after repeated washing, making them an alternative to known bactericidal preparations such as triclosan, various Quaternary ammonium salts and other toxic compounds [13,14].

In recent years, the role of practical use of silver nanoparticles has increased, in particular, in the production of nonwovens for workers of the Ministry of Emergencies. Basic technologies for modification of sanitary and hygienic and disinfectants with silver nanoparticles have been developed. A significant segment of the market for protective products is also occupied by the American companies DSM Biomedical and Agion with their lines of antifungal solutions based on silver ions with bactericidal and fungicidal properties. The technology for the introduction of active ingredients in the form of microcapsules containing solid particles (microdroplets) of antimicrobial substances that are released under certain conditions (eg by friction, pressure, dissolving the capsule shell or their biodegradation) was patented by Earth Holding (USA) for the processing of nonwovens [15,16]. Another achievement in this direction are cyclodextrins [17], which are widely used for tissue treatment, because they due to their unique chemical structure show good absorption capacity, namely form complexes with various antimicrobial and other biologically active substances.

Kathon MW (USA) based on diazolines is considered to be a universal highly effective antimicrobial agent, which has been widely used in various industries. Methods for imparting antimicrobial properties to textile materials by introducing nitrofuran preparations into spinning solutions with their subsequent fixation in the fine structure of fibers during molding have also been developed. A significant place among them is occupied by guanidine compounds as physiologically active substances. Their bactericidal action is determined by their ability to bind to bacterial membranes, penetrate the cell nucleus and produce cellular enzymes [18]. But today it is classified as a toxic biocide. Considering the above, we face the task of finding new ecological biocidal preparations that would be not only safe, but also have a duration of action, would be economically expedient and resource-saving; simple in application, in particular, they did not require a change of equipment and the purchase of new devices when introduced into textile production.

METHODOLOGIES

Despite existing developments, and taking into account the changing general biological resistance of the human body, new species of microorganisms' resistant to most biocidal products are emerging, and ways, modes of transmission and duration of life are changing [11, 2, 19-21]. Therefore, scientists are faced with the task of finding new, more effective and environmentally friendly long-acting biocidal products.

The aim of our research is to obtain an effective resource-saving method of providing antimicrobial properties to textile materials. Given the above, we have a task to investigate the antimicrobial activity of new BPTS by determining their effective concentration and to develop effective conditions for prescription-technological regime of processing of cellulose-containing tissues. In this regard, we have selected new biocidal preparations of thiosulfonate structure (BPTS) [22-24], which have no analogues in the market of Ukraine and abroad. They have a wide range of antimicrobial action and are presented by developers as low-toxic, and can be used for antimicrobial protection in various industries, namely:

- ethylthiosulfanilate (ETS) - ethyl biocide;
- allylthiosulfanilate (ATS) - allyl biocide;
- methylthiosulfanilate (MTS) - methyl biocide.

These thiosulfonates were synthesized at the Department of Technology of Biologically Active Compounds, Pharmacy and Biotechnology of the National University "Lviv Polytechnic" according to the scheme (Fig. 1).

Biocidal products are close to structural analogues of natural volatiles - garlic Allium sativum, onion Allium cepa, various types of cabbage, especially cauliflower. It is known that synthetic esters of thiosulfonic acids exhibit a wide range of biological activity, which often exceeds the effectiveness of natural analogues. They are effective sulfenylating agents in organic synthesis, water-insoluble, and have valuable properties for solving complex problems of molecular biology and biochemistry [22].

These biocides are tested, patented and effectively used to protect paints and varnishes, as additives to protect against bio-damage to lubricants and coolants, biocidal component of anticorrosive composition for pipelines of circulating water supply systems, petroleum products, building materials and structures, algaecides for surface protection sterilization of culture fluid in biotechnological productions. But these biocides have not yet been tested in light industry, and we decided for the first time to experimentally investigate the protective properties of these drugs for textiles. This is dictated not only by the wide range of action of these drugs, but also by the attempt to solve the problem of finding ecological biocides [24].

ETS, MTS, and ATS, in our opinion, may be ideal for the term "environmental biocides", as they are also active substances for the treatment of various skin mycoses and onychomycosis of the nail, competitive with nizoral and clotrimazole. Environmental friendliness and safety of these drugs have also been confirmed by developers in tests on rats [25,26]. Given the above, we can assume that these preparations are completely harmless to the human body and the environment and their use is appropriate in the textile industry, where the human body is in direct contact with tissues.

The object of research is a fabric for making overalls. Pure cotton (100%) fabric of Toctals Fabrics TM (Netherlands) with a surface density of 245 g / m2, twill weave, porosity – 41,2%, fabric thickness is 1.37 mm, linear density is 58 tex, linear density, the number of threads per 10 cm - by warp - 307, by weft - 292. The choice of fibrous composition of the fabric is due to the fact that natural fabrics are more susceptible to destruction and for sewing overalls pure cotton fabric is popular due to its natural properties, taking into account the operating conditions.

The following fungi cultures were used for testing *Trihoderma viride Pers. ex S.F. Gray, Aspergillus niger van Tieghem, Penicillium funiculosum Thom, Paecilomyces variotii Bainier, Chaetomium globosum Kunze*, which have a devastating effect on textiles.

The study of fungicidal and fungistatic activity of biocidal substances of thiosulfonate structure was carried out in accordance with GOST 9.802-84. The studies used fungal cultures deposited at the National Center for Microorganism Strains of State Research and Control Institute of Biotechnology and Strain of Microorganisms: *Trihoderma viride Pers. ex S.F. Gray, Aspergillus niger van Tieghem, Penicillium funiculosum Thom, Paecilomyces variotii Bainier, Chaetomium globosum Kunze*. The activity of the compounds was determined by suspension method. Fungal cultures were grown in Saburo medium for 2 days and kept for 3-5 days in a dark place, then made a suspension of spores in saline with cell load 2 · 109 CFU / ml according to the optical standard of turbidity (Densilameter, Czech Republic, Brno) 0.05% solutions of test compounds were prepared, which were added to tubes with Saburo medium, followed by three serial dilutions up to 0.0002%. a test tube of test fungus suspension, with a cell load in a medium of 106 CFU / ml, mixed the contents, beveled on a tripod to increase the area.

Studies of bacterial resistance and fungal resistance of tissue samples were performed according to standard methods. Tissue samples (20 x 20 mm) were pre-treated with thiosulfonates (control tissue samples did not contain thiosulfonates). Sterile meat-peptone agar (MPA) for bacteria and wort agar (CA) for fungi were used for the experiment. The following types of microorganisms were used in the tests: bacteria Escherichia coli, Staphylococcus aureus, Mycobacterium luteum and fungi Candida tenuis, Aspergillus niger, which mostly destroy textile fibers. Sterile agar medium cooled to 40-450C was poured into Petri dishes, in which a suspension of microorganisms had been previously inoculated (microbial load: bacteria 109 CFU / ml; fungal spores 107 CFU / ml). The prepared samples were immersed in agar medium, cups with experimental and control samples were incubated in a thermostat for 24-48 hours. at a temperature of 37 ° C for germination of bacteria and 48-72 hours at a temperature of 28-30 ° C for fungi.

Tensile strength characteristics of tissue samples with working dimensions of the elementary sample of 25 × 50 mm were measured on a tensioner RT-250M-2 by standard methods (GOST 3813-72 (ISO 5082-82. Textile materials. Textile fabrics and piece-articles. Methods for determination of brearing under tension), the lowering speed of the lower clamp of the tensile testing machine is 100 mm/min, clamped length is 50 mm/ Guarantee error of variation coefficient (mc) was within 0,5 - 1.5%.

EXPERIMENTAL AND RESEARCH RESULTS

As a result of tests on the sensitivity of fungi to ETS, MTS and ATS, it was determined that the minimum effective concentration of all three preparations is 0.05% (Table 1). As can be seen from table 1, all three drugs at a concentration of 0.05% are resistant to molds and can be used for fungicidal and fungistatic treatment of textile materials [27].

Table 1. Minimum effective concentration of thiosulfonate preparations for fungicidal (A) and fungistatic (B) treatment.

Type of microorganisms	Minimum effective concentration, [%]					
	ETS		MTS		ATS	
	A	B	A	B	A	B
Trichoderma viride	0,006	0,055	0,0185	0,055	0,015	0,006
Aspergillus niger	0,0185	0,055	0,0185	0,055	0,015	0,006
Penicillium funiculosum	0,006	0,0185	0,006	0,0185	0,015	0,006
Paecilomyces variotii	0,006	0,0185	0,002	0,055	0,015	0,006
Chaetomium globosum	0,006	0,055	0,006	0,055	0,008	0,006

Table 2. Optimal modes of antimicrobial treatment of tissue with biocidal products of thiosulfonate structure.

Biocide	Operation	The composition of the solution [%]	Processing mode
ethylthiosulfanilate (ETS)	Seepage (immersion) to full wet growth Squeezing Drying (Duration)	The minimum effective concentration is 0.05%, 0.5% was used Alcohol solution	T: 70°C t: 5-7 min.
allylthiosulfanilate (ATS)	Seepage (immersion) to full wet growth Squeezing Drying (Duration)	The minimum effective concentration is 0.05%, 0.5% was used Alcohol solution	T: 50°C t: 5-7 min.
methylthiosulfanilate (MTS)	Seepage (immersion) to full wet growth Squeezing Drying (Duration)	The minimum effective concentration is 0.05%, 0.5% was used Alcohol solution	T: 60°C t: 5-7 min.

Table 3. Influence of temperature and concentration on the breaking load of 100% cotton treated with ETS, MTS and ATS.

Processing temperature [°C]	Before treatment	The breaking load [N]					
	The breaking load [N]	ETS		MTS		ATS	
		Concentration of preparations [%]					
		0,1	0,5	0,1	0,5	0,1	0,5
50	745	757	759	755	760	759	763
60		761	761	760	763	757	759
70		764	767	757	759	755	757

Note: The guarantee error of the coefficient of variation (mc) was within 0.5%.

Among the effective ways to provide antimicrobial properties to textile materials, the simplest and most economical is impregnation. Therefore, this method was chosen for processing. Heat treatment was carried out at a temperature of from 50 to 70 ° C, because such parameters of the temperature regime do not destroy the microstructure of the fibers, and the biocides themselves do not lose their properties.

Antimicrobial treatment of the studied samples of textile materials was carried out in the Analytical Research Laboratory "Textile-TEST", Kyiv (Kyiv National University of Technology and Design). Tissue samples were impregnated with a prepared alcohol-water (60% / 40%) solution of biocidal products with a concentration of 0.5% at room temperature (18-20 ° C) and relative humidity of 63-65% for 1-2 minutes [28]. Then the samples were squeezed on a plate and dried at a temperature of 50-70 ° C for 5-7 minutes (Table 2). The results of tests for the selection of effective tissue treatment regimens for each biocidal product are presented in Table 2. In order to obtain longer-acting antimicrobial textile materials, we decided to increase the concentration of drugs in the next experiment. Table 3 shows the results of the treatment of pure cotton fabric ETS, MTS and ATS at a concentration of 0.1% and 0.5%.

It is known that microbiological destruction of tissues occurs due to the action of bacteria and fungi, which also leads to a decrease in physical and mechanical properties and functionality of clothing. Therefore, improving the tensile strength of textile products is one of the priorities before us, given the working conditions of workers, so when developing technology to provide antimicrobial properties, one of the determinants was mechanical properties, in particular tensile load, which is directly related to wear factors. The research results are shown in Table 3. On the basis of the received data (Tab. 3) mathematical modelling by a method of full factorial experiment was carried out (Fig. 2-4).

From the analysis of graphic dependence, we see that for all 3 biocides increase in concentration leads to increase in indicators of breaking load. Based on the results of table 3, it can be stated that for ETS the optimal processing temperature is 70 ° C, for MTS - 60 ° C, for PBX - 50 ° C, at which the breaking load of pure cotton fabric is maximum: when treated with ethyl biocide - increases at 22 N (2.95%); methyl and allyl - by 18 N (2.4%).

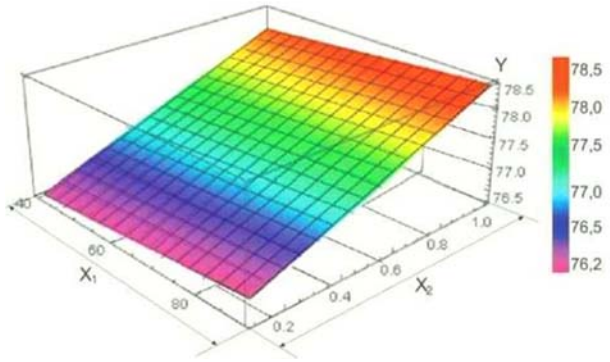

Figure 2. Dependence of breaking load Y on the concentration of ETS (X1) and heat treatment parameters (X2); Y = 75.8 + 0.0075 * X1 + 2 * X2 (three-dimensional graph).

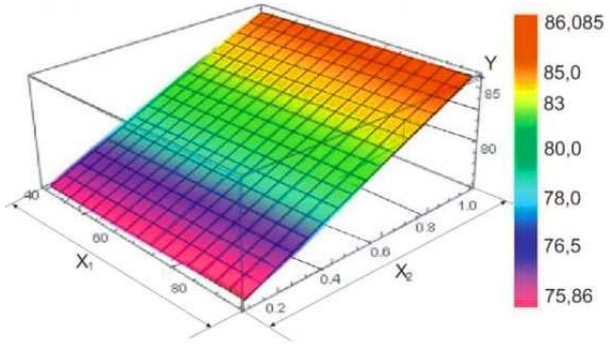

Figure 3. Dependence of breaking load Y on the concentration of MTS (X1) and heat treatment parameters (X2); Y = 74.5 + 0.0065 * X1 + 11 * X2 (three-dimensional graph).

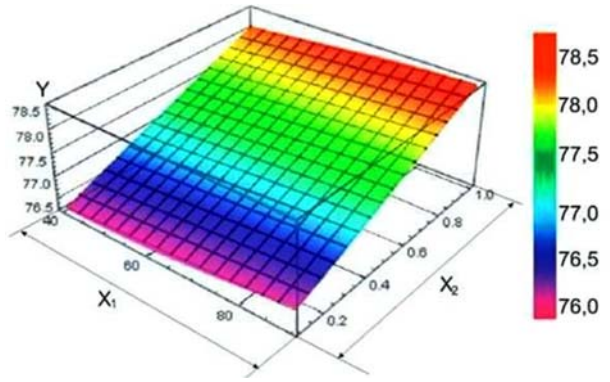

Figure 4. Dependence of breaking load Y on the concentration of ATS (X1) and heat treatment parameters (X2); Y = 75.8 - 0.0025 * X1-0.02 * X2 (three-dimensional graph).

However, given the importance of the regression coefficient, it can also be argued that the temperature of the treatment in the range of 50 - 70 °C does not significantly affect the strength of cotton fabric, so heat treatment of all 3 biocides can be carried out at 50 °C, which is more economical and resource efficient.

To determine the antimicrobial activity of textile materials treated with ETS, MTS and PBX according to the developed method, we investigated the effect of biocides on inhibiting the growth of microorganisms that are more common in the environment and have destructive effects, including Escherichia coli, Staphylococcus aureus, Mycobacter and Aspergillus niger. The test results are given in table. 4.To determine the antimicrobial activity of textile materials treated with ETS, MTS and PBX according to the developed method, we investigated the effect of biocides on inhibiting the growth of microorganisms that are more common in the environment and have destructive effects, including Escherichia coli, Staphylococcus aureus, Mycobacter and Aspergillus niger. The test results are given in Table. 4.

The results of Table. 4 confirm that the concentration of 0.5% has a better fungi-bactericidal effect, which can simultaneously increase not only the rupture characteristics, but also prolong the duration of antimicrobial action. Therefore, further studies will be conducted based on the concentration of preparations - 0.5%. However, it can also be seen that at concentrations of 0.05% and 0.1% the antimicrobial activity of textile materials remains high enough for all three biocides.

CONCLUSION

The developed technology of obtaining textile materials with antimicrobial properties has low advantages:

- this technology of obtaining antimicrobial properties does not require additional costs and efforts on the part of enterprises in the textile industry, as all the necessary equipment is available in the production line of any enterprise specializing in the production of textile materials;
- there is no need to change the technological line and stages of production, as the fabric is processed in the finished form, it is possible both in the final process and after sewing the finished product;
- low temperature regime and duration of heat treatment are energy saving;
- biocidal products of thiosulfonate structure have a high bactericidal and bacteriostatic effect. conditions and modes of processing do not affect the aesthetic properties, also do not impair the microstructure of the fibers, moreover, allow to increase the breaking load, in particular, ETS is the most effective.

It was found that all 3 biocides are effective at a minimum concentration of 0.05%, but when increasing the concentration to 0.5% has a better effect of antimicrobial activity, where the breaking load increases by 2.95%, for MTS and ATS - by 2.4%.

Thus, the presented technology of textiles with antibacterial properties can be considered promising and resource-saving.

Table 4. Fungicbactericidal activity of the test compounds (method A) on pure cotton tissue treated with BPTS.

Preparation	Concentration, [%]	Diameter of zones of suppression of growth of microorganisms, [mm]				
		E. coli	S.aureus	M. luteum	C. tenuis	A. niger
ETS	0,05	6,5	7,7	7,0	12,1	10,5
	0,1	11,0	12,0	20,0	36,0	18,0
	0,5	28,0	34,7	49,0	69,0	40,0
MTS	0,05	5,0	8,3	6,1	10,2	9,6
	0,1	9,0	15,0	12,4	25,7	15,7
	0,5	35,0	32,0	67,5	56,0	44,0
ATS	0,05	4,3	5,0	6,0	9,5	9,0
	0,1	8,5	11,0	12,7	15,4	13,7
	0,5	25,0	33,7	43,0	50,0	20,0

REFERENCES

1. Martirosyan I., Pakholiuk E.: Modern assortment and actuality of the use biocidal preporesions in the textile industry, Integration of education, science and business in the modern environment: summer disputes, International scientific-practical conference, Dnipro, 2019, pp. 433-437.
2. Emam H. E.: Antimicrobial cellulosic textiles based on organic compounds, 3 Biotech 9(29), 2019, pp. 1152-1163. https://doi.org/10.1007/s13205-018-1562-y
3. Nikolaichuk L. G., Galyk I. S., Semak B. D., et al.: The role of nanotextile si the formation of the domestic market of special clothing and application in logistic provision of military units, Herald of Lviv University of Trade and Economics. Technical Sciences. 23, 2020, pp. 49-57. https://doi.org/10.36477/2522-1221-2020-23-06
4. Martirosyan I., Pakholiuk E.: Investigation of the resistance of textile materials to the action of sea fungi. Innovations in the management of the range, quality and safety of goods and services. In: 4th International scientific-practical conference, Lviv, 2018, pp. 87-90.
5. Gutarowska B., Pietrzak K., Machnowski W., et al.: Historical textiles–a review of microbial deterioration analysis and disinfection methods, Textile Research Journal, 87(19), 2017, pp. 2388-2406. https://doi.org/10.1177/0040517516669076
6. Borkow G., Gabbay J.: Biocidal textiles can help fight nosocomial infections, Medical Hypotheses, 70(5), 2018, pp. 990-994. https://doi: 10.1016/j.mehy.2007.08.025
7. Black S.: Fashion and function: factors affecting the design and use of protective clothing, Textiles for Protection, 1(16), 2015, pp. 60-89.
8. Agarwal Ch., Csoka L.: Functionalization of wood/plant-based natural cellulose fibers with nanomaterials, TAPPI Journal, 17(02), 2018, pp. 92-111. https://doi.org/10.32964/TJ17.02.92
9. Biocides in textile global report. 2018. Available from: https://www.researchandmarkets.com/reports/4662348/biocides-in-textiles-global-report-2018/
10. Ahamed M., Akhtar M. J., Raja M, et al.: ZnO nanorod-induced apoptosis in human alycolar adenocarcinoma cells via p53, surviving and bax/bel-2 pathways: role of oxidative stress, Nanomedicine, 7(6), 2011, pp. 904-913. https://doi.org/10.1016/j.nano.2011.04.011
11. Lin J., Chen X. Y., Chen Ch. Y., et al.: Durably antibacterial and bacterially antiadhesive cotton fabrics coated by cationic fluorinated polymers, ACS Applied Materials & Interfaces, 10(7), 2018, pp. 6124-6136. https://doi.org/10.1021/acsami.7b16235
12. Martirosyan I., Pakholiuk E.: Ecological safety of textile materials for the production of overalls. Materials of the international scientific and practical conference of the applicants of higher education and young scientists "Youth - Science and Production", Innovative Technologies of Light Industry", Kherson, 2018, pp. 107-109.
13. Zhang C., Cui F., Zeng G., et al.: Quaternary ammonium compounds (QACs): A review on occurrence, fate and toxicity in the environment, Science of The Total Environment, 2(518), 2015, pp. 352-362. https://doi.org/10.1016/j.scitotenv.2015.03.007
14. Galik I. S., Semak B. D.: Problems of formation and evaluation of ecological safety of textiles, Herald of Khmelnytskyi National University, 4(239), 2016, pp. 71-76.
15. Industries LNC. Cotton-Products, Available from: http://www.lnchemicals.com/cotton-products2.html
16. Sciessent. Agion antimicrobial-technology, Available from: http://www.sciessent.com/agion
17. Singh N., Sahu O: Sustainable cyclodextrin in textile applications, The Impact and Prospects of Green Chemistry for Textile Technology, 11, 2018, pp. 83-105. https://doi.org/10.1016/B978-0-08-102491-1.00004-6
18. Morais D. S., Guedes R. M., Lopes M. A. Antimicrobial approaches for textiles: From research to market, Materials, 9, 2016, pp. 498-512. https://doi.org/10.3390/ma9060498
19. Hanczvikkel A., Vig A., Toth A.: Survival capability of healthcare-associated, multidrug-resistant bacteria on untreated and on antimicrobial textiles. Journal of Industrial Textiles, 48(7), 2019, pp. 1113-1135. https://doi.org/10.1177/1528083718754901
20. Salieri B., Turner D.A., Nowack B., et al.: Life cycle assessment of manufactured nanomaterials: Where are we? NanoImpact, 1, 2018, pp. 108-120. https://doi.org/10.1016/j.impact.2017.12.003
21. Xu Q., Ke X., Ge N., et al.: Preparation of copper nanoparticles coated cotton fabrics with durable antibacterial properties, Fibers and Polymers, 19(5), 2018, pp.1004-1013. https://doi.org/10.1007/s12221-018-8067-5
22. Lubenets V., Karpenko O., Ponomarenko M., et al.: Development of new antimicrobial compositions of thiosulfonate structure, Chemistry & Chemical Technology, 7(2), 2013, pp.119-124.
23. Pakholiuk O. V., Martirosyan I. A., Lubenets V. I.: The influence of biocidal treatment of cellulose textiles to replace its properties, Herald of Khmelnytskyi National University 6, 2018, pp. 94-98. https://doi:10.31891/2307-5732-2018-267-6(2)-94-95
24. Lubenets V. I.: Thiosulphonic acids derivatives: synthesis and properties, Ukrainian Chemistry Journal 69(3), 2003, 109-117.
25. Lubenets V.I., Havryliak V.V., Pylypets A.Z., et al.: Changes in the spectrum of proteins and phospholipids in tissues of rats exposed to thiosulfanilates, Regulatory Mechanisms in Biosystems, 9(4), 2018, pp. 295-500. https://doi.org/10.15421/021874
26. Pylypets A.Z., Iskra R.Ya., Havryliak V.V., et al.: Effects of thiosulfonates on the lipid composition of tissues, The Ukrainian Biochemical Journal, 89(6), 2017, pp. 56-62. https://doi.org/10.15407/ubj89.06.056
27. Martirosyan I., Pakholiuk E., Lubenets V., et al.: Investigation on stability of textile materials for overalls processed by new biocidal preparation, Technological Complexes, 1(15), 2018, pp. 52-59.
28. Martirosyan I., Pakholiuk O., Semak B., et al.: Investigation of wear resistance of cotton-polyester fabric with antimicrobial treatment, Lecture Notes in Mechanical Engineering. Springer International Publishing, 2020, pp.433-441. https://doi.org/10.1007/978-3-030-40724-7_44

THE INFLUENCE OF CONSTRUCTION OF NON-WOVEN TEXTILES ON AIR PERMEABILITY FOR THEIR APPLICATION IN THE COMMUNITY FACE MASKS

BALOGOVÁ ĽUDMILA* AND HULJAKOVÁ KAMILA

VÚTCH – CHEMITEX, spol. s.r.o., Rybníky 954, 011 68, Žilina, Slovak Republic

ABSTRACT

The article is aimed at evaluating the air permeability of various types of non-woven fabrics prepared by Spunbond, Spunbond-Meltblown-Spunbond technology and non-woven fabrics reinforced mechanically by needling and thermal calendering. These are commercially available non-woven fabrics with various mass per unit area and thickness made of 100 % polypropylene, without special surface finish. By combining individual types of non-woven fabrics, three-layer and four-layer textile materials were prepared, meeting the minimum requirement of technical standardization information TNI CWA 17553 for air permeability, intended for application in the community face masks. As part of the experimental works, the effect of increased humidity on the air permeability of three-layer non-woven fabrics was verified as well.

KEYWORDS

Non-woven fabric; Spunbond; Meltblown; Air permeability; Community face masks.

INTRODUCTION

The pandemic of a new type of human coronavirus (SARS-CoV-2), causing a serious infectious disease of the upper respiratory tract, COVID-19, is an ongoing threat to public health worldwide [1]. It is transmitted by droplet infection up to a distance of approximately 1 m, especially when sneezing, coughing, or talking, by releasing aerosol droplets with a diameter greater than 5 μm, contaminated with pathogens [2].

Determining the quality and effectiveness of face masks is a comprehensive topic which is still an active research area. Face masks are one of the most powerful public health tools we can use to slow and stop the spread of the virus, especially when used in places where social distancing cannot be maintained [3]. The community face masks cover part of the face in the area of the mouth, nose, chin and do not contain any inhalation and exhalation valves. The inhaled air penetrates through the material of the face mask directly into the area of the nose and mouth, the exhaled air penetrates through the material of the face mask in the opposite direction directly into the surrounding atmosphere. The community face masks are suitable for ordinary people who do not have clinical symptoms of viral infection and who are not in direct contact with people with this viral disease. In fact, they act as a temporary filter that, depending on time, reduces the rate of transmission of droplets of saliva, mucus or respiratory secretions of the user when communicating, coughing or sneezing. In addition, they can also prevent these droplets from entering the nose and mouth from the outside environment. Face masks also have a protective function preventing the user from accidental touch of the covered face areas with potentially contaminated hands.

Currently, the community face masks are produced with a very high diversity in terms of material quality, level of protection, but also the potential group of their users. The main part of a disposable face mask is a filter able to filter liquids and/or particles of specific size according to the purpose the face mask is intended for. It enables trouble-free breathing and provides long-term comfort to its user. The filtration component can consist of several layers of filtration material with different configurations [4]. Main part of disposable face mask consists of three layers of nonwoven fabric with a structure SMS spunbond – meltblown – spunbond. The outer layer does not pass droplets, the middle layer fulfils function of a filter and the inner layer absorbs humidity. Medical face masks N95 consist of 5 layers with a structure spunbond – meltblown – meltblown – meltblown – spunbond. Two the most important source materials for manufacture of the medical face masks are spunbond and meltblown type nonwovens. The outer and inner layer

* **Corresponding author:** Balogová Ľ., e-mail: balogova@vutch.sk

Received September 22, 2022; accepted November 22, 2022

of the spunbond type nonwovens is made of polyester and polypropylene, while the middle layer is meltblown type nonwoven made of high-melting polypropylene [5]. It is ideal when the face mask has maximum filtration efficiency and at the same time also high breathability. A solution can be also a filtration web filtering bacteria from humid air with a high efficiency, preserving it for a long time and still having a sufficient breathability [6].

As part of our own research focused on the quality of commercially available alternative face masks, 21 types of masks were analyzed in terms of construction, material composition and air permeability parameter. A survey showed that the masks were made of different types of materials (woven knitted and, non-woven fabrics), most often of cotton and blended fabrics, made of one, two or more textile layers, coated, with a membrane, or with surface treatment, disposable or reusable types. The protective masks, which were constructed in three layers of woven and knitted materials with an intermediate membrane layer, achieved air permeability at the level of 0 l/s/m^2. The highest air permeability was achieved by single-layer protective masks made of non-woven fabric at the level of approx. 700 l/s/m^2. The three-layer protective masks made of non-woven fabric achieved air permeability at the level of 100-250 l/s/m^2. In the case of cotton protective masks, the air permeability was influenced by the weave and sett of the woven fabric. With a single-layer cotton mask with satin weave and with a higher density of threads, the air permeability was achieved at the level of approx. 60 l/s/m^2, with a 2-layer mask of the same quality, the air permeability was at the level of approx. 40 l/s/m^2. It follows from the above that performance of the face masks from a viewpoint of air permeability influences mainly kind of textile material used (woven fabric, knitted fabric, nonwoven fabric), its construction parameters (e.g. weave, sett) as well as construction solution of the face mask itself (one-layer, more-layer one) [7]. This knowledge was used, among other things, to co-ordinate course of the experiment, result of which are a subject of this article.

According to the available studies aimed at evaluating the effectiveness of common commercially available types of face masks, it was found that some types of alternative masks provide very low protection [8]. In a study aimed at evaluating the effectiveness of face masks using the method of optical measurement of the transmission of droplets expressed as relative number of droplets released by breathing and during normal speaking, the researchers compared different types of commonly available face masks (Figure 1, samples 1-13) with a filtering face mask (Figure 1, sample 14).

Figure 1. Commercial types of face masks (samples 1-13) and filtering half mask (sample 14).

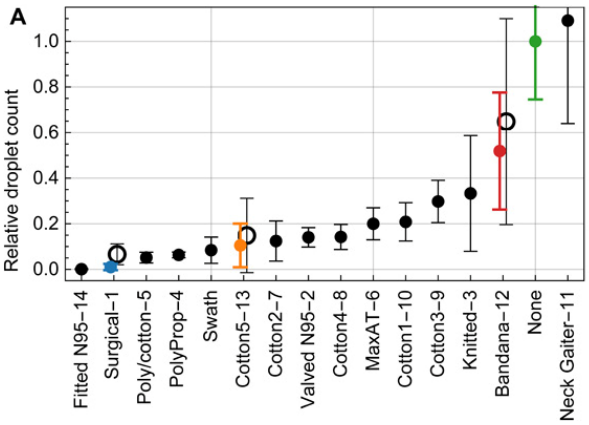

Figure 2. Relative transfer of droplets through the corresponding mask/gown.

Figure 2 shows relative number of droplets transferred through the specific face mask. Each full data point represents an average value of relative number of droplets from 10 measurements performed on the same face mask with calibration on the base of control experiment (without any face mask), while each face mask was tested on the same speaker. The hollow data points represent an average value of relative number of droplets measured on four speakers. Figure 2 shows a diagram with logarithmic scale on y-axis and numbers on x-axis correspond to the numbers of face masks on Figure 1. The results showed that some types of face masks approach the performance of standard surgical masks (Sample 1), while some alternatives to masks, such as neck scarves, provide very low barrier protection.

Table 1. Characteristics of the non-woven fabrics

No.	Designation of the sample	Production technology	Thickness [mm]	Mass per unit area [g/m^2]
1	S20	Spunbond	0,35	20
2	S25	Spunbond	0,26	25
3	S35	Spunbond	0,36	35
4	S40	Spunbond	0,38	40
5	SMS60	Spunbond/Meltblown/Spunbond	0,39	60
6	SMS80	Spunbond/Meltblown/Spunbond	0,52	80
7	VK90	Needled, calendered	0,63	90
8	VK100	Needled, calendered	0,68	100
9	VK150	Needled, calendered	0,98	150
10	VK200	Needled, calendered	1,28	200
11	VK250	Needled, calendered	1,48	250
12	VK300	Needled, calendered	1,74	300

The results of measuring the actual number of droplets released by breathing showed that the mask actually acts as a temporary low-pass filter [8]. An important recommendation in the selection of materials suitable for the construction of face masks was to improve the characteristics of virus capture by reducing the openings in the fabric while simultaneously ensuring the comfort of the user's breathing. The above-mentioned recommendation was taken into account on designing optimum material construction for use of the face masks, meeting the requirement of the Technical Standardization Information TNI CWA 17553 concerning air permeability, which guarantees the required breathing comfort with simultaneous provision of filtering efficiency. The subject of the article is to compare the protective effect of selected types of non-woven fabrics of different construction prepared by various technological procedures, potentially suitable for the production of face masks from a viewpoint of the air permeability parameter. The goal of the paper is to get as close as possible to the air permeability value required by the Technical Standardization Information TNI CWA 17553, as there is a high probability of meeting also the other minimum requirements for filtration efficiency and breathing resistance when it is achieved.

EXPERIMENTAL PART

Technical requirements and test methods

Technical parameters of the community face masks are specified in the Technical Standardization Information TNI CWA 17553 "Community face masks. Guide to minimum requirements, methods of testing and use' (hereafter 'TNI'). Basic functional parameters of the community face masks include filtration efficiency of the material, respiratory resistance and air permeability [9]. These parameters depend on each other and are mainly influenced by the construction of the material used. When choosing material intended for production of the face masks, its ability to absorb moisture and health safety are equally important.

Air permeability R, as one of the above-mentioned properties determining quality of the face masks, is defined as the speed of air flow passing perpendicularly through the test fabric under specific test conditions (area, pressure drop, time). According to TNI, materials intended for the production of the community face masks must not exceed the limit requirement $R \geq 96$ l/s/m^2 at a pressure drop of 100 Pa. Our effort was to achieve air permeability just above the required minimum limit value, in order to come as close as possible to meeting other functional requirements related to the quality of the material used (filtration efficiency, breathing resistance).

The method for measuring permeability of fabrics to air is defined by the EN ISO 9237 standard. Principle of the test is determination of the speed of air flow passing perpendicularly through a given surface of a textile material at a specified pressure difference between two sides of the test surface during a specified time interval. The source materials were tested and conditioned for 24 hours in standard atmosphere with a temperature of 20 °C and a relative humidity of 65 %. The conditioned materials were tested under the same conditions at a pressure drop of 100 Pa and a test area of 20 cm^2 at 10 different locations. The arithmetic mean of air permeability R expressed in millimeters per second (mm/s) [10] is calculated from the individual results, which corresponds to the unit liter per square meter per second (l/s/m^2).

Source materials

One of the materials suitable for production of community face masks are non-woven fabrics, the construction and properties of which depend on the technology of their production and material composition. When choosing non-woven fabrics potentially suitable for the production of community face masks, we mainly took into account compatibility of the structure, the thickness and the weight of the fabric. Commercially available nonwoven fabrics, nonwoven fabrics prepared using Spunbond (designation "S"), Spunbond-Meltblown-Spunbond (designation "SMS") technology and nonwoven fabrics reinforced mechanically by needling and

thermal calendering (designation "VK") were procured. All non-woven fabrics are made of 100% polypropylene, without special surface finish. As these are commercially available materials, the non-woven fabrics have different mass per unit area and thickness (Table 1).

RESULTS AND DISCUSSION

The air permeability R of the non-woven fabrics was measured in one, two and three layers of the same non-woven fabric. The resulting average air permeability values, together with the standard deviations (standard deviation "s" and coefficient of variation "v") are listed in Table 2 and shown in Figure 3, in which the minimum limit value of air permeability specified in the TNI at the level of 96 l/s/m^2 is marked as well.

The highest air permeability was achieved with non-woven fabrics in one layer, as the number of layers increased, the air permeability decreased. The most breathable were non-woven fabrics prepared by Spunbond technology and non-woven fabrics reinforced mechanically by needling and thermal calendering with mass per unit area of 90 g/m^2 and 100 g/m^2. The air permeability of these textiles was on average 10 times higher than its minimum limit value set by the standard. As mass per unit area and thickness increased, the air permeability of nonwovens of the VK type decreased. The least breathable were non-woven fabrics prepared by SMS technology, while the lowest air permeability in one layer exhibited the non-woven fabric SMS60. The air permeability of this non-woven fabric was 2.5 times higher than the minimum limit value set by TNI.

By adding the second layer of the same non-woven fabric, the air permeability of the non-woven fabrics, compared to the air permeability of a single layer, was reduced by an average of 30-60 %. Despite such a significant decrease, we consider the measured air permeability values to be high. The exception is the non-woven fabric SMS60, whose air permeability has fallen below the minimum limit value, which is unacceptable from a viewpoint of the potential use of the fabric in the range of facial masks.

By adding the third layer of the same non-woven fabric, the air permeability of the non-woven fabrics, compared to the air permeability of a single layer, was reduced by an average of 50-70 %. The samples SMS80 and VK150 up to VK300, whose air permeability was in the range of 126–167 l/s/m^2, came closest to the required limit value.

On the three-layer non-woven fabrics, except for sample SMS60, the influence of humidity on the change in air permeability of non-woven fabrics was verified. The aim of the experiment was to simulate the conditions of wearing the face masks, when the humidity of the air increases during breathing and talking, which can affect the breathability of the face mask. The air permeability was measured under the same climatic and test conditions, at the same air temperature of 20 °C, but different relative air humidity: 65 %, 75 % and 85 %. The average value of air permeability at individual climatic and test conditions is listed in Table 3 and shown in Figure 4.

The change in air humidity was most pronounced in non-woven textiles of the VK type. Compared to the results measured under the standard conditions (t = 20 °C, Rh = 65 %), the air permeability of these textiles decreased by approx. 1-26% at a relative air humidity of 75 % and by approx. 2- 29 % at a relative air humidity of 85 %. Due to the technology of their production, non-woven fabrics of the VK type have, compared to the non-woven fabrics of the S and SMS types, a higher mass per unit area and thickness, thanks to which they have the ability to capture in their construction a larger amount of water vapor, which can negatively affect the air permeability parameter. In the case of non-woven fabrics of S and SMS type, there was a slight decrease in air permeability by 1-4 % with increasing humidity, which will be further taken into account in the specification of materials.

When looking for a suitable combination of materials intended for application in the construction of face masks, it is important to take into account their mass per unit area and thickness, in addition to their functional properties. It would be undesirable for the face mask to be uncomfortable and distracting for the user due to its high mass per unit area and thickness. It is equally important in the case of increasing the protective function of the mask, e.g. by the surface finish applied on the outer layer of the face mask, to take into account also quality of the non-woven fabric in terms of compatibility and homogeneity of its surface.

Taking into account the above-mentioned requirements, a series of three-layer material constructions was designed. They consist of a combination of individual types of non-woven textiles. When selecting the outer layer, a compromise solution was adopted between air permeability and weight per unit area of the non-woven fabric. The outer layer of each structure is S40 non-woven fabric, which belongs to the thin low weight non-woven fabrics of the Spunbond category, has a compatible structure and a smooth calendered surface. The middle layer always consists of a different sample of non-woven fabric (Table 1, samples No. 1-12). The inner layer (the layer that will be in direct contact with the human skin) of each structure will be the low weight non-woven fabric S20, which is soft, pleasant to touch and, thanks to this, it will ensure wearing comfort of the mask.

The measurement conditions and the resulting average value of the air permeability of the three-layer combination of the non-woven fabrics with the basic Spunbond non-woven fabric (sample No. 4: S40) are listed in Table 4 and shown in Figures 5 and

6, in which weight per unit area and total thickness of the individual combinations is also shown for a comprehensive assessment.

The combinations 4/5/1 and 4/6/1 show the lowest air permeability. The middle layer of the combinations consists of non-woven fabrics produced by Spunbond-Meltblown-Spunbond (SMS) technology. These are non-woven fabrics made by laminating of Spunbond (technology based on spinning from the melt) and Meltblown (technology based on melt blowing) layers, thanks to which the SMSs have better filtration, insulating and barrier properties than non-woven fabrics prepared only by Spunbond technology (combinations 4/1/1 to 4/4/1). Compared to combinations including the non-woven fabrics reinforced mechanically by needling and thermal calendering (combinations 4/7/1 up to 4/12/1), their additional advantage is a lower overall weight per unit area and thickness. Despite the fact that air permeability of the 4/5/1 combination is higher only by 36 l/s/m^2 than the minimum limit value set by the standard, we consider this value to be high even after taking into account the effect of humidity on air permeability (min. 4% decrease).

The solution how to reduce the air permeability of combinations 4/5/1 and 4/6/1 was addition of the fourth layer, which consists of the non-woven fabric SMS60 (sample No. 5), or SMS80 (sample No. 6). The non-woven fabrics were inserted into the existing combinations between the original second and third layer. The measurement conditions and the resulting average value of air permeability of the four-layer combination of non-woven fabrics with the basic Spunbond non-woven fabric (sample No. 4: S40) are listed in Table 5 and shown in Figures 7 and 8.

The four-layer combinations brought the expected shift of the air permeability parameter to lower values. While the air permeability of the 4/5/5/1 combination is below the limit value and does not meet the requirement of the standard, the 4/6/6/1 combination can still be considered less risky. The combinations 4/5/6/1 and 4/6/5/1 meet requirement of the standard, but after taking into account the influence of humidity, only sample 4/5/6/1 was evaluated as a satisfactory one. From the results, achieved so far, it follows that the construction of a community face mask should consist of at least three or more layers of non-woven fabrics, the appropriate combination of which would meet the minimum limit requirement of the standard regarding air permeability.

Since our goal is to achieve not only satisfactory functional properties, but also the lowest possible mass per unit area and thickness of the combination of materials intended for application in the face mask, a new series of three-layer material constructions was prepared. Their outer layer is SMS60 non-woven fabric, the middle layer always consists of a different sample of non-woven fabric (Table 1, samples No. 1 -12) and the inner layer is the low weight non-woven fabric S20. The measurement conditions and the resulting average air permeability value of the three-layer combination of non-woven fabrics with the basic SMS non-woven fabric (sample No. 5: SMS60) are listed in Table 6 and shown in Figures 9 and 10.

Compared to the three-layer combinations with the basic Spunbond non-woven fabric (sample No. 4: S40), the air permeability of the three-layer combinations with the basic SMS non-woven fabric (sample No. 5: SMS60) was significantly reduced by changing the outer layer. It has been repeatedly confirmed that by a combination of min. two SMS60 (Figures 3, 9 and 10 - sample 5/5/1) the air permeability falls below the minimum limit value required by the standard and this combination is not suitable for preparation of the face masks. From the series of above-mentioned three-layer combinations, we consider the most suitable 5/1/1 and 5/6/1 combinations whose air permeability as well as weight per unit area and thickness are acceptable for application in the construction of the community face masks.

CONCLUSION

Air permeability is only one of three qualitative parameters to be met by the community face masks. For the formulation of definitive recommendations, it is therefore necessary to continue the experiment by determining the filtration efficiency and breathing resistance of the specified types of material combinations and verifying the wearing comfort of the face mask by the user. Based on the achieved results, it is possible to formulate the following partial recommendations and conclusions:

- construction of the face mask made of non-woven fabrics should consist of at least three or more layers. This conclusion corresponds to the requirement of TNI CWA 17553, which recommends to make the community face masks from two or three layers;

Table 2. Air permeability of the non-woven fabrics in 1, 2 and 3 layers

No.	Designation of the sample	Air permeability								
		1 layer			2 layers			3 layers		
		***R* [l/s/m^2]**	*s* [l/s/m^2]	*v* [%]	***R* [l/s/m^2]**	*s* [l/s/m^2]	*v* [%]	***R* [l/s/m^2]**	*s* [l/s/m^2]	*v* [%]
1	S20	**623**	16,9	2,7	**321**	8,0	2,5	**228**	3,9	1,7
2	S25	**1 053**	24,2	2,3	**728**	9,3	1,3	**544**	6,5	1,2
3	S35	**957**	4,4	0,5	**646**	2,2	0,4	**427**	2,1	0,5
4	S40	**873**	16,6	1,9	**564**	9,6	1,7	**363**	6,0	1,7
5	SMS60	**228**	7,3	3,2	**89**	1,3	1,5	**0** [1)]	0,0	0,0
6	SMS80	**442**	9,7	2,2	**242**	5,1	2,1	**137**	2,6	1,9

7	VK90	**1 000**	31,0	3,1	**633**	19,0	3,0	**420**	12,3	2,9
8	VK100	**950**	28,5	3,0	**425**	12,4	2,9	**271**	6,8	2,5
9	VK150	**371**	10,8	2,9	**247**	7,4	3,0	**164**	4,7	2,8
10	VK200	**374**	10,1	2,7	**249**	6,7	2,7	**156**	3,9	2,5
11	VK250	**425**	13,2	3,1	**230**	6,7	2,9	**133**	3,5	2,6
12	VK300	**383**	11,1	2,9	**220**	6,2	2,8	**126**	3,5	2,8

Note: [1)] At a pressure drop of 100 Pa, it was not possible to measure air permeability on the sample.

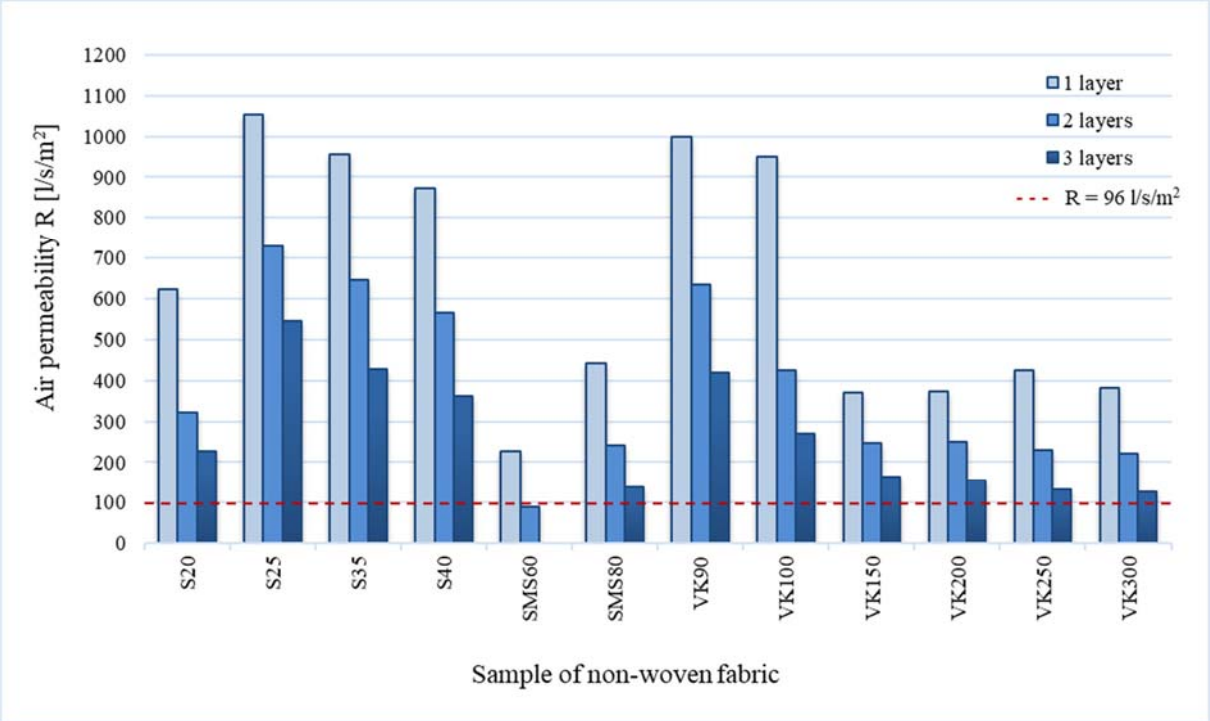

Figure 3. Air permeability of the non-woven fabrics in 1, 2 and 3 layers.

Table 3. Air permeability of non-woven fabrics in **3 layers** under different climatic and test conditions

No.	Designation of the sample	Climatic and test conditions								
		***t* = 20 °C, *RH* = 65 %**			***t* = 20 °C, *RH* = 75 %**			***t* = 20 °C, *RH* = 85 %**		
		Air permeability								
		***R* [l/s/m²]**	*s* [l/s/m²]	*v* [%]	***R* [l/s/m²]**	*s* [l/s/m²]	*v* [%]	***R* [l/s/m²]**	*s* [l/s/m²]	*v* [%]
1	S20	**228**	3,9	1,7	**229**	7,3	3,2	**226**	6,3	2,8
2	S25	**544**	6,5	1,2	**544**	15,8	2,9	**543**	16,3	3,0
3	S35	**427**	2,1	0,5	**418**	14,6	3,5	**411**	13,6	3,3
4	S40	**363**	6,0	1,7	**358**	11,1	3,1	**354**	8,8	2,5
6	SMS80	**137**	2,6	1,9	**140**	4,3	3,1	**131**	3,7	2,8
7	VK90	**420**	12,3	2,9	**416**	14,1	3,4	**412**	7,8	1,9
8	VK100	**271**	6,8	2,5	**233**	6,5	2,8	**226**	7,0	3,1
,9	VK150	**164**	4,7	2,8	**143**	4,4	3,1	**141**	3,4	2,4
10	VK200	**156**	3,9	2,5	**116**	2,6	2,2	**111**	2,1	1,9
11	VK250	**133**	3,5	2,6	**107**	1,6	1,5	**102**	3,0	2,9
12	VK300	**126**	3,5	2,8	**103**	2,1	2,0	**98**	2,6	2,7

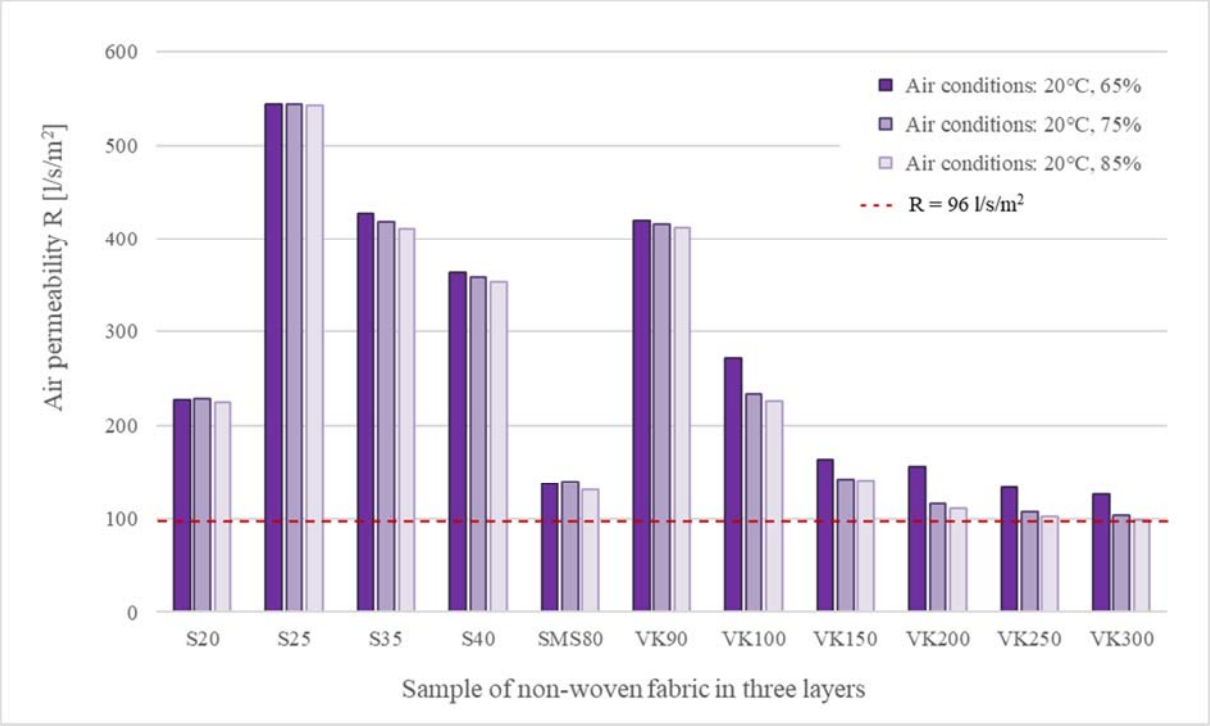

Figure 4. Air permeability of non-woven fabrics in 3 layers under different climatic and test conditions.

Table 4. Parameters of the three-layer combination with the basic Spunbond non-woven fabric (sample No. 4: S40)

Designation of the sample	Three-layer combination of non-woven fabrics	Air permeability			Thickness [mm]	Weight per unit area [g/m²]
		R [l/s/m²]	*s* [l/s/m²]	*v* [%]		
4/1/1	S40 / S20 / S20	263	5,4	2,0	1,09	80
4/2/1	S40 / S25 / S20	329	9,9	3,0	1,00	85
4/3/1	S40 / S35 / S20	326	8,9	2,7	1,06	95
4/4/1	S40 / S40 / S20	309	5,0	1,6	1,14	100
4/5/1	S40 / SMS60 / S20	132	4,5	3,4	1,14	120
4/6/1	S40 / SMS80 / S20	211	5,7	2,7	1,24	140
4/7/1	S40 / VK90 / S20	297	7,7	2,6	1,33	150
4/8/1	S40 / VK100 / S20	277	6,9	2,5	1,43	160
4/9/1	S40 / VK150 / S20	250	3,5	1,4	1,64	210
4/10/1	S40 / VK200 / S20	245	7,1	2,9	1,98	260
4/11/1	S40 / VK250 / S20	264	6,8	2,6	2,17	310
4/12/1	S40 / VK300 / S20	240	6,7	2,8	2,31	360

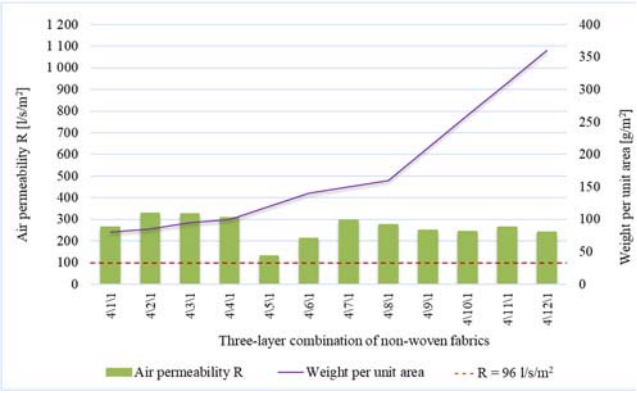

Figure 5. Air permeability and weight per unit area of the three-layer combination with the Spunbond non-woven base fabric (sample No. 4: S40).

Figure 6. Air permeability and thickness of the three-layer combination with the Spunbond non-woven base fabric (sample No. 4: S40).

Table 5. Parameters of the four-layer combination with the base Spunbond non-woven fabric (sample No. 4: S40)

Designation of the sample	Four-layer combination of non-woven fabrics	Air permeability			Thickness [mm]	Weight per unit area [g/m²]
		R [l/s/m²]	*s* [l/s/m²]	*v* [%]		
4/5/5/1	S40 / SMS60 / SMS60 / S20	81	2,1	2,6	1,54	180
4/5/6/1	S40 / SMS60 / SMS80 / S20	102	2,4	2,3	1,66	200
4/6/5/1	S40 / SMS80 / SMS60 / S20	96	1,9	2,0	1,67	200
4/6/6/1	S40 / SMS80 / SMS80 / S20	132	2,3	1,7	1,76	220

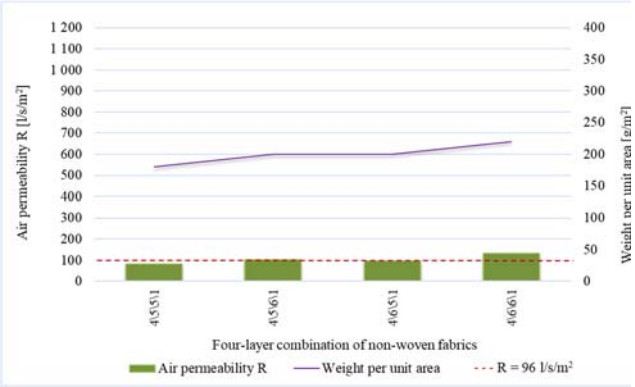

Figure 7. Air permeability and weight per unit area of the four-layer combination with the basic Spunbond non-woven fabric (sample No. 4: S40).

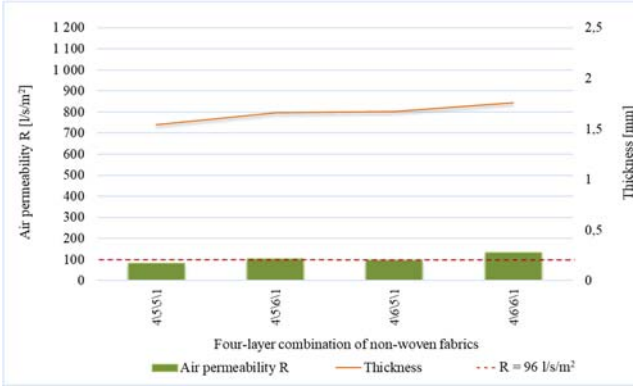

Figure 8. Air permeability and thickness of the four-layer combination with the basic Spunbond non-woven fabric (sample No. 4: S40).

Table 6. Parameters of the three-layer combination with the base Spunbond-Meltblown-Spunbond non-woven fabric (sample No. 5: SMS60)

Designation of the sample	Three-layer combination of non-woven fabrics	Air permeability			Thickness [mm]	Weight per unit area [g/m²]
		R [l/s/m²]	*s* [l/s/m²]	*v* [%]		
5/1/1	SMS60 / S20 / S20	117	2,7	2,3	1,12	100
5/2/1	SMS60 / S25 / S20	129	3,0	2,3	1,05	105
5/3/1	SMS60 / S35 / S20	131	1,3	1,0	1,09	115
5/4/1	SMS60 / S40 / S20	127	2,6	2,1	1,15	120
5/5/1	SMS60 / SMS60 / S20	86	2,5	2,9	1,16	140
5/6/1	SMS60 / SMS80 / S20	105	3,0	2,9	1,26	160
5/7/1	SMS60 / VK90 / S20	127	3,2	2,5	1,35	170
5/8/1	SMS60 / VK100 / S20	127	2,6	2,0	1,45	180
5/9/1	SMS60 / VK150 / S20	108	1,6	1,5	1,69	230
5/10/1	SMS60 / VK200 / S20	112	2,5	2,2	2,06	280
5/11/1	SMS60 / VK250 / S20	98	2,1	2,1	2,22	330
5/12/1	SMS60 / VK300 / S20	97	1,4	1,5	2,34	380

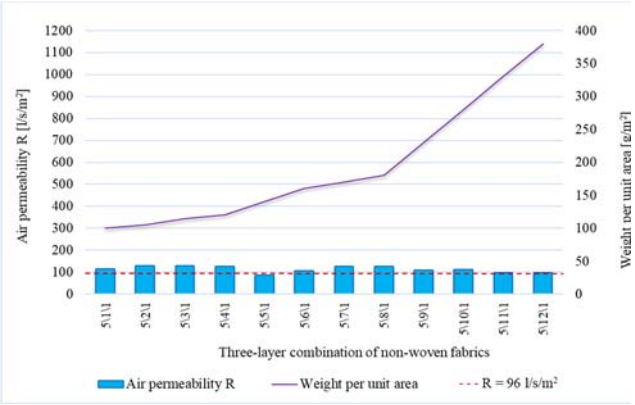

Figure 9. Air permeability and weight per unit area of the three-layer combination with the basic Spunbond-Meltblown-Spunbond non-woven fabric (sample No. 5: SMS60).

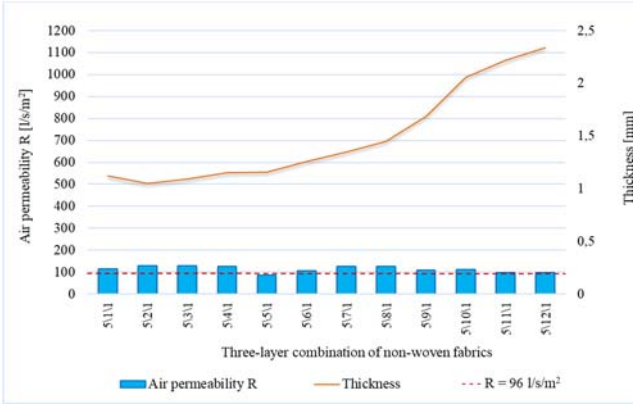

Figure 10. Air permeability and thicness of the three-layer combination with the basic Spunbond-Meltblown-Spunbond non-woven fabric (sample No. 5: SMS60).

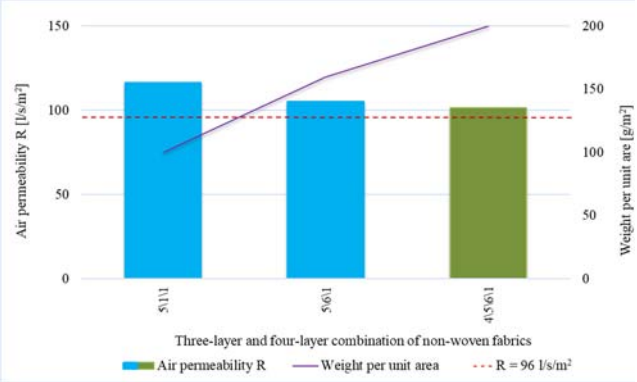

Figure 11. Air permeability and weight per unit area of the recommended three-layer and four-layer combinations of non-woven fabrics.

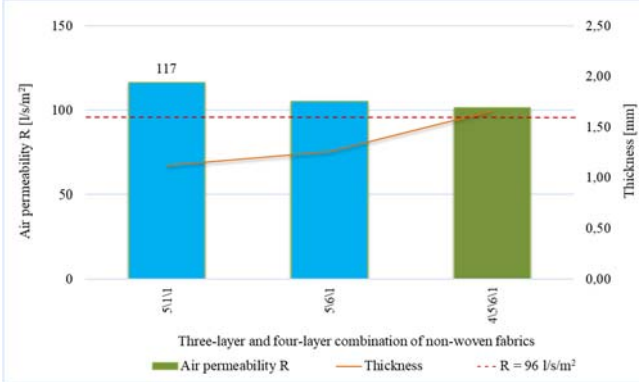

Figure 12. Air permeability and thickness of the recommended three-layer and four-layer combinations of non-woven fabrics.

- it is recommended to use a layer of non-woven fabric prepared by SMS technology in the construction of the face mask. The use of two or more layers of SMS60 non-woven fabric reduces air permeability below the minimum limit value required by TNI;
- it is recommended to make the inner layer of the face mask from a non-woven fabric prepared using Spunbond technology, which will ensure wearing comfort of the face mask;
- it is recommended, when designing the face mask structure, to take into account weight per unit area and thickness of the non-woven fabrics, which affects the resulting weight as well as wearing comfort of the face mask;
- recommended combination of non-woven fabrics for application in the face mask construction are the three-layer combinations 5/1/1 and 5/6/1 and the four-layer combination 4/5/6/1 (Figures 11 and 12), whose air permeability value is even after taking into account the effect of an increase in humidity up to 85%, at the level of the minimum limit value required by TNI.

Acknowledgement: *This work was supported by the Slovak Research and Development Agency under the Contract no. APVV-20-0234.*

REFERENCES

1. Lockhart S. L., Duggan L. V., Wax R. S., et al.: Personal protective equipment (PPE) for both anesthesiologists and other airway managers: principles and practice during the COVID-19 pandemic, Canadian Journal of Anesthesia, 67(8), 2020, pp. 1005-1015. https://doi.org/10.1007/s12630-020-01673-w
2. Leung N.H.L, Chu D.K.W., Shiu E.Z.C. et al.: Respiratory virus shedding in exhaled breath and efficacy of face masks, Nature Medicine, 26(5), 2020, pp. 676-680. https://doi.org/10.1038/s41591-020-0843-2
3. Higgins-Dunn N.: CDC director says face masks may provide more protection than coronavirus vaccine, Health and Science, 2020. Available from: https://www.cnbc.com/2020/09/16/cdc-director-says-face-masks-may-provide-more-protection-than-coronavirus-vaccine-.html
4. US5724964A: Disposable face mask with enhanced fluid barrier.
5. Protective clothing and face mask: Types of raw materials. Available from: https://testexmaskmachine.com/types-of-raw-materials-for-face-mask-and-protective-clothing-production/
6. US3316904A: Filtering web for face masks and face masks made therefrom.
7. Rástočná Illová D.: Annual project report, no. APVV-20-0234 for year 2021, APVV Bratislava, 2022, pp. 2-3.
8. Fischer E.P., Fischer M.C., Grass D., et al.: Low-cost measurement of face mask efficacy for filtering expelled droplets during speech, Science Advances, 6(36), pp. 3083. https://doi.org/10.1126/sciadv.abd3083
9. TNI CWA 17553:2020. Face masks for the public. A guide to minimum requirements, test methods and use. (Document CWA 17553: 2020 was developed with the support of the CCMC and the AFNOR Secretariat, was introduced into the STN system as Technical Standardization Information and is provided to users free of charge)
10. STN EN ISO 9237:1998. Textile. Determination of air permeability of flat textiles (ISO 9237:1995).

INFLUENCE OF MICROENCAPSULATION PARAMETERS ON THE SIZE AND MORPHOLOGY OF MICROCAPSULES BY ECO-FRIENDLY SOLVENT EVAPORATION METHOD ORIENTED TO MEDICAL TEXTILES

THUY DAO THI CHINH[1], SINTES-ZYDOWICZ NATHALIE[2] AND HUONG CHU DIEU[1*]

[1] School of Textile-Leather and Fashion, Hanoi University of Science and Technology, Vietnam
[2] University of Lyon, Université Claude Bernard Lyon 1, IMP@Lyon1, UMR5223, France

ABSTRACT

Application of microcapsules in medical textile has been studied and commercially developed widely in recent years. The aim of this work was to propose an eco-friendly microencapsulation by solvent evaporation method that can contribute to the manufacture of medical textile products using microcapsules. Quillaja saponin was used as bio-sourced surfactant and ethyl acetate was used as the less toxic, non-halogenated organic solvent. The influences of saponin concentration, stirring speed during emulsification step and the volume of ethyl acetate used to saturate the aqueous phase before emulsification on the microcapsule size and morphology were investigated. The results showed that eudragit microcapsules of ibuprofen with diameter in range from 17 to 34 μm, which were suitable for medical textile applications, were successfully elaborated. The saponin concentration varied from 0.025 to 0.1 wt%. The stirring speed was changed from 700 to 600 rpm. The volume of ethyl acetate used in saturation step was 0, 8 and 12 ml. In the scope of investigation, the saponin concentration and the volume of ethyl acetate used in saturation step did affect the microcapsule size and morphology while the stirring speed did not. The saturation step really helped to reduce the formation of irregular microparticles and to narrow the size distribution, but the microcapsules became more porous, weaker and were deformed significantly by drying in the fabric treatment process.

KEYWORDS

Medical textile; Microcapsule; Solvent evaporation method; Quillaja saponin; Ethyl acetate.

INTRODUCTION

Microcapsules are microparticles in which solid, liquid or gaseous active ingredients (the core) are packaged within the second materials (the shells or the membranes) [1], [2]. With advantages such as the ability of protecting the active ingredients from surrounding environment and controlling the release of active ingredients, microcapsules have been applied in many fields of textile industry including the medical textile [3]–[7].

The size is a very important characteristic of microcapsules because for normal spherical microcapsules, the diameter is in inverse proportion to surface area and therefore, strongly affects the active release rate of active ingredients from microcapsules [1], [5], [8]. The relation between the particle size and release characteristic of aromatic microcapsules for the functional textile applications have been reported by Zhao H. et al. [5]. It was found that the release rate of essential oil (Rose® 7289) from melamine-formaldehyde microcapsules significantly increased with the decrease in microcapsule particle size. As predicted according to the Peppas model, after one year of release, the small microcapsules with mean diameter of around 6.67 μm would be substantially depleted while larger microcapsules with mean diameter of around 37.69 μm would release only approximately 10% of the core material. Besides, the size of microcapsules also affected the textile impregnation efficiency and broken release intensity of microcapsule treated fabric. The last one was characterized by the peak height of 1,8-eucalyptin composition of essential oil (Rose® 7289) measured in the SPME-GC-MS elution curves. The composition 1,8-eucalyptin was considered as the essential oil quantity released from the microcapsule treated fabrics which had been followed the hitting process. The highest impregnation efficiency and broken release intensity were reached when the microcapsule size was similar to the textile fiber diameter (25 ÷ 30 μm) [5].

[*] **Corresponding author:** Huong Ch. D., e-mail: huong.chudieu@hust.edu.vn
Received September 29, 2022; accepted November 24, 2022

Microcapsule size requirements in textile application depend on many factors, especially the use of end products and the structures of textile substrates. In general, microcapsules used in medical textile often have average diameters in range of 10 ÷ 60 μm [3], [4], [6]–[8]. Chu C. D. et al. [9] have proposed the suitable size of microcapsules, which was in the range of 15 ÷ 20 μm, for some popular knitted structures (Single, Rib1x1 and Interlock 1x1 fabrics). Their proposal based on the observation of the fabric structure by the optical microscopy and the scanning electron microscopy to determine the width and the height of the knitted loops.

Along with the size, the microcapsule morphology is also the interest of many studies about the microcapsule elaboration and application. Most of the models and equations used to predict and calculate the size and the release rate of active ingredients from microcapsules are based on an assumption that microcapsules are spherical in shape [10] [11]. However, for textile applications, the drying step, which is always obligatory in the finishing process, often makes microcapsules deflate significantly [4], [12]–[14]. Mollor P. et al. [13] studied the influence of drying temperature on the deformation of melamine formaldehyde microcapsules containing peppermint fragrance after being applied to cotton fabrics by padding technique. Three levels of drying temperatures investigated were 120, 140 and 160°C (all for 10 minutes). Their results showed that the presence of apparently unaltered microcapsules could be observed on the fabric treated by air at 120°C, some deflated microcapsules appeared when heated at 140°C and the swelling was reduced considerably in each microcapsule at drying temperature of 160°C. Based on FTIR spectrum of microcapsule padded fabrics at different drying temperatures, along with thermal analysis of microcapsules, the authors confirmed that microcapsule deformation was due to the fragrance loss from microcapsules during the drying step.

Microencapsulation by solvent evaporation method has been used to elaborate microcapsules for most of textile applications, including the field of medical textile products [7]. The basic principle of solvent evaporation technique from oil/water emulsion consists of two continuous stages: the emulsification stage and the solvent evaporation stage. In the first stage, an emulsion is created from the oil phase (a homogenous mixture of polymer, active ingredients, and a proper solvent) and the aqueous phase (a solution in water of a suitable surfactant). In the later stage, the emulsion is then subjected to reduced pressure and elevated temperature to gradually remove the solvent from the emulsion droplets. Eventually, when the droplet composition reaches the bimodal boundary, the polymer phase separates as small droplets of liquid, which are rich in solvent and polymer within the emulsion droplets. These droplets are mobile and migrate to the oil/water interface where they fuse and spread to engulf the original oil droplet if the wetting conditions are correct. Further solvent removal causes the polymer to precipitate at the interface, forming the shell [10].

Surfactant concentration and stirring rate are the two most important parameters that affect the size of microcapsules in the solvent evaporation method [10], [15], [16]. There is a general trend of many works indicating that the microcapsule size will decrease when the surfactant concentration increases because of the reduced interfacial tension. In the study of Valot P. et al. [15] on the microencapsulation of ibuprofen by solvent evaporation technique, the concentration of the PVA surfactant ranged from 0.1 to 2.0 wt%. Their results showed that the mean diameter of microcapsules was not influenced by the surfactant concentration above 0.2 wt%, whereas it significantly decreased below 0.2 wt%, the variation suggested that the droplet cover was insufficient at this level and could not prevent the droplet from coalescence. Besides, the PVA concentration also impacted the size distribution of microcapsules, which were relatively narrow only for the concentration of 0.2 wt%. In the study of Urbaniak T. and Musiał W. [16], the size of lavumidine-loaded microsphere was reported to decrease with the increase of homogenization speed. The microspheres were prepared by solvent evaporation method, using a laboratory rotor-stator homogenizer. When the homogenization speed increased from 10,000 to 35,000 rpm, the hydrodynamic diameter of microspheres decreased from around 2400 nm to 400 nm, respectively. This effect was explained by the increased shear stress at faster rotation rates, which caused the larger tangential stress, resulting in smaller emulsion droplets.

The halogenated solvents such as methylene chloride and chloroform have been the most used solvents for the solvent evaporation technique because of its high volatility, quite low boiling temperature and very low solubility in water. However, these solvents are confirmed carcinogenic according to EPA (Environmental Protection Agency) data and many researchers are making great efforts to find less toxic replacements [10]. Ethyl acetate is a non-halogenated solvent that has been used recently for microencapsulation by solvent evaporation method in the attempt to cut down the use of methylene chloride. Sah H. [17] was successful in producing PLGA microspheres by solvent evaporation method that used ethyl acetate as the solvent. The elaborated microspheres had the average diameter of 44 μm, which were obviously smaller than that of microspheres made by solvent extraction technique (93 μm). Moreover, the amount of residual solvent in the microspheres made by solvent evaporation technique, which was 2.62 wt%, was also much lower than that in the microspheres made by solvent extraction technique (6 wt%). Merabedini S. M. et al. [18] also made successfully

ethyl cellulose microcapsules containing plant oils by solvent evaporation method with the ethyl acetate solvent, the microcapsule size and the microencapsulation efficiency were equal to those of microcapsules made from the chloroform solvent. A big disadvantage of using ethyl acetate for the microencapsulation by solvent evaporation method is its high solubility in water (90 g/l at 20°C, which is 4.5 times higher than that of methylene chloride), which causes the fast diffusion of solvent from emulsion droplets to aqueous phase, leading to the fast precipitation of polymer wall, resulting in non-spherical microcapsules [17], [19]. The solvent diffusion rate could be slowed down by saturating the aqueous phase with a certain volume of ethyl acetate before the emulsification step [19], [20].

Quillaja saponin is a group of bio-sourced surfactants extracted from the *Quillaja Saponaria Molina* tree. With the presence of hydrophobic quillaic acid aglycone group and two hydrophilic sugar chains in molecular structure, quillaja saponin is amphiphilic and possesses surfactant properties due to the high surface activity and the ability to form micelles. Therefore, quillaja saponin has been used widely as stabilizer and emulsifier in the food and pharmaceutical fields [21]–[24]. However, so far, there has not been much research on the use of saponin as the surfactant in the microencapsulation.

This work aims to investigate the ability of quillaja saponin as natural surfactant and ethyl acetate as non-halogenated solvent for an eco-friendly microencapsulation by solvent evaporation method. The elaborated microcapsules of ibuprofen are oriented to medical textile applications due to their suitable size and morphology. The influence of saponin concentration, stirring speed during emulsification and volume of ethyl acetate added to aqueous phase before emulsification on the microcapsule size and morphology was investigated.

EXPERIMENTS

Materials

2-(4-Isobutylphenyl) propanoic acid (Ibuprofen) from BASF (Germany) and medium-chain triglyceride oil (Miglyol 812) supplied by SASOL (Germany) were used as model active ingredients, which help to diffuse the active agent ibuprofen and apply it to skin of user. The poly(ethyl acrylate-co-methyl methacrylate-co-trimethylammonioethyl methacrylate chloride) Eudragit RSPO polymer was from EVONIK Industry (Germany). Quillaja saponin ($C_{36}H_{54}O_{11}$) from *Quillajar* bark (Sapogenin content 20 ÷ 35 %) was purchased from SIGMA-ALDRICH. Ethyl acetate solvent with purity of 99.9 % was supplied by CARLO ERBA. All chemicals for the microencapsulation process have been used as providing without any more purification.

The textile substrate used was cotton interlock fabric knitted from cotton yarn (Ne20) with the loop length of 3.78 mm, the horizontal density of 122 wales/10 cm and the vertical density of 147 courses/10 cm. The interlock fabric meter square weight was 396 g/m2. The knitting process were carried out on the flat knitting machine SSR-112 (knitting gauge R16) of Shima Seiki (Japan). The grey fabrics were then scoured and bleached at Doximex Knitting Company (Vietnam).

Microencapsulation

The microencapsulation based on the solvent evaporation method, which was often used to elaborate the ibuprofen-loaded microcapsules. Ethyl acetate solution (15 ml) containing ibuprofen (8.33 mg/ml), miglyol 812 (33.33 mg/ml) and eudragit RSPO (116.67 mg/ml) was added dropwise for 5 minutes to 100 ml of a quillaja saponin aqueous solution under blade stirring at 700 rpm. The evaporation of ethyl acetate at reduced pressure (300 ÷ 350 Torr) was initiated 5 minutes after the emulsification start with a stirring rate of 600 rpm. Microcapsules collected after 5 hours of evaporation were washed three times with distilled water and then preserved in type of microcapsule suspension in the lab fridge.

To investigate the influence of quillaja saponin concentration on the characteristics of microcapsules, saponin concentration varied by four levels of 0.025, 0.05, 0.075 and 0.1 wt%, the microcapsule lots were coded as C0.025, C0.050, C0.075 and C0.100, respectively.

To investigate the influence of stirring rate during the emulsification stage on microcapsule characteristics, the stirring rate changed in three levels of 700, 650 and 600 rpm, the correlative microcapsule lots were coded as R600, R650 and R700.

To investigate the influence of the solvent volume added to the continuous phase before emulsification on microcapsule characteristics, the volume of ethyl acetate added to the saponin solution was manipulated by 0 ml, 8 ml and 12 ml, and the correlative microcapsule lots were coded as S0, S8 and S12.

Application of microcapsules to the fabric

The washed microcapsules were re-dispersed in distilled water to make the microcapsule suspension with concentration of 12.5 mg/ml. Circle fabric sample with diameter of 25 mm was placed into a plastic cup having the same diameter. The microcapsule suspension (5 ml) was poured into the cup. After 12 hours of soaking, the fabric sample was taken out and then dried in a vacuum drier at 25°C until totally dry.

Microcapsule characterization

The microcapsule suspension was diluted two times for the optical microscopy observation with an

Olympus EX microscope. The microcapsule morphology was also observed by scanning electron microscopy on an ESEM (XL SERIES – Philips) at low vacuum mode (3 ~ 3.5 Torr, 15 kV).

The microcapsule - treated fabric was observed by Olympus EX microscope and by the scanning electron microscope (SEM) QUANTA FEG 250.

The average diameter and the size distribution of microcapsules were determined by static laser light scattering using a Mastersizer 2000 (Malvern instruments, UK). The broadness of the size distribution curve was expressed by Span value calculated as below:

$$Span = \frac{d(0.9) - d(0.1)}{d(0.5)} \quad (1)$$

In which, *d* (0.5) indicated that 50% of total particles were smaller than this size, it was similar for *d*(0.9) and *d* (0.1) value.

According to (1), the smaller span value represented the narrower size distribution, meaning that the size of microcapsules was more homogeneous.

RESULTS AND DISCUSSION

Influence of saponin concentration on the microcapsule size and their morphology

The surfactant concentration has been reported to have strong effect on the size of emulsion droplets and, consequently, the size of elaborated microcapsules [10], [15], [16]. For this work, in order to reveal the influence of saponin concentration on the microcapsule size and morphology, the saponin concentration varied by four levels of 0.025, 0.050, 0.075 and 0.100 wt%. The microcapsule lots were coded by C0.025, C0.050, C0.075 and C0.100, respectively.

The *d*(0.5) diameter and the span values of four microcapsule lots were presented at Table 1 and the influence of saponin concentration on the microcapsule size distribution was shown in Fig. 1.

It could be seen that the average diameter of elaborated microcapsules was in range of 17.1 ÷ 34.3 µm, which was popular for most medical textile applications [3]–[5]. When the saponin concentration increased from 0.025 to 0.1 wt%, the *d*(0.5) diameter of microcapsules decreased respectively from 34.3 to 17.1 µm. This result was similar to the trend reported in some literatures for various types of surfactant, including quillaja saponin [15], [16], [25]–[27]. At high concentration, more surfactant molecules could be oriented at the interface of aqueous - oil phases to reduce efficiently the interfacial tension, which resulted in the formation of smaller emulsion droplets, and then smaller microcapsules.

Table 1. Effect of saponin concentration on the diameter and size distribution of microcapsules.

Lot	Saponin concentration [wt%]	*d*(0.5) diameter [µm]	Span value
C0.025	0.025	34.3 ± 0.3	2.4
C0.500	0.050	23.2 ± 0.2	2.8
C0.075	0.075	21.5 ± 0.2	3.0
C0.100	0.100	17.1 ± 0.2	3.9

The decrease of the microcapsule *d*(0.5) diameter was especially important when the saponin concentration increased from 0.025 to 0.05 wt%. The significant size decrease (from 34.3 to 23.2 µm) might be connected to the cmc value of quillaja saponin from Sigma Aldrich, which was reported about to 0.05 wt% [28]. With a saponin concentration lower than the cmc value, the droplet surface was only partially covered, the interfacial tension between the organic and aqueous phases decreased significantly according to the addition of surfactant concentration. When the saponin concentration reached the cmc value, the effect of the increase in saponin concentration became less significant on the interfacial tension, and consequently, did not quite affect the microcapsule size.

The optical microscope images (Fig. 2) helped to confirm the results of laser diffractometry. Besides, the optical microscope images revealed that most of microcapsules were in spherical shape while some of them were in elliptical or rod shape. Since most equations used to predict the active release rate from microcapsules were only based on spherical ones, those irregular microparticles would be a big disadvantage in predicting the drug release profile from microcapsule-treated fabric.

The similar phenomenon was mentioned in some referred researches on the microencapsulation by solvent evaporation/extraction methods with the use of ethyl acetate [17], [19].

The solubility in water of ethyl acetate (90 g/l at 20°C) was much higher than that of halogenated solvents most used in solvent evaporation method such as dichloromethane (20 g/l at 20°C). With high stirring rate during the emulsification, ethyl acetate in oil droplets diffused quickly to the aqueous phase, inducing the fast polymer precipitation and eventually, increasing the formation of elliptical or rod shape microparticles as shown in Fig. 2.

Span value was quite high in the range of 2.4÷3.9 (Table 1), which presented the broad size distribution of microcapsule lots. The fast polymer precipitation could be a reason for this phenomenon because the emulsion droplets did not have enough time to be divided into smaller and more stable ones.

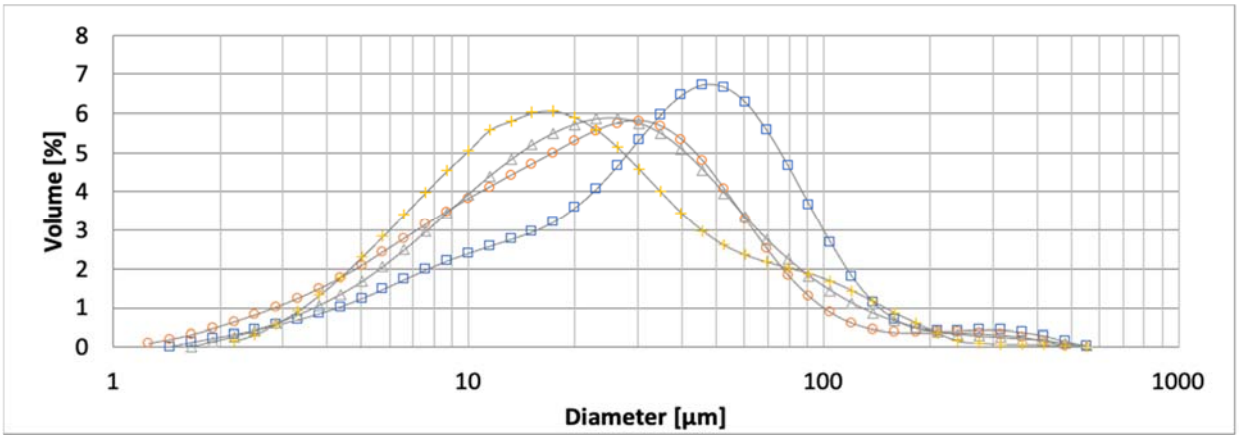

Figure 1. Size distributions of microcapsules at different saponin concentrations.

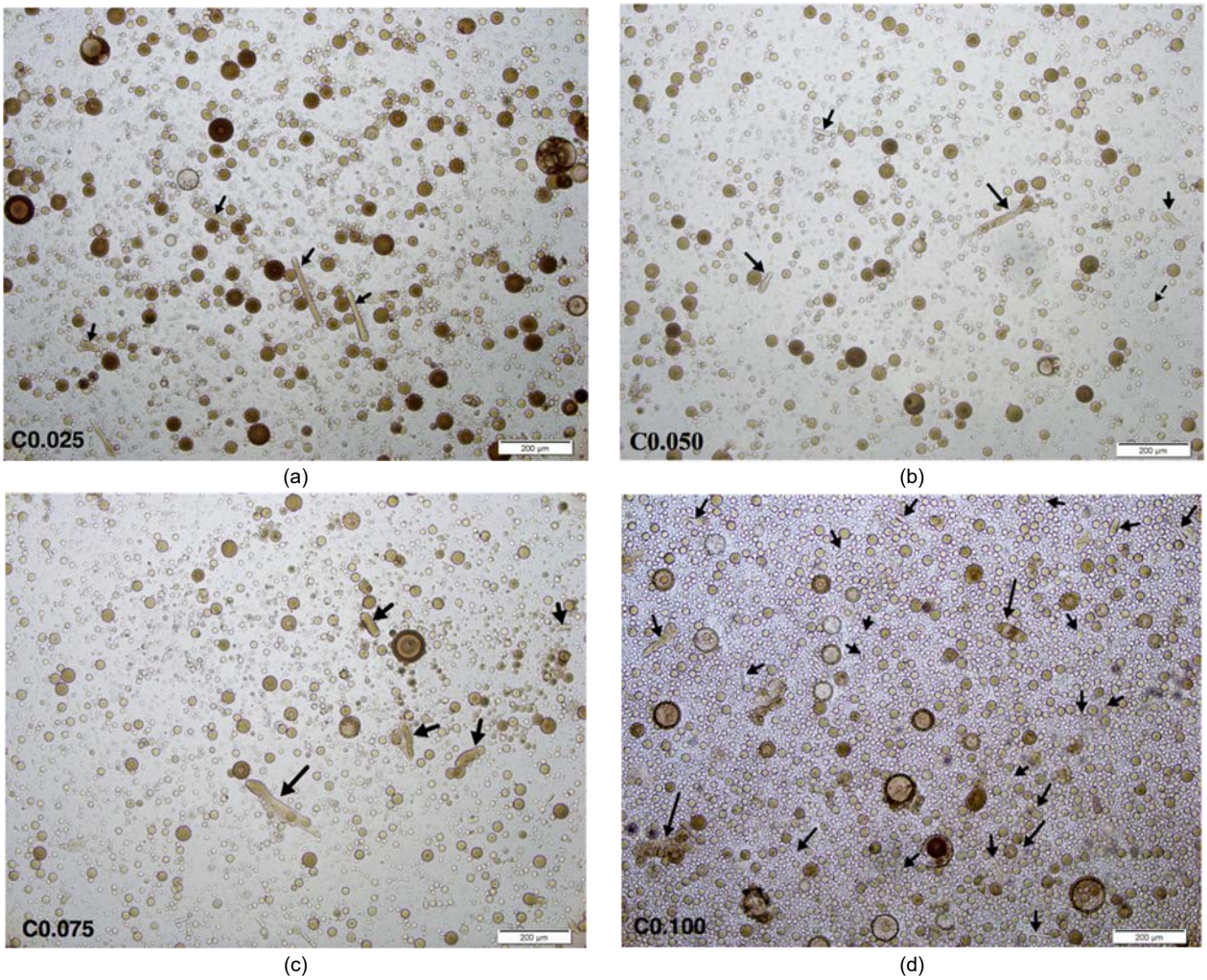

(a) (b) (c) (d)

Figure 2. Optical microscope images of microcapsules obtained at different saponin concentrations. C0.025 (a), C0.050 (b), C0.075 (c) and C0.100 (d). ⟶: irregular microparticles.

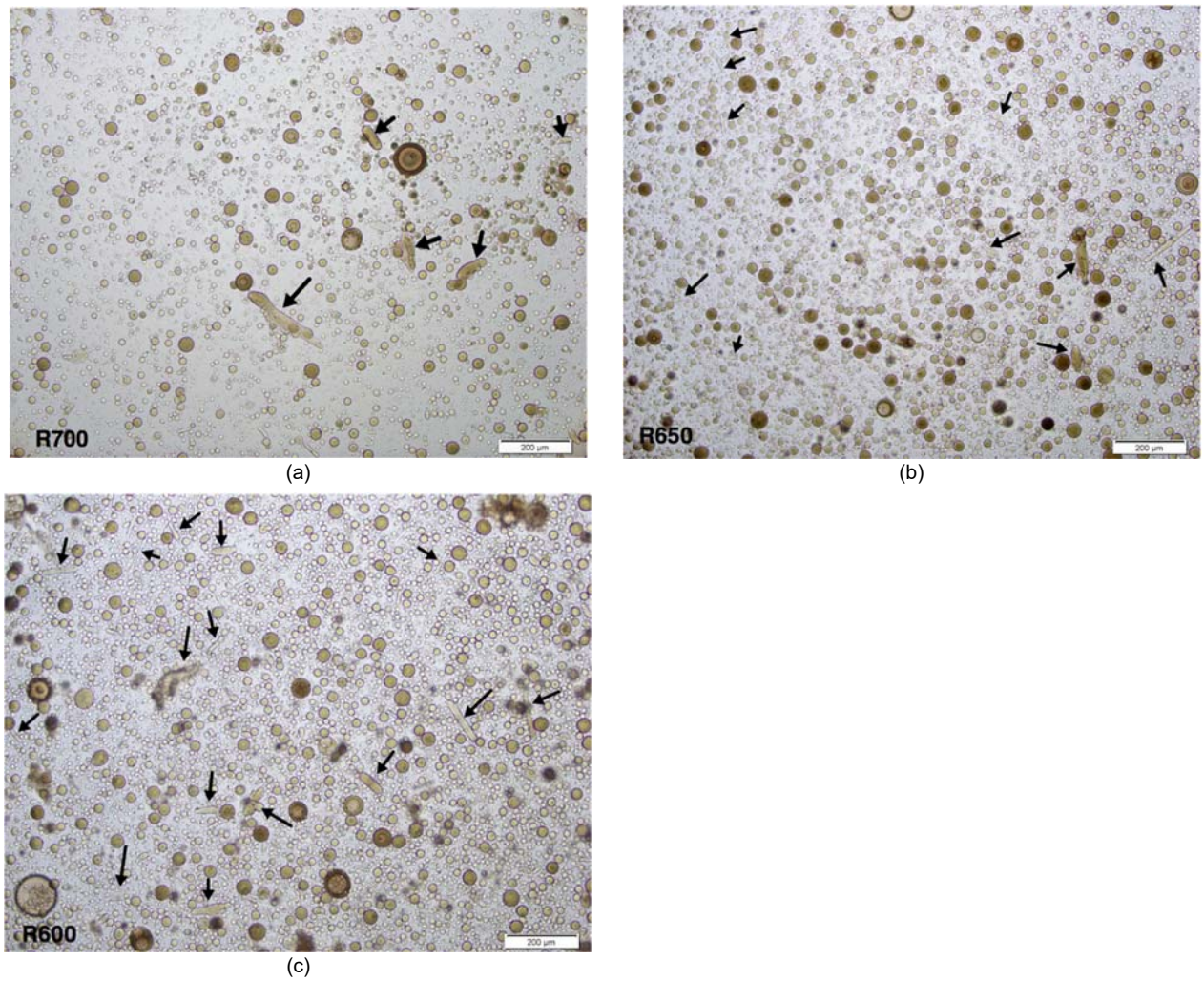

Figure 3. Optical microscope images of microcapsules obtained at different stirring rates. R700 (a), R650 (b) and R600 (c). ⟶: irregular microparticles.

Moreover, the span value increased at higher concentration of saponin surfactant and the most incline was from 3.0 to 3.9 when saponin concentration varied from 0.075 to 0.1 wt%. Might be the high saponin concentration above the cmc value (0.05 wt%) promoted the solubility of ethyl acetate in water, accelerating the diffusion of solvent from oil droplets to the aqueous phase and the polymer precipitation, resulting in broader microcapsule size distribution. This assumption will be verified in a further research.

Influence of stirring rate during emulsification stage on microcapsule size and morphology

As discussed above, high stirring rate during the emulsification step could be a reason for the presence of irregular microparticles in microcapsule lots. The high shear stress induced by the strong stirring action not only accelerated the diffusion of ethyl acetate solvent from the oil droplets to aqueous phase but also pulled along the oil droplets, resulting in the formation of irregular microparticles [19]. So, in order to reduce the number of the non-spherical microparticles and to get a narrower size distribution, the influence of stirring rate on microcapsule size and morphology was investigated. Because the rate of 700 rpm was nearly the upper limit of the mechanical stirrer, three levels of stirring rate investigated were: 700, 650 and 600 rpm. The correlative microcapsule lots were coded as R700, R650 and R600, with a saponin concentration equal to 0.075 wt%.

The optical microscope images of three investigated microcapsule lots were shown in Fig. 3 and it could be seen that reducing stirring rate did not help to decrease the number of irregular microparticles as expected.

Besides, reducing stirring rate from 700 to 600 rpm did not seem to affect the mean diameter of microcapsules, which was still about 21 ÷ 22 µm (Table 2). However, the size distribution became broader (Fig. 4) with the span value increased considerably from 3.0 to 3.9 (Table 2), it could be due to the less uniform mixing force throughout the emulsion mixture at low stirring speed.

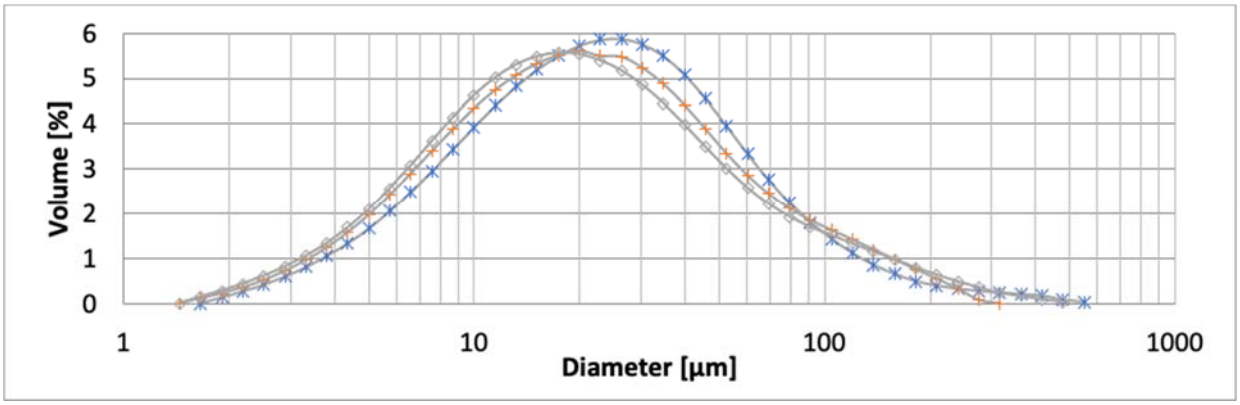

Figure 4. Effect of stirring rate on size distributions of microcapsules.

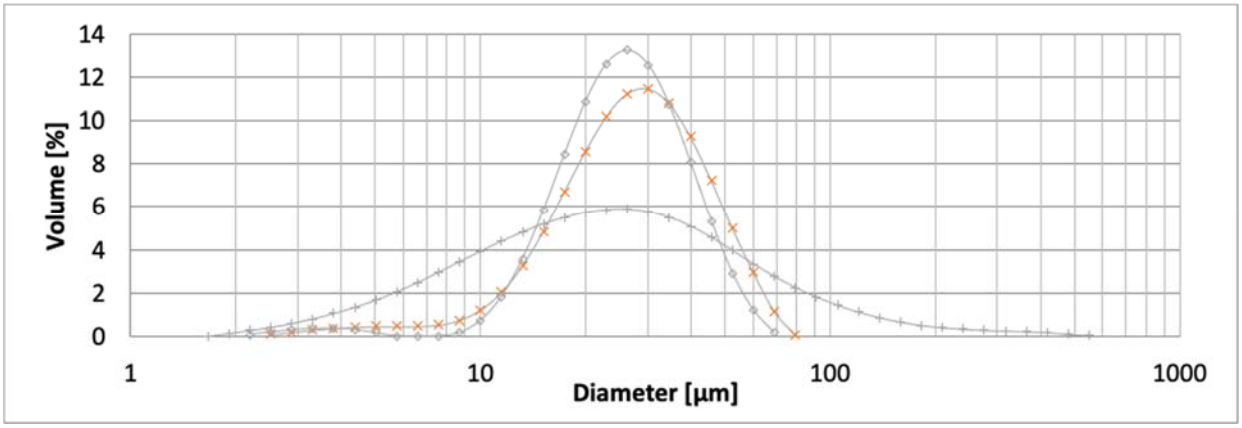

Figure 5. Effect of stirring rate on size distributions of microcapsules.

Table 2. Effect of stirring rate on the diameter and size distribution of microcapsules.

Lot	Stirring rate during emulsification [rpm]	*d*(0.5) diameter [µm]	Span value
R700	700	21.5 ± 0.2	3.0
R650	650	22.4 ± 0.2	3.5
R600	600	21.0 ± 0.1	3.9

Influence of the volume of ethyl acetate added to the aqueous phase

The fast diffusion of ethyl acetate from oil droplets to aqueous phase was the main reason for the formation of elliptical and rod shape microparticles because it induced the rapid polymer precipitation, so disturbing the emulsification step. In literature, the diffusion rate was reported to be slowed down by saturating the outer aqueous phase with a certain volume ethyl acetate prior to the emulsification step [19], [20]. Therefore, in this work, a certain volume of ethyl acetate was added to the aqueous phase before the emulsification step for an effort of reducing the irregular microparticles and narrowing the size distribution. At saponin concentration of 0.075 wt% and the stirring rate of 700 rpm, the volume of ethyl acetate added to the aqueous phase varied by three levels: 0 ml (without saturation of aqueous phase with ethyl acetate), 8 ml and 12 ml. The microcapsule lots were coded by S0, S8 and S12, respectively. It should be noted that the S0 microcapsules were exactly the C0.025 and R700 microcapsules in the previous investigation.

Table 3. Effect of ethyl acetate volume on the diameter and size distribution of the microcapsules.

Lot	Volume of ethyl acetate added to the aqueous phase [ml]	*d*(0.5) diameter [µm]	Span value
S0	0	21.5 ± 0.2	3.0
S8	8	29.5 ± 0.2	1.3
S12	12	27.5 ± 0.2	1.1

The mean diameter and size distribution of microcapsule lots were presented in Table 3 and Figure 5.

According to data in Table 3 and Fig. 5, the addition of ethyl acetate to the aqueous phase before emulsification really helped to narrow the microcapsule size distribution. When 8 ml of ethyl acetate was added to the aqueous phase, the span value decreased obviously from 3.0 (for S0 microcapsules) to 1.3 (for S8 microcapsules) while the *d*(0.5) diameter of microcapsules increased slightly from 21.5 µm (for S0 microcapsules) to 29.5 µm (for S8 microcapsules). However, with more ethyl acetate added to the aqueous phase (12 ml for S12 microcapsules), the microcapsule diameter (27.5 µm) and the span value (1.1) did not change much.

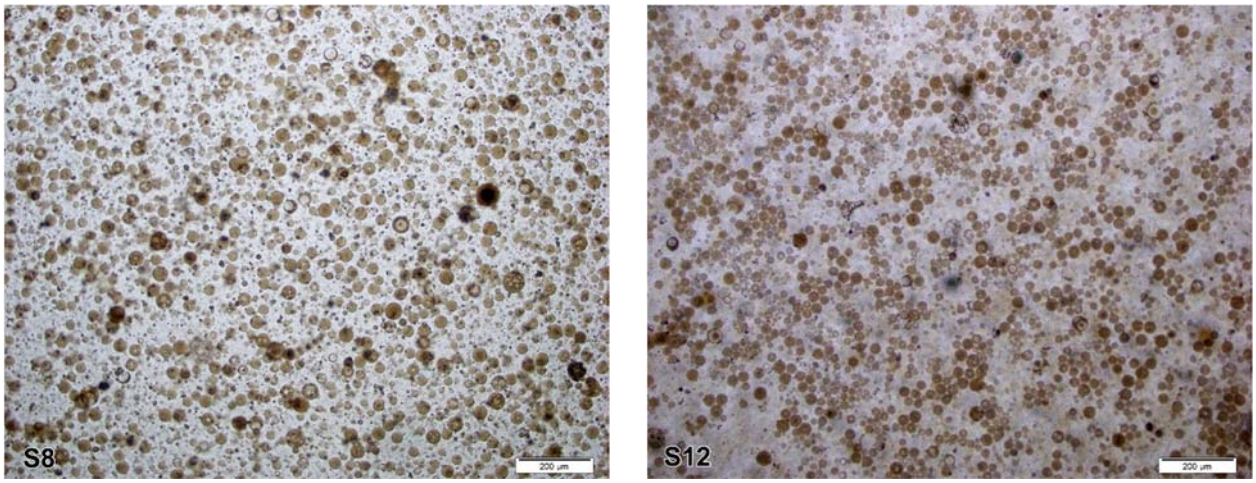

(a) (b)

Figure 6. Optical microscope images of microcapsules S8 (a) and S12 (b).

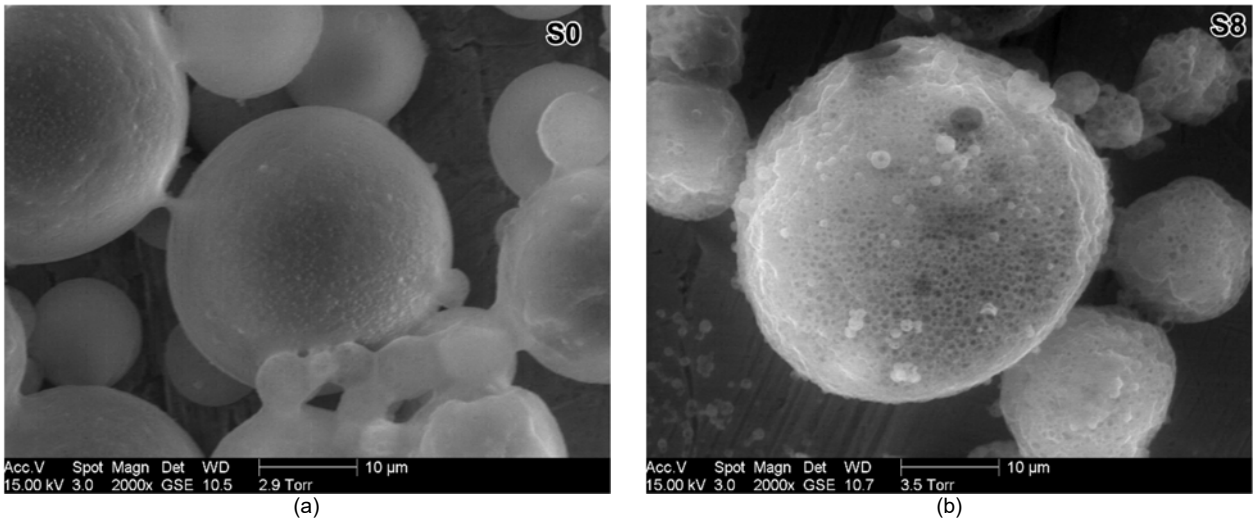

(a) (b)

Figure 7. SEM images of microcapsules S0 (a) and S8 (b).

The optical microscope images and S8 and S12 microcapsules (Fig. 6) showed the similar trend obtained by the laser diffractometry. Moreover, it was revealed that the irregular microparticles almost disappeared in the S8 and S12 microcapsule lots.

Since the solubility in water of ethyl acetate at 20°C is 90 g/l that equals to 100 (ml/l), with 8 ml of ethyl acetate added to 100 ml of aqueous phase, the solvent was completely dissolved and almost reached the water saturation. The diffusion rate of ethyl acetate from the oil droplets to the aqueous phase was then significantly reduced, resulting in the delay of the polymer precipitation, increasing the efficiency of the emulsification step through the formation of smaller droplets with spherical shape. With more than 8 ml of ethyl acetate was added to the aqueous phase (for example in case of S12 microcapsules), the aqueous phase might be completely saturated by the solvent, so the mean diameter and the size distribution of microcapsules did not change much in comparison to the S8 lot.

SEM images of S0 microcapsule (Fig. 7(a)) and of S8 microcapsule (Fig. 7(b)) showed the clear difference in the microcapsule surface morphology.

The external surface of S0 microcapsules (without saturation) appeared quite smooth (Fig. 7(a)) while S8 microcapsules (saturating the aqueous phase by 8 ml of ethyl acetate) exhibited very porous surface with many pinholes larger than 1 µm (Fig. 7(b)). This difference also was reported in literatures [29], [30] in which, the fast removal of solvent from oil droplets tended to form the smoother surface of microcapsules and in contrast, the slow removal of solvent would cause the microcapsule structure more porous. Besides, in the case of ethyl acetate, the high miscibility between ethyl acetate and water favored the uptake of water into the dispersed phase and created water pockets inside the microcapsule core when the polymer precipitated. The more water entrapped inside the droplets, the more porous the microcapsule would be. The saturation step delayed the solvent removal during the emulsification step

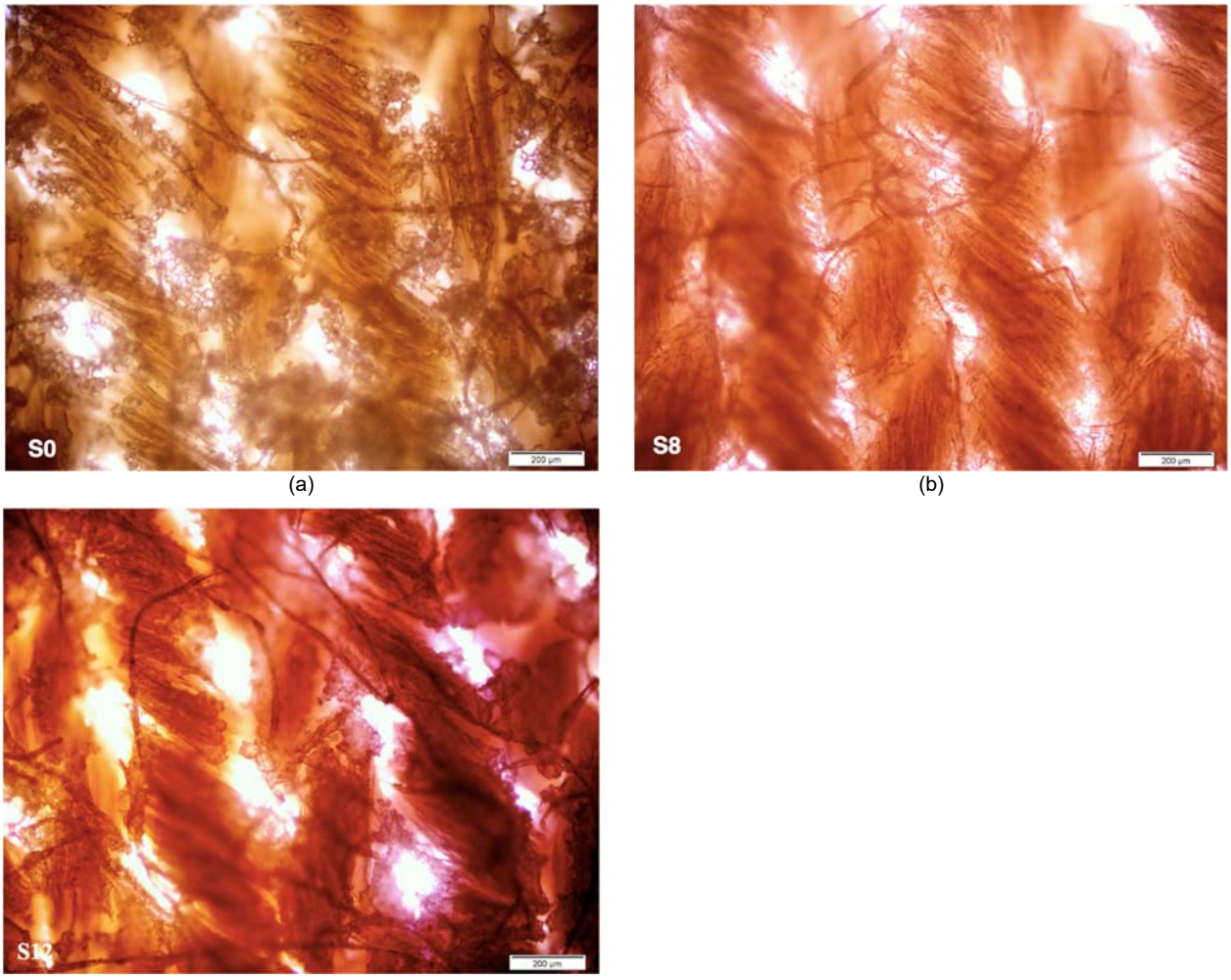

Figure 8. Optical microscope images of cotton interlock knitted fabric treated with microcapsules obtained at different ethyl acetate added volume.

and therefore slowed down the solidification of droplets, favoring the water diffusion into the semisolid microcapsules that eventually created more porous microcapsules.

The S0, S8 and S12 microcapsules were then applied to cotton interlock knitted fabric to test their drying ability during the fabric finishing process. The microscopic images of microcapsule treated fabrics were presented at Fig. 8.

It was shown that after the fabric treatment, which required a vacuum drying stage at 25ºC for 24 hours, the S0 microcapsules were still spherical (Fig. 8(a)) while the S8 and S12 microcapsules deformed strongly, no completely spherical microcapsules could be observed on the fabric surface (Fig. 8(b,c). The addition of ethyl acetate to the aqueous phase decreased the diffusion rate of solvent from the oil droplets to the aqueous phase. After the same duration of solvent evaporation step (5 hours), the content of residual solvent in S8 and S12 microcapsules were higher than that in S0 microcapsules. Since the water solubility in ethyl acetate is equal to 3.3 wt% [17], the content of residual water in S8 and S12 microcapsules might also be higher than that of S0 microcapsules. Therefore, the polymer structure of S8 and S12 microcapsules was softer and weaker than of S0 microcapsules, resulting in their serious deformation after the drying process.

CONCLUSION

In conclusions, it was successful to produce microcapsules by solvent evaporation method using quillaja saponin as bio-sourced surfactant in the combination with ethyl acetate as non-halogenated and less toxic solvent. The microcapsules were in spherical shape with the size range of 17 ÷ 34 µm, suitable for the medical textile applications.

When the saponin concentration increased from 0.025 to 0.1 wt%, the $d(0.5)$ diameter of microcapsules decreased from 34.3 to 17.1 µm while the span value increased from 2.4 to 3.9, respectively. The irregular microparticles with elliptical or rod shapes were observed in all four microcapsule lots.

The stirring rate during emulsification step was slowed down gradually by 700, 650 and 600 rpm in an effort of reducing the number of irregular microparticles, but it did not work. The *d*(0.5) diameter almost did not change at around 21.5 μm while the span value increased quickly from 3.0 to 3.9.

Another solution to overcome the formation of irregular microparticles was saturating the aqueous phase by a certain volume of ethyl acetate prior to the emulsification step. With 8 and 12 ml of ethyl acetate added to the aqueous phase, the irregular microparticles almost disappeared in the microcapsule lots. The *d*(0.5) diameter increased slightly from 21 to 28 μm while the size distribution of microcapsules became obviously narrower with span value decreased from 3.0 to 1.1. However, the saturation step made the microcapsules more porous, softer, and weaker, so they were easily deformed during the drying stage, leaving a polymer coating on the fabric surface rather than individual dried microcapsules after the fabric treatment.

For the medical textile applications, the microcapsules always need to pass a drying process. Therefore, in the scope of research, despite of the broad size distribution and the formation of some irregular microparticles, the microcapsule lot C0.075 (R700 or S0) was chosen to be the best candidate for medical textile applications due to their capability of keeping spherical shape during the drying step.

Acknowledgement: *This research is funded by Hanoi University of Science and Technology (HUST) under project number T2021-PC-044. The authors are thankful to Principal of the University, Direction of the School of Textile Garment and Fashion Design, Department of Textile Technology, for providing necessary facilities to carry out this work.*

REFERENCES

1. Dubey R.: Microencapsulation technology and applications, Defence Science Journal 59(1), 2009, pp. 82-95. https://doi.org/10.14429/dsj.59.1489
2. Jyothi N. V. N, Prasanna P. M., Sakarkar S. N., et al.: Microencapsulation techniques, factors influencing encapsulation efficiency, Journal of Microencapsulation 27(3), 2010, pp. 187–197. http://doi.org/10.3109/02652040903131301
3. Karagonlu S., Basal G., Özyildiz F., et al.: Preparation of thyme oil loaded microcapsules for textile applications, International Journal of New Technology and Research 4(3), 2018, pp. 01-08.
4. Fiedler J. O., Carmona O. G, Carmona G. C, et al.: Application of Aloe vera microcapsules in cotton nonwovens to obtain biofunctional textiles, The Journal of The Textile Institute 111(1), 2020, pp. 68-74. https://doi.org/10.1080/00405000.2019.1625607
5. Zhao H., Fei X., Cao L., et al.: Relation between the particle size and release characteristics of aromatic melamine microcapsules in functional textile applications, RSC Advances, 9(3), 2019, pp. 25225–25231. https://doi.org/10.1039/C9RA05196A
6. Beşen B. S, Balcı O., Güneşoğlu C., et al.: Obtaining medical textiles including microcapsules of the ozonated vegetable oils, Fibers and Polymers, 18(6), 2017, pp. 1079-1090. https://doi.org/10.1007/s12221-017-1212-8
7. Boh Podgornik B., Šandrić S., Kert M.: Microencapsulation for functional textile coatings with emphasis on biodegradability - A systematic review, Coatings 11(11), 2021, pp. 1371. https://doi.org/10.3390/coatings11111371
8. Hsieh W. C., Chang C. P, Gao Y. L.: Controlled release properties of Chitosan encapsulated volatile Citronella Oil microcapsules by thermal treatments, Colloids and Surfaces B: Biointerfaces, 53(2), 2006, pp. 209-214. https://doi.org/10.1016/j.colsurfb.2006.09.008
9. Chu D. H, Vu. T. H. K, Sintes-Zydowicz N.: Determination of size of Ibuprofen microcapsule using for textile application and research influence of stirring speed during microencapsulation on their dimension, Journal of Science and Technology Technical Universities, 102, 2014, pp. 144-148.
10. Li M., Rouaud O., Poncelet D.: Microencapsulation by solvent evaporation: State of the art for process engineering approaches, International Journal of Pharmaceutics, 363(1), 2008, pp. 26-39. https://doi.org/10.1016/j.ijpharm.2008.07.018
11. Carr E. J., Pontrelli G.: Drug delivery from microcapsules: How can we estimate the release time?, Mathematical Biosciences, 315, 108216, 2019. https://doi.org/10.1016/j.mbs.2019.108216
12. Yang Z., Zeng Z., Xiao Z. Ji H.: Preparation and controllable release of chitosan/vanillin microcapsules and their application to cotton fabric, Flavour and Fragrance Journal 29(2), 2014, pp. 114-120. https://doi.org/10.1002/ffj.3186
13. Monllor P., Sánchez L., Cases F., et al.: Thermal behavior of microencapsulated fragrances on cotton fabrics, Textile Research Journal, 79(4), 2009, pp. 365-380. https://doi.org/10.1177/0040517508097520
14. Azizi N, Chevalier Y., Majdoub M.: Isosorbide-based microcapsules for cosmeto-textiles, Industrial Crops and Products, 52, 2014, pp. 150-157. https://doi.org/10.1016/j.indcrop.2013.10.027
15. Valot P., Baba M., Nedelec J-M., et al.: Effects of process parameters on the properties of biocompatible ibuprofen-loaded microcapsules, International journal of pharmaceutics, 369 (1-2), 2009, pp. 53-63. https://doi.org/10.1016/j.ijpharm.2008.10.037
16. Urbaniak T., Musiał W.: Influence of solvent evaporation technique parameters on diameter of submicron lamivudine-poly-ε-caprolactone conjugate particles, Nanomaterials, 9(9), 2019, pp. 1240. http://doi.org/10.3390/nano9091240
17. Sah H.: Microencapsulation techniques using ethyl acetate as a dispersed solvent: effects of its extraction rate on the characteristics of PLGA microspheres, Journal of Controlled Release, 47(3), 1997, pp. 233-245. https://doi.org/10.1016/S0168-3659(97)01647-7
18. Mirabedini S. M., Dutil I., Farnood R. R.: Preparation and characterization of ethyl cellulose-based core–shell microcapsules containing plant oils, Colloids and Surfaces A: Physicochemical and Engineering Aspects, 394, 2012, pp. 74-84. https://doi.org/10.1016/j.colsurfa.2011.11.028
19. Meng F. T., Ma G. H., Qiu W., et al.: W/O/W double emulsion technique using ethyl acetate as organic solvent: effects of its diffusion rate on the characteristics of microparticles, Journal of Controlled Release, 91(3), 2003, pp. 407-416. http://doi.org/10.1016/s0168-3659(03)00273-6
20. Kim H. K., Park T. G.: Microencapsulation of dissociable human growth hormone aggregates within poly(D,L-lactic-co-glycolic acid) microparticles for sustained release, International journal of pharmaceutics, 229(1-2), 2001, pp. 107-116. http://doi.org/10.1016/s0378-5173(01)00852-3
21. Chung C., Sher A. , Rousset P., et al.: Formulation of food emulsions using natural emulsifiers: Utilization of quillaja saponin and soy lecithin to fabricate liquid coffee whiteners, Journal of Food Engineering, 209, 2017, pp. 1-11. https://doi.org/10.1016/j.jfoodeng.2017.04.011

22. Rai S., Acharya-Siwakoti E., Kafle A., et al.: Plant-derived saponins: A review of their surfactant properties and applications, Sci 3(4):44, 2021. https://doi.org/10.3390/sci3040044
23. Schreiner T. B, Dias M. M., Barreiro M. F., et al.: Saponins as natural emulsifiers for nanoemulsions, Journal of Agricultural and Food Chemistry, 70(22), 2022, pp. 6573-6590. https://doi.org/10.1021/acs.jafc.1c07893
24. Liao Y., Li Z., Qing Z., et al.: Saponin surfactants used in drug delivery systems: A new application for natural medicine components, International journal of pharmaceutics, 603, 2021, pp. 120709. https://doi.org/10.1016/j.ijpharm.2021.120709
25. Wojciechowski K.: Surface activity of saponin from Quillaja bark at the air/water and oil/water interfaces, Colloids and surfaces. B, Biointerfaces, 108, 2013, pp. 95-102. https://doi.org/10.1016/j.colsurfb.2013.02.008
26. Yang Y., Leser M. E., Sher A. A., et al.: Formation and stability of emulsions using a natural small molecule surfactant: Quillaja saponin (Q-Naturale®), Food Hydrocolloids, 30(2), 2013, pp. 589-596. https://doi.org/10.1016/j.foodhyd.2012.08.008
27. Yang Y., McClements D. J.: Encapsulation of vitamin E in edible emulsions fabricated using a natural surfactant, Food Hydrocolloids, 30(2), 2013, pp. 712-720. https://doi.org/10.1016/j.foodhyd.2012.09.003
28. Mitra S., Dungan S. R.: Micellar properties of quillaja Saponin. 1. Effects of Temperature, Salt, and pH on Solution Properties, Journal of Agricultural and Food Chemistry, 45(5), 1997, pp. 1587-1595. https://doi.org/10.1021/jf960349z
29. Chung T. W., Huang Y. Y., Liu Y. Z.: Effects of the rate of solvent evaporation on the characteristics of drug loaded PLLA and PDLLA microspheres, International Journal of Pharmaceutics, 212(2), 2001, pp. 161-169. https://doi.org/10.1016/S0378-5173(00)00574-3
30. Izumikawa S., Yoshioka S., Aso Y.: Preparation of poly(l-lactide) microspheres of different crystalline morphology and effect of crystalline morphology on drug release rate, Journal of Controlled Release, 15(2), 1991, pp. 133-140. https://doi.org/10.1016/0168-3659(91)90071-K

INFLUENCE OF SOME WINDING PARAMETERS ON HAIRINESS OF YARN AFTER WINDING PROCESS

TRAN DUC TRUNG, CHU DIEU HUONG* AND DAO ANH TUAN*

Hanoi University of Science and Technology, Hanoi, Vietnam

ABSTRACT

Hairiness is an important quality parameter of yarn after winding process. It affects not only the quality of yarn, but also the productivity of the warping, weaving, knitting machines as well as the quality of produced fabrics. Hairiness is influenced by the factors of raw materials, technology and equipment at all stages of yarn production. This article presents the results of experimental research on the simultaneous influence of four typical winding parameters, including: Winding speed (Z_1), the load on the friction discs of the yarn tensioner (Z_2), the distance between the bobbin and the yarn guide (Z_3) and the pressure of package on the grooved drum (Z_4) to the increasing percentage of the hairiness of the yarns after winding compared to that before winding. Yarn hairiness was measured by Uster tester 5. By using the second-order orthogonal experimental planning, together with the support of Excel 2019 and Design Expert 11 software, an experimental matrix and mathematical models describing the relationship between the four winding parameters and increasing percentage of the hairiness of three types of yarn (carded Ne 31/1 CVCD, combed Ne 30/1 CVCM, combed Ne 30/1 COCM) are established. The research result is the scientific basis for selecting the optimal winding parameters in order to achieve the required increase in hairiness of the yarn after winding or predict hairiness increase of the yarns before winding.

KEYWORDS

Winding; Winding parameters; Yarn hairiness; Hairiness measurement.

INTRODUCTION

The ends of the fibers, the very small loops of yarn protruding from the surface of the yarn, cause the yarn hairiness. In fact, especially when spinning from short fibers such as cotton... it is inevitable that the yarn will have hairiness. High yarn hairiness increases the breakage rate of yarn on winding, warping, weaving and knitting machines. Depending on the use of the yarn, the hairiness requirement of the yarn will change. Products of sewing thread, woven fabric, and knitted fabric need to clearly show the weaving pattern, beautiful surface, and very little hairiness of the yarns. In contrast, for the production of napped fabric or felt fabric, yarns with high hairiness are needed to form a good layer of snow on the surface of the fabrics.

Hairiness is expressed in a variety of ways including the number of protruding fiber ends per unit of the length of yarn (usually 1m), the average length of the fiber ends, the total length of the fiber ends, the total area of the fiber ends. Of all, the expression of hairiness by the number of protruding fiber ends has been widely applied. Currently, the hairiness of a 1000m yarn test sample is understood as the average value of the length of the ends protruding from the main connection of the yarn body in one unit length of one centimeter [1].

The level of hairiness is affected by the properties of the raw material, yarn parameters, and processing parameters. Here, only a few studies on the influence of winding technology on yarn properties including hairiness are mentioned.

Zhigang Xia et al [2] studied the effect of repeated winding on carded ring cotton yarn properties, including hairiness, winding speed at 840m/min, the load applied to the friction discs of the tensioner is 45g. According to this study, the yarn after winding had a yarn count decrease in T (tex) due to partial loss of the yarn mass. Unevenness U% and imperfection index (IPI) (thin (-50%), thick (+50%), neps (+200%)) are improved, breaking strength as well as breaking work declines. The hairiness was measured by the YG172 hairiness meter. This study also shows that hairiness of all yarns is largely increased after windings, total yarn hairs per 10 meters increase and the largest increasing percentage of the hairiness are almost designated to the hairs ranged in the length from 2 to 4mm.

* **Corresponding author:** Dao Anh T., Chu Dieu H., e-mail: *tuan.daoanh@hust.edu.vn*, *huong.chudieu@hust.edu.vn*

Received November 4, 2022; accepted December 9, 2022

MD Zahidul Islan [3] studied the effect of winding speed on the properties of the yarn after winding. In this work, two yarns of Ne 22 carded hosiery and Ne 22 combed hosiery were wounded in Autoconer winding Machine at the speed of 1400m/min, 1500m/min and 1600m/min. The research results showed that the parameters U%, IPI, hairiness H of the yarn after winding increased with the winding speed respectively. When winding at the speed of 1600m/min, U% of the yarn after winding increased by 17%, the IPI increased by 43.03%, the H increased by 40% compared to before winding, while with the Ne 22 carded cotton yarn, U% of the yarn after winding increased by 21.7%, the IPI increased by 47.6%, the H increased by 48.5% compared to before winding. The level of U%, IPI, H% of the carded yarn is higher than that of the combed yarn with the same Ne 22.

According to R. Senthil Kumar [4], in the case of winding from a bobbin, the parameters of the yarn after winding increase at the average level as follows: U% = 3 ÷ 5%, Thin (-50%): 0 ÷ 0.5%, Thick (+50%): 15 ÷ 20%, Neps (+200%): 5 ÷ 10%, hairiness H = 25 ÷ 30% is acceptable. However, to achieve the above increases, it is necessary to wind with reasonable parameters to be able to achieve.

Jun Lang and Sukang Zhu [5,6] investigated the hairiness change of yarn during winding by analyzing forces acting on the fiber ends protruding from the yarn body. According to this study, the cause of yarn hairiness is due to the yarn's friction with the friction discs of the tensioner and the grooved drum of the winding machine. This is a theoretical study, the established equations of the effects of the tension disks and the grooved drum on the yarn hairiness contain many unknowns (coefficients), so it is difficult to apply this research in practice.

Rafael Beltran et al [7] established a winding model in which an air nozzle was positioned between the tensioner and the grooved drum. The air pressure in the nozzle is 0.7 bar. Research results have shown that, when equipped with an air nozzle on the motion trajectory of the yarn, the hairiness of the yarn (the number of fiber ends with a length of 3mm) was reduced by 33% compared to when there was no air nozzle.

Noman Haleen and Tungai Wang [8] summarized and developed the research on hairiness. In this study, the authors summarized the methods of measuring hairiness, material factors, and technology (mainly in the pre-winding stages) affecting hairiness. According to this study, over 600 research studies directly or indirectly related to hairiness have been reported proving that hairiness is very interesting.

It can be seen that the properties of the yarn after winding have changed compared to before winding [9, 10], in which the hairiness increases sharply with the winding speed. In fact, the hairiness of the yarn after winding not only influenced by the winding speed, but also by many other winding parameters such as the load placed on friction discs of the tensioner, the position of the bobbin, the pressure of the package on the grooved drum... these parameters also affect yarn tension and also affect hairiness but have not been studied.

Thus, in order to achieve the yarn hairiness or hairiness increase of the yarn after winding, it is necessary to study the simultaneous influence of some typical winding parameters on the hairiness of the yarn, establishing mathematical models showing the relationship between the increase in yarn hairiness after winding and some typical winding parameters creating a scientific basis to select the optimal winding parameters to achieve the required hairiness of the yarn. This is a topical issue that interests the enterprises producing and using yarn after winding, because the hairiness of the yarn is not only related to the quality of textile products but also related to the cost of yarn in the market.

MATERIAL AND METHODS

Materials

Three types of ring yarns: Ne 31/1 CVCD (Carded yarn Ne 31/1 60% Cotton 40% Polyester); Ne 30/1 CVCM (Combed yarn Ne 30/1 60% Cotton 40% Polyester); Ne 30/1 COCM (Combed yarn Ne 30/1 100% Cotton) were wound on the same kind of bobbin produced by Vinatex Nam Dinh factory in Vietnam (Table 1). These are also 3 types of yarns being produced by many spinning mills in Vietnam to export to China. Procedure for selecting test samples according to ASTM D 2258-99 Standard Practice for sampling yarn for testing. Each winding was conducted for 2 minutes to ensure the same yarn length on the package and enough yarn length to test the yarn hairiness.

Methods

The winding model

The winding model is developed in Hanoi University of Science and Technology has the principle diagram in Figure 1.

Yarn 10 is removed from the bobbin 9, through the yarn guide 11, yarn tensioner 12, yarn clearer 13, yarn guide 14, grooved drum 7 and then wound on the package 8.

Table 1. The parameters of three types of yarns.

Parameters	Yarn 31/1CVCD	Yarn 30/1CVCM	Yarn 30/1COCM
Type of yarn	*Carded (60% cotton, 40% polyester)*	*Combed (60% cotton ,40% polyester)*	*Combed (100% Cotton)*
Yarn count [hank/pound]	31/1	30/1	30/1
Yarn twist [t/m]	760	744	766
Breaking Force [cN]	284.7	289.7	277.8
Elongation [%]	6.2	6.25	4.44
Tenacity [cN/tex]	15.04	14.91	14.34
Hairiness	5.61	5.55	5.7
Unevenness U [%]	11.01	9.44	8.94

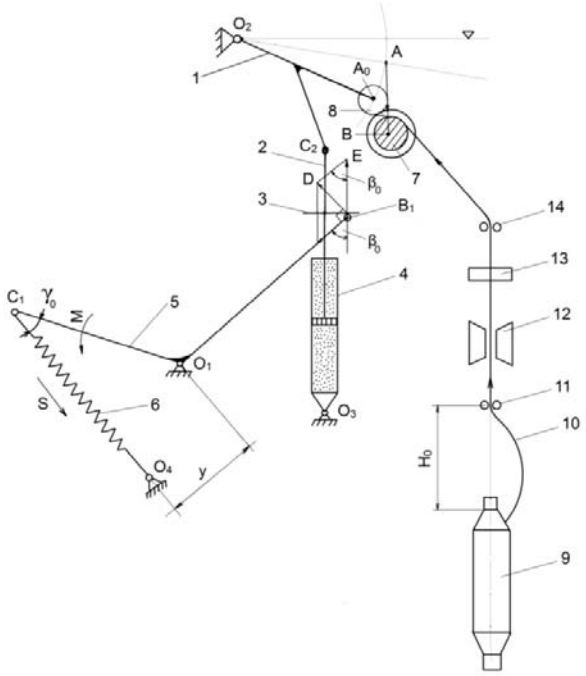

Figure 1. Principle diagram of the winding model.

Short branch of the package holder 1 connected to piston rod 2 moving in cylinder containing air (oil) 4. One end of lever 5 rests on stop plate 3 fastened on the piston rod, the other end of this lever is connected to spring 6. Details 2, 3, 4, 5, 6 create a mechanism to balance the pressure of the package on the grooved drum. With such a structure, when the diameter (mass) of package 8 increases, lever 1 will have to rotate counter-clockwise around O_2, lever 5 will rotate counter-clockwise around O_1, pulling force S of spring 6 will decrease but the distance y from spring to O_1 increases to compensate, force D at B_1 remains constant because moment M considering O_1 remains constant:

$$M = D.B_1O_1 = S.y = constant \quad (1)$$

As a result, the angle β^0 decreases, the force Eat B_1 increases according to equation (2) and keeps the pressure of the package on the grooved drum constant during winding.

$$E = \frac{D}{\sin \beta_0} \quad (2)$$

The fabricated winding model is a similar physical model, facilitating the calculation and adjustment of winding parameters for research purposes.

Measuring the hairiness

The hairiness of the yarn before and after winding is measured according to ASTM D1425/D 1425 M - 14 (2020) by Uster tester 5. The machine has 160 channels, can also measure the evenness, imperfection... of slivers, raw yarns, yarns of all kinds. Measuring range: From 10 dtex to 2500 dtex (Nm 1000 ÷ Nm 4). Sensitivity: +/- 5% to + 500% / - 100%. Speed level: 25 to 800m/min, measuring time: from 6 seconds to 20 minutes. The hairiness measuring principle is presented in Figure 2.

At the measuring slot there is a constant monochrome parallel light source. As the yarn passes through the measuring slot, the scattered light formed from the refracted, diffracted and reflected rays of the individual fibers and the fibers protruding from the main bonding part of the yarn body is clearly seen. As a result, the hairiness is measured and displayed at the receiver and converted into the corresponding electrical signal.

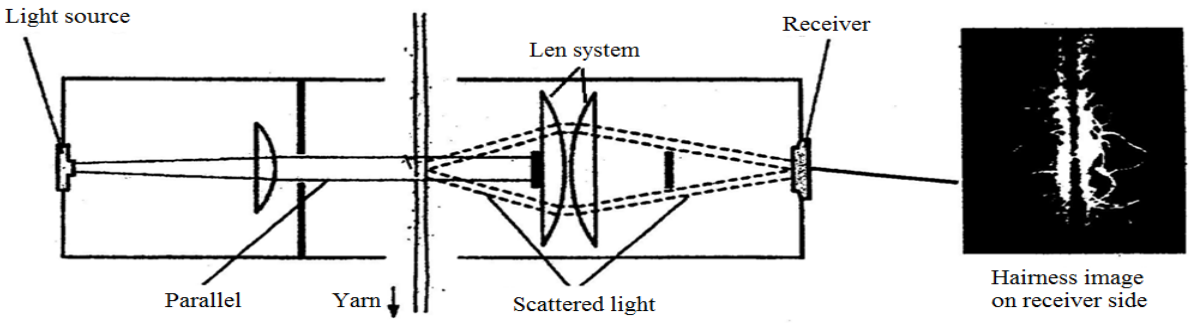

Figure 2. Hairiness measuring principle.

Table 2. Central value and variation range of winding parameters.

Parameters	Actual values				Coded values			
	Z_1 [m/min]	Z_2 [cN]	Z_3 [cm]	Z_4 [N]	x_1	x_2	x_3	x_4
Top level	1200	30	18	21	+1	+1	+1	+1
Base level Z_j^0	900	20	14	14	0	0	0	0
Bottom level	600	10	10	7	-1	-1	-1	-1
Variation range ΔZ_j	300	10	4	7	-	-	-	-

The intensity of the light on the receiver is proportional to the amount and length of fibers protruding from the yarn body. In other words, it is proportional to the hairiness. It is then converted to a digital value and evaluated by the Uster tester 5 computer. The parameters installed into the Uster tester 5 include type of test: normal, measuring slot No. 4, sample pulling speed 400m/min, measuring time 1min, environmental conditions: temperature 20 ± 20C, relative humidity 65 ± 2%.

The experimental planning method

The second-order orthogonal experimental planning method was used (BOX - WILSON planning) to establish the experimental matrix and mathematical models showing the relationship between increasing percentage of the hairiness of the yarn after winding and the selected winding parameters with the help of Excel 2019 and Design Expert 11 software.

RESULTS AND DISCUSSION

Determination of variation range of winding parameters

When winding, the winding parameters that are considered to have a great influence on the hairiness or increase in hairiness of the yarn after winding compared to before winding include: Winding speed (Z_1), the load on the friction discs of the yarn tensioner (Z_2), the distance between the bobbin and the yarn guide (Z_3) and the pressure of package on the grooved drum (Z_4). In this study, the values of winding parameters in Table 2 were selected on the basis of inheriting the studies [3,9], surveying the winding conditions of common yarns in enterprises, yarn quality before winding and the ability of the winding model.

Coding and experimental matrix establishing

The experimental regression equation of the hairiness increase of the yarn after winding for coding variables has the following general form:

$$H = b_0 + b_1x_1 + b_2x_2 + b_3x_3 + b_4x_4 + b_{12}x_1x_2 + b_{13}x_1x_3 + b_{14}x_1x_4 + b_{23}x_2x_3 + b_{24}x_2x_4 + b_{34}x_3x_4 + b_{11}x_1^2 + b_{22}x_2^2 + b_{33}x_3^2 + b_{44}x_4^2$$

Where:

b_0, b_1, b_2, b_3, b_4, b_{12}, b_{13}, b_{14}, b_{23}, b_{24}, b_{34}, b_{11}, b_{22}, b_{33}, b_{44}: Regression coefficients

x_1, x_2, x_3, x_4: The encoding variables of winding parameters

To establish an experimental matrix, Z_j is converted to x_j according to the formula:

$$x_j = \frac{Z_j - Z_j^0}{\Delta Z_j} \quad (3)$$

Then, a full experimental table is made. The number of experiments N with the number of variables k = 4 is determined by the $N = 2^k + n_0 + 2k$ where, n_0 is the number of experiments in the center ($n_0 = 1$). So, N = 25. Coefficient $\alpha = \sqrt{\sqrt{N.2^{k-2}} - 2^{k-1}} = \sqrt{\sqrt{25.2^2} - 2^3} = 1.414$.

Experimental matrix and experimental results are shown in Table 3 in which, h_1%, h_2%, h_3%are the increasing percentage of the hairiness of three types of yarns Ne 31/1 CVCD, Ne 30/1 CVCM, Ne 30/1 COCM after winding compared to before winding determined according to each experiment. Each experiment wound 4 bobbins (each bobbin has a mass of 48g) so that the package has enough length for hairiness measurement. The increasing percentage of the hairiness (hairiness increase) of the yarns after winding is calculated by the formula:

Table 3. Experimental matrix and experimental results (k = 4; n_0 = 1).

N⁰	x_0	x_1	x_2	x_3	x_4	Z_1	Z_2	Z_3	Z_4	Ne 31/1 CVCD		Ne 30/1 CVCM		Ne 30/1 COCM	
										h_1	h_1 [%]	h_2	h_2 [%]	h_3	h_3 [%]
1	+	-	-	-	-	600	10	10	7	7	24.78	7.02	26.49	7.03	23.33
2	+	+	-	-	-	1200	10	10	7	7.56	34.76	7.49	34.95	7.28	27.72
3	+	-	+	-	-	600	30	10	7	7.18	27.99	7.19	29.55	7.18	25.96
4	+	+	+	-	-	1200	30	10	7	7.48	33.33	7.44	34.05	7.4	29.82
5	+	-	-	+	-	600	10	18	7	6.99	24.60	6.95	25.23	7.23	26.84
6	+	+	-	+	-	1200	10	18	7	7.08	26.20	7.08	27.57	7.37	29.30
7	+	-	+	+	-	600	30	18	7	7.02	25.13	7.04	26.85	7.21	26.49
8	+	+	+	+	-	1200	30	18	7	7.14	27.27	7.16	29.01	7.35	28.95
9	+	-	-	-	+	600	10	10	21	6.88	22.64	6.7	20.72	6.92	21.40
10	+	+	-	-	+	1200	10	10	21	6.99	24.60	7.02	26.49	7.44	30.53
11	+	-	+	-	+	600	30	10	21	7.24	29.06	7.22	30.09	7.05	23.68
12	+	+	+	-	+	1200	30	10	21	7.3	30.12	7.23	30.27	7.33	28.60
13	+	-	-	+	+	600	10	18	21	7.32	30.48	7.26	30.81	7.09	24.39
14	+	+	-	+	+	1200	10	18	21	7.65	36.36	7.69	38.56	7.43	30.35
15	+	-	+	+	+	600	30	18	21	7.34	30.84	7.34	32.25	7.2	26.32
16	+	+	+	+	+	1200	30	18	21	7.86	40.11	7.76	39.82	7.52	31.93
17	+	0	0	0	0	900	20	14	14	7.33	30.66	7.04	27.43	7.26	27.37
18	+	α	0	0	0	1324	20	14	14	7.42	32.26	7.42	33.69	7.5	31.58
19	+	-α	0	0	0	475	20	14	14	6.94	23.71	6.91	24.50	7.01	22.98
20	+	0	α	0	0	900	34.14	14	14	7.38	31.55	7.4	33.33	7.32	28.42
21	+	0	-α	0	0	900	5.86	14	14	7.17	27.81	7.18	29.37	7.19	26.14
22	+	0	0	α	0	900	20	19.65	14	7.41	32.09	7.41	33.51	7.42	30.18
23	+	0	0	-α	0	900	20	8.34	14	7.14	27.27	7.17	29.19	7.08	24.21
24	+	0	0	0	α	900	20	14	23.9	7.34	30.84	7.34	32.25	7.15	25.44
25	+	0	0	0	-α	900	20	14	4.1	7.22	28.70	7.2	29.73	7.22	26.67

$$h_u = \frac{h - h_0}{h_0}.100\% \quad (4)$$

Where:

h_0: Hairiness of yarn before winding (determined from yarn wound on bobbins of the respective yarns in Table 1)

h: Hairiness of yarn after winding (determined from yarn wound on packages) according to each experiment of the respective yarns.

Experimental results have shown that the increasing percentage of the hairiness of all three types of yarns after winding is quite high (up to 40.11%) because when winding, the yarn is influenced by the winding parameters, so it is pulled, friction with the guides, friction discs of the tensioner, notches of grooved drum, so the number and the length of the ends fibers are pulled out of the yarn body increase, causing hairiness increase (increase in hairiness).

Establishing the regression equations

By using the Design Expert software, the regression coefficients have been calculated and tested according to Student's standards. After removing the insignificant coefficients, we get the regression equations of the following form:

$H_1 = 29.3262 + 2.4677x_1 + 1.2361x_2 + 1.0265x_3 + 1.1584x_4 + 0.7910x_2x_4 + 3.0637x_3x_4$

$R^2 = 0.8773$

$H_2 = 30.2285 + 2.5867x_1 + 1.3334x_2 + 1.1799x_3 + 0.9436x_4 + 3.1407x_3x_4$

$R^2 = 0.9184$

$H_3 = 27.1439 + 2.5464x_1 + 0.5560x_2 + 1.0972x_3 - 0.3180x_1x_2 - 0.3618x_1x_3 + 0.7785x_1x_4$

$R^2 = 0.9239$

The regression coefficients represent the influence of winding parameters on the increasing percentage of the hairiness of the yarn after winding. It can be seen that:

In the selected range, the four winding parameters: the winding speed (x_1), the load on the friction discs of the yarn tensioner (x_2), the distance between the bobbin and the yarn guide (x_3) and the pressure of package on the grooved drum (x_4) all have the effect on the hairiness increase of the yarns after winding.

In the four winding parameters selected to study the influence, the winding speed parameter (x_1) has the greatest influence on the hairiness increase of the yarn (coefficients b_1 in equations H_1, H_2, H_3 all have maximum values and are equal to 2.4677, 2.5867, 2.5464), followed by the effect of the load on the friction discs of the yarn tensioner (x_2) (coefficients b_2 equals 1.2361, 1.3334, 0.5560 in equations H_1, H_2, H_3), followed by the effect of the distance (x_3) (coefficients b_3 equals 1.0265, 1.1799, 1.0972 in equations H_1, H_2, H_3). All these three parameters have a positive influence on the hairiness increase of the yarn after winding.

To determine the influence of two parameters: winding speed (x_1) and the load on the friction discs of the tensioner (x_2) on the hairiness increase of the yarn after winding and check the reliability of mathematical models have been established,

Table 4. The hairiness increase H and the difference of the hairiness increase ΔH when the windingspeed (x_1) changes.

Real variable	Encoding variable	Yarn Ne 31/1 CVCD			Yarn Ne 30/1 CVCM			Yarn Ne 30/1 COCM		
Z_1 [m/min]	x_1	H_1	H_{1k}	ΔH_1	H_2	H_{2k}	ΔH_2	H_3	H_{3k}	ΔH_3
700	-0.6666	27.68	28.63	3.43	28.5	29.21	2.49	25.45	26.17	2.85
800	-0.3333	28.50	29.9	4.91	29.36	30.1	2.52	26.29	26.97	2.58
900	0	29.33	30.66	4.53	30.23	30.85	2.05	27.14	27.37	0.85
1000	0.3333	30.15	31.01	2.85	31.09	32.45	4.37	27.99	28.51	1.85
1200	+1	31.79	33.19	4.41	32.82	33.62	2.43	29.69	30.61	3.09

Table 5. The hairiness increase H and the difference of the hairiness increase ΔH when the load (x_2) changes.

Real variable	Encoding variable	Yarn Ne 31/1 CVCD			Yarn Ne 30/1 CVCM			Yarn Ne 30/1 COCM		
Z_2 [cN]	x_2	H_1	H_{1k}	ΔH_1	H_2	H_{2k}	ΔH_2	H_3	H_{3k}	ΔH_3
10	-1	28.09	28.46	1.31	28.89	29.31	1.45	26.59	26.8	0.80
15	-0.5	28.71	29.42	2.47	29.56	30.11	1.86	26.87	27.05	0.66
20	0	29.33	30.15	2.79	30.23	30.85	2.05	27.14	27.37	0.85
25	0.5	29.94	31.19	4.17	30.89	31.44	1.78	27.42	27.72	1.09
30	+1	30.56	31.92	4.45	31.56	32.34	2.47	27.7	28.25	1.98

calculated according to the regression equations and tested experimentally to measure the hairiness of the yarn under the conditions:

1. The winding speed x_1 changes, $x_2 = 0$ ($Z_2 = 20$ cN), $x_3 = 0$ ($Z_3 = 14$ cm), $x_4 = 0$ ($Z_4 = 14$ N).

2. The load x_2 changes, $x_1 = 0$ ($Z_1 = 900$ m/min), $x_3 = 0$ ($Z_3 = 14$ cm), $x_4 = 0$ ($Z_4 = 14$ N).

The calculation results and experimental determination of hairiness increase H (%) and ΔH (%) in Table 4 and Table 5.

Where:

x_1, x_2: The encoding variables are determined by the formula (3).

H_1, H_{1k}, H_2, H_{2k}, H_3, H_{3k}: The hairiness increase of the yarns after winding calculated according to the regression equations and determined by experiments when the winding speed x1 changes (table 3.3) and the load changes (Table 4).

ΔH_1, ΔH_2, ΔH_3: The difference of the hairiness increase of yarns after winding are determined by experiments compared with the calculation when the winding speed x_1 changes (Table 4) and the load changes (Table 5).

It can be seen that: The hairiness increase of the 3 types of yarn after winding increases with the winding speed Z_1 and the load on the friction disc of the tensioner Z2. Winding speed Z_1 increased by 71.4% (from 700 to 1200m/min), H_1 increased by 14.8% (from 27.68 to 31.79%), H_2 increased by 15.2% (from 28.5 to 32.82%), H_3 increased by 16.6% (from 25.45 to 29.69%). Load Z_2 increased by 200% (from 10 to 30cN), H1 increased by 8.8% (from 28.06 to 30.56%), H_2 increased by 9.2% (from 28.89 to 31.56%), H3 increased by 4.2% (from 26.59 to 27.7%).

The results of calculating the difference in hairiness increase according to the regression equations and determined experimentally with a deviation of less than 5%, proving that the established computational models achieve an acceptable level of confidence.

Under the same conditions of winding technology (Z_1, Z_2), the hairiness increase of the 3 yarns is not the same because they are also influenced by yarn count, yarn composition, yarn production technology and yarn hairiness before winding. The increase in hairiness of Ne 30/1 CVCM yarn was the highest among the three yarns mainly due to the lowest hairiness of this yarn before winding (Table 1).

The interplay among these four winding parameters is also shown quite clearly through the coefficients $b_{24} = 0.791$, $b_{34} = 3.0637$ (in equation H_1), $b_{34} = 3.1407$ (in equation H_2), $b_{12} = 0.3180$, $b_{13} = 0.3618$, $b_{14} = 0{,}7785$ (in equation H_3). Thus, when all four of these parameters change at the same time or only one of these parameters changes, the hairiness increase of the yarn after winding will change.

The value R^2 is the correlation coefficient, which indicates the error between the experimental and calculated results. As the R^2 is closer to 1, it shows that the calculated results according to the regression equations and the experimental results are very close. In this study, $R^2 = 0.873$; 0.9184; 0.9239, which shows that the calculated and experimental results are close and acceptable.

It is possible to see the image of the faces representing each relationship between the pairs of parameters of the objective function on the basis of fixing the remaining parameters at the encoding level 0 at the center through the 3D graph. Figures 3, 4, and 5 are examples.

Determination of optimal winding parameters

Inheriting the research result [4] and winding at high speed in research range to achieve high winding productivity, optimal winding parameters are determined from the point of view of achieving the required hairiness from 25 ÷ 30%.

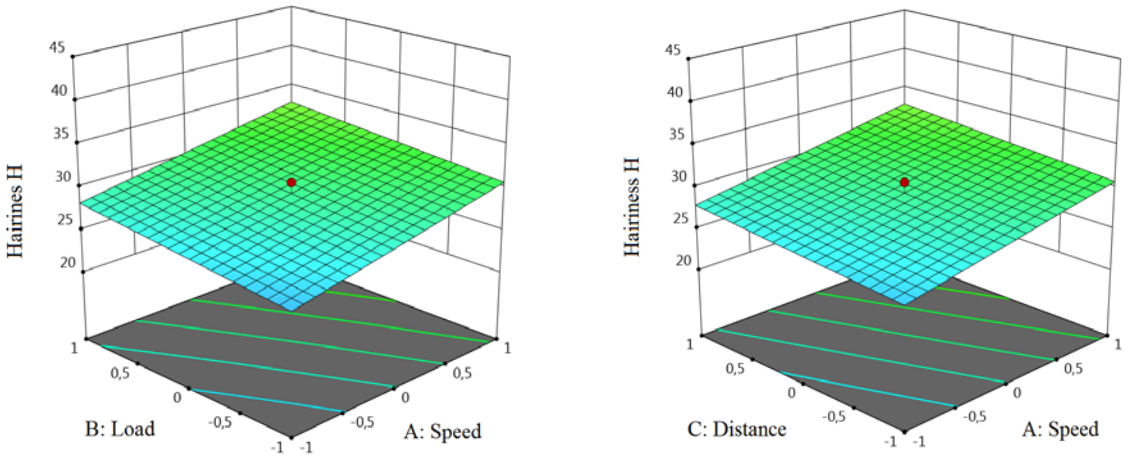

Figure 3. Yarn Ne 31/1 CVCD.

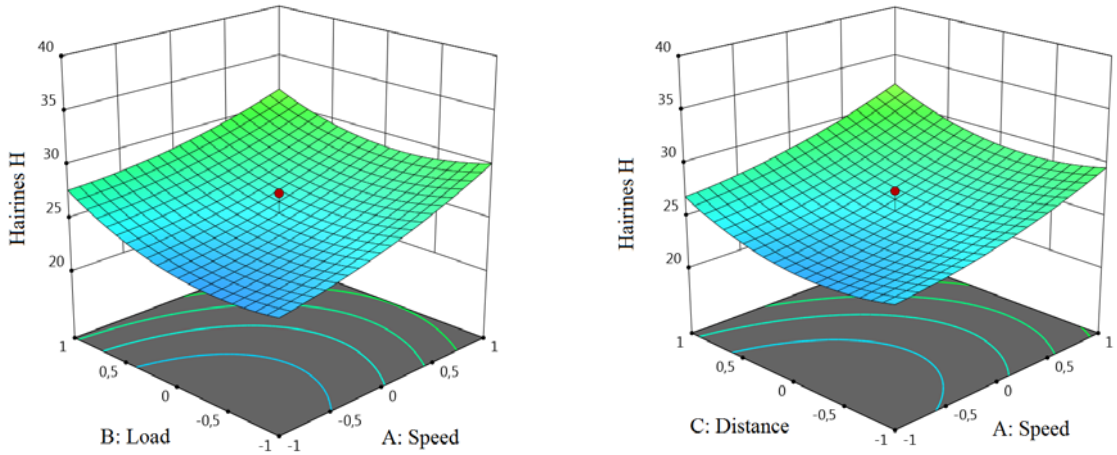

Figure 4. Yarn Ne 30/1 CVCM.

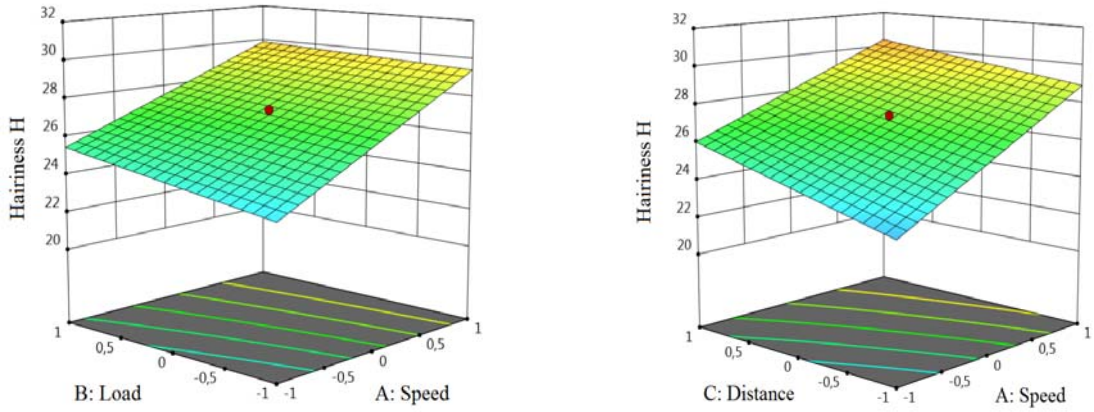

Figure 5. Yarn Ne 30/1 COCM.

However, when winding at high speed, the yarn tension is high, the breakage rate of yarn increases, the winding efficiency decreases, and the yarn hairiness increases.

To choose the optimal winding speed, an experimental study was performed in the condition of variable winding speed Z_1 = 10m/s (600m/min), 13.3m/s (800m/min), 16.6m/s (1000m/min), 20m/s (1200m/min), Z_2 = 20cN, Z_3 = 14cm, Z_4 = 14N. Winding 20 bobbins of yarns, each bobbin has a mass of m_0 = 48g, (the length is L = 1.693.Ne.m_0), monitor the breakage rate of yarn and calculate the winding efficiency taking into account the influence of the breakage rate of yarn.

Yarn Ne 31/1 CVCD, L = 2519.18 (m)

Yarn Ne 30/1 CVCM, L = 2437.9 (m)

Yarn Ne 30/1 COCM, L = 2437.9 (m)

Table 6. Results of P_0 and η when winding speed changes

Yarn	Yarn breakage P_0 (times/bobbin)	Winding speed Z_1 [m/s]			
	Winding efficiency η [%]	**10**	**13.3**	**16.6**	**20**
Yarn Ne 31/1 CVCD	P_0	0	1.3	1.5	5.0
	η	96.18	89.17	85.86	67.72
Yarn Ne 30/1 CVCM	P_0	0	1.1	1.3	4.5
	η	96.05	89.72	86.45	73.04
Yarn Ne 30/1 COCM	P_0	0	1.2	1.4	4.8
	η	96.05	89.28	85.95	71.74

Table 7. The results of determining the optimal winding parameters to achieve the required hairiness

Yarn	x_1	x_2	x_3	x_4	Z_1 [m/min]	Z_2 [cN]	Z_3 [cN]	Z_4 [N]	H [%]	h
Ne 31/1 CVCD	0.333	-1	-1	1	1000	10	10	21	25.18	7.02 ± 1.07
Ne 30/1 CVCM	0.333	-1	-1	1	1000	10	10	21	26.38	7.01 ± 1.03
Ne 30/1 COCM	0.333	-1	-1	-1	1000	10	10	7	26.30	7.19 ± 1.11

Winding efficiency η (%) is determined by the formula:

$$\eta = \frac{T_{lt}}{T_{tt}}.100 = \frac{T_{lt}}{T_{lt} + T_d}.100 \quad (5)$$

Where:

T_{lt}: Theoretical time after finish winding a bobbin,

$$T_{lt} = \frac{L}{Z_1} \quad \text{(s)}$$

T_{tt}: Actual time after finish winding a bobbin, $T_{tt} = T_{lt} + T_d$ *(s)*

T_d: Winding stop time when winding a bobbin $T_d = t\ (1 + P_0)$ where, t is the average splicing time at yarn break or change bobbin (t = 10s), P_0 is the average breakage rate of yarn after winding a bobbin (times/bobbin). After substituting the known parameters in (5), the formula for calculating the winding efficiency (%) is:

$$\eta = \frac{L}{L + Z_1.t\left(1 + P_0\right)}.100 \quad (6)$$

In order to achieve the high actual winding productivity, it is necessary to winding at a high speed but also achieve a high winding efficiency. Experimental results have shown that, winding at a low speed of 13.3m/s (800m/min), η = 89.17% and winding at a high speed of 20m/s (1200m/min), the low efficiency η = 67.72% will not achieve the high actual winding productivity. Therefore, with the three types of yarn in this study, winding at 16.6m/s (1000m/min) is reasonable, then the winding efficiency will be over 85%. To achieve the required increase in yarn hairiness after winding H_1 = 25.18%, H_2 = 26.38%, H_3 = 26.30%, by using the Design Expert software, the optimal winding parameters are determined in Table 7.

The parameters Z_j, x_j, H, h (Table 6, 7) are related to each other according to the formulas: $Z_j = x_j.\Delta Z_j + Z_j^0$; $h = h_0(0,01H+1)$, h_0 is the hairiness of the yarn before winding.

The experimental results verified with optimal technological parameters, the determined hairiness only deviated from the calculated ±6%. In practice, it is possible to choose the solution of determining the optimal winding technological parameters according to the hairiness requirements between the producer and the user of the yarn after winding.

CONCLUSION

From the obtained research results, the following conclusions can be drawn:

1. The four winding parameters: winding speed x_1 (Z_1), the load on the friction discs of the tensioner x_2 (Z_2), the distance between the bobbin and the yarn guide x_3 (Z_3) and the pressure of the package on the grooved drum x_4 (Z_4) all have influence on hairiness increase of yarns after winding: Ne 31/1 CVCM, Ne 30/1 CVCM, Ne 30/1 COCM. Of all, the effect of winding speed on the hairiness increase is the largest. That is expressed in coefficient b_1 has the largest value (equal to 2.4677; 2.5867; 2.5464) in the regression equations H_1, H_2, H_3. Winding speed increased, yarn friction with guides and grooved drum also increased lead to the yarn tension increased. The number of fiber ends and the length of the fiber ends being pulled outside the yarn body increases, causing the hairiness of the yarn increase.
2. The mathematical models of increase in yarn hairiness showing the relationships between hairiness increase of yarns after winding and the four selected winding parameters are determined. The research results are the basis for selecting optimal winding parameters to achieve the required hairiness increase or predict hairiness increase of the yarns before winding, contribute to reducing waste when producing yarn and orienting the use of yarn after winding. The methodology in this study can be applied to many different yarn samples, but the established hairiness regression models are only used for 3 types of yarns Ne 31/1 CVCD, Ne 30/1 CVCM, Ne 30/1 COCM because, these are experimental models, when the experimental conditions (yarn count, twist, production technology...) change, the experimental results and the regression models will also change.

3. The optimal winding parameters have been determined ensuse a winding efficiency of over 85% and the required increase in yarn hairiness after winding H_1 = 25.18% (with Ne 31/1 CVCD yarn), H_2 = 26.38% (with Ne 30/1 CVCM yarn), H_3 = 26.30% (with Ne 30/1 COCM yarn). The research method implemented can be applied to determine the optimal winding parameters from the point of view of achieving the required increase in hairiness and winding efficiency.

Acknowledgement: *This research is funded by Hanoi University of Science and Technology (HUST) under project number T2022-PC-094.*

REFERENCES

1. USTER 5, Application Handbook. Copyright 2008 by Uster Technologies AG.
2. Xia Z., Wang X., Ye W., et al. Effect of repeated winding on carded ring cotton yarn properties. Fiber and Polymers, 12(4), 2011, pp.534-540. http://doi.org/10.1007/s12221-011-0534-1
3. Islam MD. Z.: Effect of winding speed on yarn properties, Journal of Engineering Research and Application, 9(3), 2019, pp. 28 - 34. http://doi.org/10.9790/9622- 0903032834
4. Kumar R.S. Quality requirement ring cop for the modern cone – Winding process. The Indian Textile Journal, 2008.
5. Lang J., Zhu S., Pan N.: Changing yarn hairiness during winding - Analyzing the trailing fiber ends, Textile Research Journal, 74(10), 2004, 905-913. https://doi.org/10.1177/004051750407401010
6. Lang J., Zhu S., Pan N.: Change of hairiness during winding process: Analysis of the protruding fiber, Textile Research Journal, 76(1), 2006, pp.71-77. http://doi.org/0.1177/0040517506059710
7. Beltran R., Wang L., Wang X.: A Controlled experiment on yarn hairiness and fabric pilling, Textile Research Journal, 77(3), 2007, pp. 179 - 183. https://doi.org/10.1177/0040517507079409
8. Haleen N., Wang X. Recent research and developments on yarn hairinees, Textile Research Journal, 85(2), 2015, pp. 211-214. https://doi.org/10.1177/0040517514538692
9. Tran Duc T. Research on new modeling of winding process for controlling yarn package pressure on grooved drum. In: Aun/seed-net joint regional conferences in transportation, energy and mechanical manufacturing engineering – RCTEMME, 2021.
10. Tran Duc T., Gian Thi Thu H. Determining the effect of some technological parameters in winding process on yarn package hardness. In: Proceeding of the 2nd national scientific conference on textile, apparel and leather engineering (NCSTEX2020), 2020, pp.187.

COMPARISON OF QUANTITATIVE METHODS FOR DETERMINING THE ANTIBACTERIAL EFFECTIVENESS OF NON-WOVEN TEXTILES

ŠČASNÍKOVÁ KATARÍNA*, SIBILOVÁ ANDREA AND BÁNOVSKÁ ZUZANA

VÚTCH-CHEMITEX, spol. s r.o., Rybníky 954, 011 68 Žilina, Slovak Republic

ABSTRACT

This contribution is aimed at comparing two quantitative methods for determining the antibacterial effectiveness of non-woven textiles and assessment of permanence of the antimicrobial finish of the non-woven textile materials prepared from polypropylene fibers. Experience and results obtained by the quantitative test methods specified in AATCC TM 100 and STN EN ISO 20743 intended to evaluate the effectiveness of the antibacterial finish are published in the contribution. Emphasis is placed on comparability of the selected test methods, on the test microorganism used in the study as well as on evaluation of the results of antibacterial effectiveness. The non-woven fabrics, that were the subject of the evaluation, were pre-treated by surface activation with low-temperature plasma at atmospheric pressure and subsequently finished using antimicrobial (AMB) nanosol solution with a concentration of 15 ppm Ag+, 30 ppm Ag+, 60 ppm Ag+ and 120 ppm Ag+. Antibacterial effectiveness before washing and after 5 washing cycles is demonstrated on the specific examples obtained from practice.

KEYWORDS

Antibacterial effectiveness; Antimicrobial nanosol; Antibacterial textiles; Non–woven fabrics.

INTRODUCTION

Recently, awareness of antimicrobial textiles has come to the fore during the COVID 19 pandemic as consumers looked for ways to improve overall hygiene and well-being. Microorganisms naturally belong to human life. They are useful for a man, but some of them are dangerous as well. It has long been known that microorganisms, especially bacteria, can thrive on textile materials. Antibacterial fabrics are designed to provide protection against bacteria, mold and viruses [1].

As consumers are increasingly aware of the personal hygiene and health risks associated with certain microorganisms, the demand for antimicrobial textiles experienced a large increase in recent years. In addition to being effective against microorganisms, the antimicrobial finish of textiles must also meet various requirements, namely, it must be suitable for textile processing, durable in washing, dry cleaning, it must present a favorable safety and environmental profile, and should not damage quality or appearance of the textile material [2,3].

The growth of microorganisms on textiles causes a number of undesirable effects not only on the textiles as such, but it has also an adverse effect on the user. These effects include odor-causing, reduction of mechanical strength, discoloration and increased possibility of user contamination [4].

It is known that a large surface area of textiles and their ability to retain water provide favorable conditions for the growth of microorganisms such as bacteria and molds, which are found basically everywhere and are able to multiply very quickly depending on humidity, nutrients and temperature [5].

Due to growing public awareness of pathogenic health effects, intensive research and development has been encouraged in recent years to minimize or even eliminate bacterial growth on the textiles. Therefore, the researchers develop new means for antibacterial finish of the textiles [6].

As part of the research, we drew motivation from sources where the subject was a modified fabric providing protection of the human body against bacteria and viruses, ensuring protection of the human skin and face [7]. Subsequently, subject of the research was a barrier incorporating the modified fabric, preventing penetration of bacteria and other infectious microorganisms. The developed textile barrier can be used in the households, laboratories and in medical facilities (e.g. gown, drape, blanket...) [8].

* **Corresponding author:** Ščasníková K., e-mail: scasnikova@vutch.sk

Received September 30, 2022; accepted December 14, 2022

Microorganisms are known to cause major problems related to the transmission of diseases and infections through clothing, bedding, etc. It should be noted that bacteria are usually active at pH 7,0-8,0. Mold growth on textile materials is faster at relative humidity above 80%. At that time, microorganisms are found on the textile material in large quantities, they spread diseases and infections and also damage the fibers under normal conditions of use and storage [9]. MRSA bacterial infection caused by staphylococcus (methicillin-resistant Staphylococcus aureus) can be spread by direct contact with an infected person, as well as after contact with an object or surface touched by an infected person. It is transmitted by contact with sleepwear, bed linen and/or bed sheets. Therefore, there is an urgent need to develop textile materials effective against various microorganisms characterized by sterilizing and antimicrobial effects [10].

The goal was to prepare not only hydrophobic, but also breathable fabric, whose surface is finished with an antimicrobial agent. The fabrics according to this invention show excellent durability even in washing. This means that the fabric can be used even after repeated washing, it is not intended for one use only [11,12].

Plasma treatments are gaining popularity in the textile industry due to many advantages over traditional wet processing technologies. Equally interesting was a polypropylene non-woven fabric, made by spunbond technology and treated with hydrogen fluoride using plasma. It was found that the fabric treated in this way shows 99,04% bacterial reduction, which represents an effective barrier against the penetration of microorganisms [13].

EXPERIMENTAL PART

The experimental part describes the procedures, methods and results related to the evaluation of the antibacterial efficiency of modified non-woven fabrics. If bactericidal activity is required and/or assumed, then the quantitative assessment is necessary. Quantitative evaluation provides also a clearer picture of possible applications of the finished textile materials. One of the possibilities is also a fabric modified by surface activation with plasma and subsequent antimicrobial finish using nanosol containing an antibacterially active substance. Verification of its antibacterial effectiveness according to the appropriate standards is the subject of this article.

Methods for evaluating antibacterial effectiveness of the modified textiles

Two quantitative test methods were chosen to verify the antibacterial effectiveness of non-woven fabrics: AATCC TM 100 - 2019 [14], STN EN ISO 20743 – 2021 [15]. Both methods involve counting microbes and the results are reported as a percentage or logarithmic reduction of the contamination level.

The test microorganism Staphylococcus aureus CCM 4516 was used for testing and determination of the antibacterial effectiveness. The microorganism Staphylococcus aureus is a gram-positive coccus with dimensions of 0.5-1.5 μm in diameter. The cocci are arranged either individually, in squares, short chains, but most often in irregular grape-shaped clusters. Liquid inoculated (bacterial) solutions prepared from this microorganism were applied on the textile test samples in accordance with the test procedures.

Test method AATCC TM 100 - 2019

The test method for antibacterial finishes on textile materials AATCC TM 100 – 2019 (absorption method) is used for quantitative determination of effectiveness of antibacterial finishes applied on the textile materials. Textiles with antibacterial finishes offer the users protection from harmful bacteria and at the same time they reduce risk of disease transmission. The test method includes evaluation of the bactericidal (killing of bacteria) and bacteriostatic (inhibiting the growth of bacteria) effectiveness of the textile material during 24-hour contact with the tested bacteria.

The reduction factor was evaluated, which indicates the percentage by which the inoculated concentration of bacteria was reduced. For the test, (1.0 ± 0.1) ml of test inoculum per sample was used (i.e. in the range from 1x105 to 3x105 colonies/milliliter (CFU/ml)). After inoculation (0 contact time), a neutralizing solution was added to the sample to suppress the bactericidal effect and to maintain the correct pH balance. Serial dilutions were plated on nutrient agar medium and incubated at (37 ± 2) °C for 24 h. Evaluation of the inoculated samples took place at zero time and after 24 hours, in both cases the colony forming units were counted. The antibacterial efficiency was expressed by ratio of the number of bacteria on the antibacterially finished nonwoven fabric immediately after inoculation compared to a sample of the antibacterially finished nonwoven fabric incubated for a contact period of 24 hours. The amount of bacteria is given as the number of bacteria per sample (samples in the vessel), not as the number of bacteria per ml of neutralization solution (CFU/sample) and then the reduction R is calculated and expressed as a percentage (Tab. 3, Tab. 5):

$$100\,(C - A) / C = R \qquad (1)$$

where:

- R is reduction of bacteria as a percentage;
- C is number of bacteria regenerated from the inoculated finished test samples in a vessel, immediately after inoculation (at "0" contact time);
- A is number of bacteria regenerated from the inoculated finished test samples in a vessel, incubated for 24-hour contact time;

In this method, the microbial concentrations are standardized and the bacteria are supplied with nutrients during the entire incubation period. If the textiles tested do not have strong antibacterial potential, then this will allow bacteria to flourish and grow.

Test method STN EN ISO 20743 - 2021

The test method STN EN ISO 20743 - 2021 Determination of the antibacterial activity of textile products is a quantitative (absorption) test method to determine the antibacterial activity of the antibacterial textile products. This test method can be applied to all textile products including woven fabrics, waddings, clothing, bedspreads, household goods and textiles, yarn and material for various products, regardless of the type of antibacterial agents used.

In this method, similar to AATCC TM 100 - 2019, the test bacterial suspension was inoculated directly onto samples of the non-woven fabrics (exactly 0,2 ml of inoculum adjusted to a concentration of 1x105 - 3x105 CFU/ml is pipetted onto each sample). The concentration of bacteria (CFU) was counted at time zero (immediately after inoculation of the bacterial suspension) and after 24 hours of incubation of the bacteria on the non-woven fabric sample. The method required to perform the test on a sample of nonwoven fabric with antibacterial finish as well as on a reference sample of the nonwoven fabric. Result of the test was the antibacterial effect value, which was calculated from the CFUs:

$$A = (lgC_t - lgC_0) - (lgT_t - lgT_0) = F - G \qquad (2)$$

where:

- A is the resulting antibacterial effectiveness value;
- F is the growth value of the nonwoven fabric control sample $(F = lgC_t - lgC_0)$;
- G is the growth value of the nonwoven fabric sample with antibacterial finish $(G = lgT_t - lgT_0)$;
- lgC_t is the average decimal logarithm of the bacterial number determined from 3 test control samples of the non-woven fabric after 24-hour incubation;
- lgC_0 is the average decimal logarithm of the bacterial number determined from 3 test control samples of the nonwoven fabric immediately after inoculation;
- lgT_t is the average decimal logarithm of the bacterial number determined from 3 test samples of the non-woven fabric with antibacterial finish immediately after 24-hour incubation;
- lgT_0 is the average decimal logarithm of the bacterial number determined from 3 test samples of the nonwoven fabric with antibacterial finish immediately after inoculation.

If $C_0 > T_0$, C_0 is replaced by T_0 in the calculations.
Results of the testing will be assessed according to the achieved value of antibacterial efficiency A as shown in Tab. 1.

Table 1. Assessment of antibacterial properties according to the STN EN ISO 20743 - 2021 method

Effectiveness of antibacterial properties	Antibacterial value *(A)*
low	$A < 2$
significant	$2 \leq A < 3$ (2,3)
strong	$A \geq 3$

Materials used

For the purposes of verifying the antibacterial effectiveness using the above-mentioned methods, a sample of non-woven fabric was prepared from 100% PP using spunbond technology with mass per unit area of 40 g/m^2 and a thickness of 0,38 *mm*. The prepared sample of non-woven fabric was pre-treated with low-temperature plasma and then finished by application of antimicrobial (AMB) nanosol solutions with a concentration of 15 *ppm* Ag+, 30 *ppm* Ag+, 60 *ppm* Ag+ and 120 *ppm* Ag+ (Tab. 2).

Samples of the non-woven fabrics were subjected to five cycles of washing and drying in accordance with STN EN ISO 6330: 2012 using washing procedure 4N at a water temperature of (40±3) °*C* and a commercial detergent. Drying was carried out by procedure C, i.e. drying in a horizontal position in a spread state and then antibacterial effectiveness of the samples was evaluated (Tab. 2).

RESULTS AND DISCUSSION

Antibacterial effectiveness was quantitatively determined on samples of non-woven fabrics on which the AMB nanosol was applied under specified conditions. After incubation the bacteria are leached from the samples, their number is determined and the reduction of the number on the textile sample is calculated as a percentage or the strength of the antibacterial effect of the finished non-woven fabric is assessed. The results of testing by the absorption method according to the above-mentioned procedures are shown in Tab. 3-6.

Table 2. Identification of non-woven fabrics for verification of the antibacterial effectiveness.

Description of samples of non-woven fabrics	Marking of samples of non-woven fabrics before washing	Marking of samples of non-woven fabrics after 5 washing and drying cycles
standard PP fabric without finish	PP	
non-woven PP fabric finished by application of AMB nanosol solution with a concentration of 15 *ppm* Ag^+	PP1/15	PP2/15
non-woven PP fabric finished by application of AMB nanosol solution with a concentration of 30 *ppm* Ag^+	PP1/30	PP2/30
non-woven PP fabric finished by application of AMB nanosol solution with a concentration of 60 *ppm* Ag^+	PP1/60	PP2/60
non-woven PP fabric finished by application of AMB nanosol solution with a concentration of 120 *ppm* Ag^+	PP1/120	PP2/120

Table 3. Evaluation of antibacterial effectiveness (*R*) of non-woven fabrics **before washing** according to AATCC TM 100 – 2019.

Sample of finished non-woven fabric	PP1/15	PP1/30	PP1/60	PP1/120
Number of bacteria from inoculated test samples *(C) [CFU/sample]*	1,53 x 10^5	1,36 x 10^5	1,25 x 10^5	1,20 x 10^5
Reduction in number of bacteria (*R*) [%]	57,52	70,59	>99,92	>99,92

Table 4. Evaluation of the antibacterial effect (*A*) of the fabrics **before washing** according to **STN EN ISO 20743 -2021.**

Sample of finished non-woven fabric	PP1/15	PP1/30	PP1/60	PP1/120
Growth value *F* ($F = lg\ C_t - lg\ C_0$)	+ 2,70	+2,63	+2,53	+2,51
Growth value *G* ($G = lg\ T_t - lg\ T_0$)	-1,10	- 3,20	-4,65	-4,75
Antibacterial activity value *(A = F-G)*	3,80	5,83	7,18	7,26
Assessment of antibacterial properties from Tab.1	strong A ≥ 3			

Assessment of antibacterial effectiveness of the fabrics before washing

This work consists of two parts. In the first part, we focused on the evaluation of antibacterial effectiveness on selected fabrics before washing.

Figure 1 shows the growth of bacteria on agar after the contact time on PP non-woven fabric without antibacterial finish.

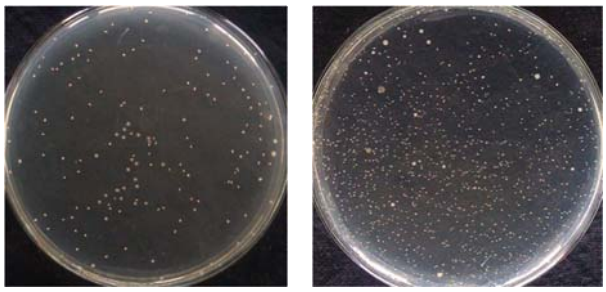

contact time: 0 hour contact time: 24 hours

Figure 1. Comparison of bacterial growth on agar: **100% PP non-woven fabric without antibacterial finish.**

To determine antibacterial effectiveness of the textile samples quantitatively, reduction in the number of bacteria *R* (Equation 1) was calculated according to the standard method AATCC TM 100 - 2019 (Tab. 3). The amount of bacteria is expressed as a number of bacteria per sample; according to the requirements of the standard, when diluted to 10^0, the value "less than 100" is indicated. The amount of inoculum per sample (1.0±0.1) *ml* of the appropriate solution of 18 *h* culture of the test organism is applied so that the amount of 1-3 x 10^5 organisms is reached on the textile test samples in "0" contact time.

The results listed in Tab.3 show, that antibacterial finish of the test samples for the microorganism *Staphylococccus aureus* CCM 4516 led to a reduction of number of bacteria at the level of **58%** on the finished PP1/15 test sample and almost **100%** on PP1/60 and PP1/ 120 samples, prepared with a higher concentration of AMB nanosol. A strong bactericidal effect was achieved on the non-woven fabrics finished by application of AMB nanosol solution before washing and drying.

Our goal was to verify reproducibility and compare the results obtained by both above-mentioned methods (Tab. 3 and Tab. 4). Table 4 shows results of determining the antibacterial effectiveness before washing and drying using another absorption method according to STN EN ISO 20743 - 2021. The test is considered effective if the test inoculum is between 1x10^5 and 3x10^5 *CFU/ml*.

Based on the results from the evaluation of the antibacterial effectiveness of the tested samples listed in Tab. 4 it can be concluded, that the finished test samples evaluated according to STN EN ISO 20743 - 2021 method show a strong antibacterial effectiveness, which is consistent compared to the AATCC TM 100 - 2019 method (Tab. 3). Comparison of the methods by evaluating the antibacterial effectiveness on non-woven fabrics before washing shows that the both test absorption methods confirmed a high antibacterial result.

Comparison of growth of bacteria on agar after contact time (0 hour and 24 hours) is shown in Fig. 2 and Fig. 3. The following section shows selected images of growth of bacteria on agar after a contact time of 0 hour and after a contact time of 24 hours, reproducibility of which was repeatedly confirmed by both test methods before washing.

Table 5. Evaluation of the antibacterial effectiveness (R) on the finished nonwoven fabric samples **after washing** according to **AATCC TM 100 – 2019.**

Sample of finished non-woven fabric after washing	PP2/15	PP2/30	PP2/60	PP2/120
Number of bacteria from inoculated test samples *(C) [CFU/sample]*	1,41 x 10^5	1,20 x 10^5	1,18 x 10^5	1,10 x 10^5
Reduction in number of bacteria (*R*) [%]	41,84	60,00	98,83	99,78

Table 6. Evaluation of the antibacterial effect **A** of the fabrics **after washing** according to **STN EN ISO 20743 – 2021.**

Sample of finished non-woven fabric after washing	PP2/15	PP2/30	PP2/60	PP2/120
Growth value *F* ($F = lg\ C_t - lg\ C_0$)	+ 2,51	+2,48	+2,40	+2,37
Growth value *G* ($G = lg\ T_t - lg\ T_0$)	- 1,00	- 2,82	- 4,68	- 4,79
Value of antibacterial activity *(A = F-G)*	3,51	5,30	7,03	7,16
Assessment of antibacterial properties from Tab.1	**strong A ≥ 3**			

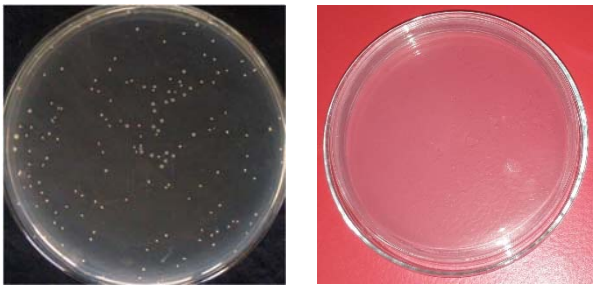

contact time: 0 hour contact time: 24 hours

Figure 2. Sample PP1/60 before washing – comparison of growth of bacteria on agar by the **AATCC TM 100 method.**

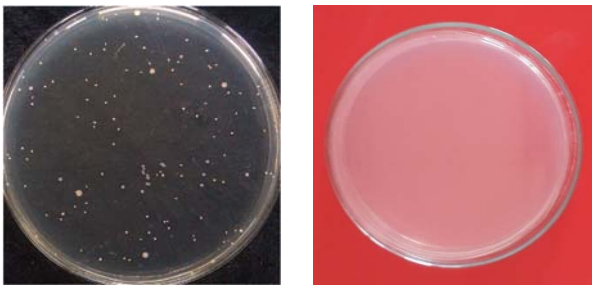

contact time: 0 hour contact time: 24 hours

Figure 3. Sample PP1/60 before washing - comparison of growth of bacteria on agar by the **STN EN ISO 20743 method.**

Assessment of antibacterial effectiveness of the fabrics after washing

The second part of this research was devoted to the evaluation of the permanence of the antibacterial finish on the samples of non-woven textiles subjected to five washing cycles. Antibacterial effectiveness was evaluated after 5 washing cycles according to the above-mentioned methods (Tab. 5, Tab. 6). The antibacterial efficiency was expressed by the ratio of the number of bacteria on the antibacterially finished nonwoven fabric immediately after inoculation compared to the sample of the antibacterially finished nonwoven fabric incubated for a contact period of 24 hours.

Results presented in Tab. 5 show, that washing did not have a significantly negative effect especially on the non-woven fabric samples PP2/60 and PP2/120 regarding reduction of the antibacterial effectiveness compared to the non-woven fabric samples before washing (Tab. 3). The highest antibacterial efficiency after washing was achieved on the sample of PP non-woven fabric finished by application of the antimicrobial nanosol solution containing 120 *ppm* Ag^+, where reduction of number of bacteria of the test microorganism *Staphylococccus aureus* CCM 4516 was approximately 99,80% after 5 washing cycles. A sample containing 60 *ppm* Ag^+, PP2/60 approx. 98,80 % achieved the same high antibacterial effectiveness after washing. The PP2/15 sample containing the AMB nanosol with concentration of 15 *ppm* Ag^+ achieved a reduction of number of bacteria over 40 %, which is a decrease by about 27 % compared to the non-woven fabric sample (PP1/15) before washing. The PP2/30 sample with nanosol concentration of 30 *ppm* Ag^+ achieved about 60 % reduction of number of bacteria, which was a decrease by 15 % compared to the non-woven fabric sample (PP1/30) before washing (Tab. 3 and Tab. 5).

Table 6 shows the results of determining the antibacterial effectiveness of nonwoven fabrics after washing using the absorption method according to STN EN ISO 20743 - 2021.

Results of the evaluation of the antibacterial activity of non-woven fabrics after washing given in Tab. 5 and Table 6 show, that the antibacterial activity is almost on the same bactericidal level for samples **PP 2/60** and **PP2/120** (*A* ≥ 3).

Selected images of bacterial growth on agar after a contact time of 0 h and after a contact time of 24 h are presented in the next part. Their reproducibility was repeatedly confirmed by both test methods **after washing** (Fig.4 and Fig.5).

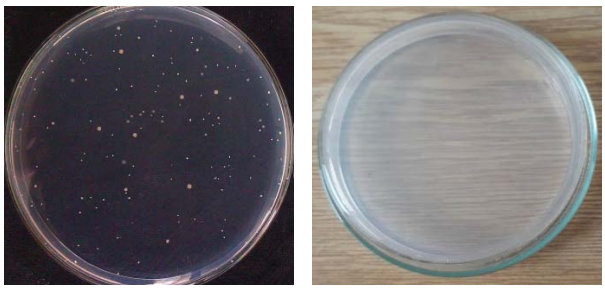

contact time: 0 hour contact time: 24 hours

Figure 4. Sample PP1/60 after washing – comparison of growth of bacteria on agar by the **AATCC TM 100 method.**

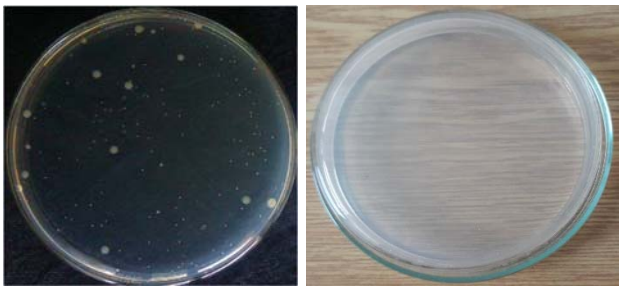

contact time: 0 hour contact time: 24 hours

Figure 5. Sample PP1/60 after washing - comparison of growth of bacteria on agar by the **STN EN ISO 20743 method.**

Reproducibility of both above-mentioned methods was verified for each sample by parallel measurements, from which the average values, necessary for the calculations to determine the antibacterial effectiveness, were obtained. Colonies on the agar plates were counted according to the AATCCTM 100-2019 method (at zero time and after 24 hours) and also according to the STN EN ISO 20743-2021 method. After counting the colonies on the agar plates, the values, according to the AATCC TM 100 method, were substituted into the equation $100\ (C\text{-}A)/C = R$, from which the result of antibacterial effectiveness (reduction) in *%* can be seen.

In accordance with the STN EN ISO 20743, colonies on agar plates were counted as well. The average values of the number of bacteria were converted to a decimal logarithm according to the specified procedure. The value of the antibacterial effect *(A)* was calculated according to the equation given in the standard: $A = (lgC_t - lgC_0) - (lg\ T_t - T_0)$. Antibacterial properties of the non-woven fabric are assessed on the basis of the calculated *A* value. This standard defines the antibacterial effectiveness as strong ($A \geq 3$) - shown in Tab.1.

Figure 6 clearly shows the number of bacteria recovered from inoculated finished test samples in a vessel, incubated for 24 hours. Figure 7 clearly shows the average logarithmic values (lgT_t) of the number of bacteria obtained from three antibacterially finished non-woven test samples after 24 hours of incubation.

No viable bacteria were detected on the antibacterially finished nonwoven fabrics (PP1/60, PP1/120) on which the *Staphylococcus aureus* bacterium was applied (incubated for 24 hours in a microbiological incubator at (37±2) °C) or a significant reduction in the number of viable bacteria (PP1/15, PP1/30) has been found. After 24-hour cultivation, the number of colonies on agar plates was determined and counted (*CFUs*), and then the antibacterial effectiveness was calculated according to the AATCC TM 100 (Fig. 6) and STN EN ISO 20743 standard (Fig. 7).

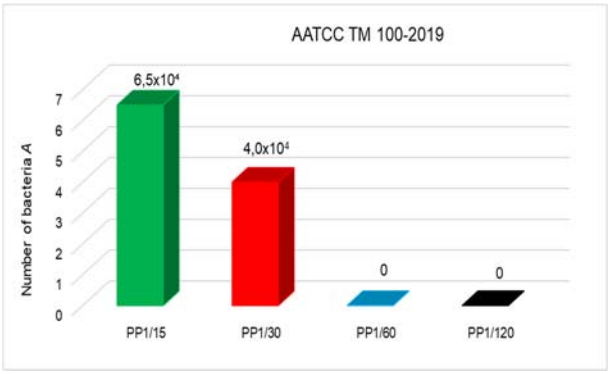

Figure 6. Number of viable *Staphylococcus aureus* bacteria on antibacterially finished textiles before washing according to the AATCC TM 100 method: ***A*** – average number of bacteria recovered from inoculated finished test samples incubated for 24 hours.

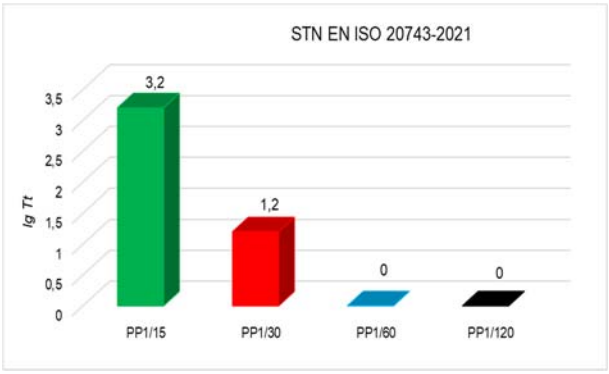

Figure 7. Number of viable *Staphylococcus aureus* bacteria on antibacterially finished textiles before washing according to the STN EN ISO 20743 method: ***lgT$_t$*** – decimal logarithm of the arithmetic mean of the number of bacteria per non-woven fabric after 24 hour incubation

Based on comparison of the antibacterial effectiveness results on 100 *%* PP non-woven fabric, it can be concluded that bactericidal effectiveness with a high degree of bacterial reduction was achieved according to the AATCC TM 100 - 2019 method and strong antibacterial effectiveness according to the STN EN ISO 20743 -2021 method (PP1/60, PP1/120), PP2/60, PP2/120). Values with less low reductions and/or significant value of antibacterial effectiveness, obtained by the methods, mentioned in the text above, could be caused by lower stability of the antimicrobial finish on PP nonwoven fabrics (PP1/15, PP2/15, PP1/30, PP2/30). Suitability of the selected test methods, together with the selection and finish of the non-woven fabric and laboratory verification of the test methods for the assessment of antibacterial activity showed us that after verifying reproducibility of the results by both absorption methods, it is possible to consider the test methods STN EN ISO 20743 - 2021 and AATCC TM 100 - 2019 sufficiently sensitive and equally reliable from the experimental viewpoint.

CONCLUSION

The antimicrobial finish protects textiles from odors and ensures their freshness, as well as protection against degradation caused by bacteria and mold. However, differences in test results between specific laboratories and failure to meet effectiveness expectations due to the use of inappropriate test methods often lead to uncertainty on the market of the antimicrobial products. Information allowing comparison of the effectiveness of antimicrobial finishes is often misleading due to differences in methodologies, as a result of inappropriate tests as well as different level of laboratory experience with their evaluation. The only way how to ensure comparability of the results is to perform side-by-side tests in the same laboratory using the same test methods.

It is possible to conclude that the assessment of antibacterial effectiveness according to the quantitative methods AATCC TM 100 - 2019 and STN EN ISO 20743 - 2021 is based on the same principle with slight deviations, while the result is expressed in a different way. Each methodology has its own expression of results, and by comparing the methods it was possible to find a correlation between the results. All samples of the non-woven fabrics had a strong antibacterial effect. Washing did not show any negative effect on reduction of the antibacterial effectiveness in comparison with the samples of nonwoven fabrics before washing. In order to determine significant level of antibacterial effect and low level of antibacterial effect, it would be necessary to test materials with AMB nanosol concentration of less than 15 *ppm* Ag^+ and number of bacteria less than 40%. The effect of low-temperature plasma on increased adhesion of AMB nanosol to the surface of PP non-woven fabric was demonstrated.

Acknowledgement: *This work was supported by the Research and Development Support Agency under contract no. APVV-20-0234.*

REFERENCES

1. Antimicrobial textiles: promoting hygiene during the COVID-19 pandemic and beyond, Performance Apparel Markets, 71, 2021.
2. Gao Y., Cranston R.: Recent advances in antimicrobial treatments of textiles, Test. Res. J., 2008, 78(1), pp. 60-72. https://doi.org/10.1177/00405175070823
3. Windler L., Height M., Nowack B.: Comparative evaluation of antimicrobials for textile applications., Environ. Int., 53, 2013, pp. 62 -73. https://doi.org/10.1016/j.envint.2012.12.010
4. Venugopala K. N., Rashmi V., Odhav B.: Review on natural coumarin lead compounds for their pharmacological activity. BioMed Res. Int., 2013, pp. 563-568. https://doi.org/10.1155/2013/963248
5. Zanoaga M.,Tanasa F.: Antimicrobial reagents as funcional finishing for textiles intended for biomedical applications. I. Synthetic organic compounds. Chem. J. Mold., 9(1), 2014 pp.14-32. https://doi.org/10.19261/CJM.2014.09(1).02
6. Morais S., D., Guedes R., M., Lopes M., A.: Antimicrobial Approaches for Textiles: From Research Market, Materials, 9, 2016, pp. 1 – 21. https://doi.org/10.3390/ma9060498
7. Fan Y.: Composite medical protective clothing, CN2669636Y, 2003.
8. Woodcock A.: Infection barrier, EP0398611A1, 1989.
9. Rajendran S.: Infection control and barrier materials: An overview, Medical Textiles and Biomaterials for Healthcare, 2006, pp. 131-135. https://doi.org/10.1533/9781845694104.3.131
10. Virus inactivation sheet, KR101759363B1, 2010.
11. Nano Motion Technology Co Ltd.: Protective clothing system for preventing respiratory system infectious disease, and the clothing, CN100506096C, 2003.
12. Sieren Co. Ltd.: Virus barrier laminated fabric excellent in washing durability, JP2015013391A.
13. Parthasarathi V., Thilagavathi G.: Development of plasma enhanced antiviral surgical gown for healthcare workers, Fashion and Textiles 2, 2015, 4. https://doi.org/10.1186/s40691-015-0028-7
14. AATCC TM 100-2019. Test Method for Antibacterial Finishes on Textile Materials. Assessment of.
15. STN EN ISO 20743-2021. Textiles – Determination of antibacterial activity of textile products.

USE OF ARDUINO-COMPATIBLE SYSTEMS IN DEVICES FOR DETERMINATION OF COLOR INDICATORS OF FLAX FIBER

TOLMACHOV VOLODYMYR[1*] AND RIABKO ANDRII[2]

[1] Department of Professional Education and Computer Technologies of the Olexander Dovzhenko Hlukhiv National Pedagogical University, Kyievo-Moskovska str. 24, Hlukhiv, Ukraine
[2] Department of Physics and Mathematics Education and Informatics of the Olexander Dovzhenko Hlukhiv National Pedagogical University, Kyievo-Moskovska str. 24, Hlukhiv, Ukraine

ABSTRACT

The paper substantiates the use for Hue, Saturation, Value color model to determine the color coordinates of flax fiber, based on it proposed a new device for determining the color indicators of flax fiber using of arduino-compatible systems, outlines the principle of its operation and design features, and tests of the developed device using reference samples of flax fiber.

KEYWORDS

Flax fiber; Algorithm; Color group; Arduino; Device.

INTRODUCTION

To determine the parameters of scutched flax fiber in Ukraine use the methods set out in State Standard 4015-2001 [1], which determines the fiber number by the sum of the scores of such indicators as handful length, tensile load, flexibility and color group. To determine the color group of flax, each of the 30 handfuls previously prepared according to the method defined by the standard should be assigned the number of the group to which it is closest in color. There are 4 color groups in total. The first group of colors corresponds to a brown, green, bast-like color of a handful of flax; the second group - yellow, yellow with shades, gray and dark gray with shades; the third is gray and dark gray; the fourth is light gray.

During the visual examination, the main analyzers are the organs of vision, ie the eyes, whose light receptors are excited by waves of light rays in the visible region of the spectrum. However, the unequal perception of the color components by the eye leads to the fact that the brightness of different parts of the visible spectrum is perceived differently. This can distort the results during the visual assessment. The perception of color depends on subjective factors: the physiological characteristics of the expert, his age, qualifications, color vision disorders, the purpose of the study. All methods developed so far to determine the color of the fiber are based on organoleptic evaluation, so they do not provide the necessary accuracy of analysis, which directly depends on the spectral sensitivity of the visual organs and the accuracy of their determination. In addition, based on the obtained values of the intensity of light reflected from the surface of the test sample, it is possible to determine both the degree of retting of the stems, and the rate of separation of the fiber.

To determine the color indicators of an object, raw material or material, its image must be somehow recorded for further analysis or analyzed immediately in real time. Existing devices use either computer technology with a webcam, scanner, camcorder, digital camera connected to it, or electronic signal processing circuits to which photosensors are connected. In the second case, the measurement results depend on the characteristics of the photosensor and lighting. If the level of illumination of the sample is insufficient, the base colors are shifted to the corresponding dark shades, if on the contrary - the base colors are shifted to light shades, and then to white. The use of photosensors, such as photodiodes, phototransistors, color and light sensors, allows them to be used in relatively small devices, which provides autonomy and mobility of the measuring system.

Thus, the actual and expedient task is to develop instrumental methods for assessing color as one of the indicators of the quality of flax fiber. The use of these methods in practice will increase the objectivity of quality assessment and reduce the time for research.

Unlike cotton, flax fibers do not have objective standards for testing or classification. Flax fibers are

* **Corresponding author:** Tolmachov V., e-mail: tvs-@ukr.net

Received July 3, 2022; accepted January 9, 2023

evaluated and graded within countries or individual companies, but only one test method (ISO 2370 for flax fiber fineness) is recognized on an international level. Marketing of flax fiber is generally based on subjective methods of evaluation, but strong interest has existed for developing objective standards such as those that exist for cotton [2].

To study the properties of flax fiber, gas–liquid chromatographic methods, 13C CPMAS NMR spectrometry, histochemistry, electron microscopy and UV absorption microspectrophotometry are used to assist in determining the structure and composition of these cell walls in relation to quality and utilization [3]. But Saeideh G. [4] was shown that the spectrophotometer geometry influences the color coordinates of the samples.

Color is an important factor in the evaluation of functionality of many products, but especially of textile industry ones. Color evaluation can be done visually or using specialized test instruments such as colorimeters or spectrometers, therefore a high accuracy of measurements must be achieved. Standards describe different procedures and testing techniques depending on the product type and the quality level required by the customer [5].

Color is one quality parameter that is very dependent upon retting methods, and new procedures such as enzyme-retting greatly expand the color choices. To determine color values, use the well accepted CIElab method [6]. It is generally known that scientific analysis and interpretation of natural dyeing processes is essential to demonstrate the economic feasibility of dyeing flax and other natural fibers with environmentally benign natural colorants [7].

Color measurements are made of various kinds of flax retted by dew, water or enzymes. Two sets of samples are analyzed under different conditions using different spectrophotometers and by reflectance in the visible and near infrared spectral regions. Sample set one consists of 55 samples of various flax types retted by traditional dew and water methods and various experimental enzyme retted samples. Means and standard deviations of CIELAB color values for each of the classes are displayed as spheroid plots. The enzyme retted fiber flax class forms a separate group that is substantially lighter and slightly yellower than dew retted flax [8].

Weisnerova D. and Weisner I. [9] applied computer image analysis to group together flax cultivars (Linum usitatissimum L.) according to their similarity in commercially important dry seed traits. Both the seed shape and seed-colour traits were tested on 53 cultivars from world germplasm collections. Four shape traits (Area, Perimeter, MeanChord, and MinFeret) and three color traits (L*, a*, b* calculated from original RGB color channels as CIE color space coordinates) were computer extracted from digital images of 62349 seeds with 1200 seeds per cultivar in average. Cultivar clustering was generated by two independent methods of multivariate analysis.

Epps H.H., Akin D.E., Foulk, J.A., Dodd R.B. [10] use twenty-seven samples representing variations of retted flax fibers are analyzed using a color spectrophotometer and CIELAB models. Variables included enzyme or dew retting, fiber or seed flax, enzyme and chelator concentrations, and sequential cleaning steps. In addition to differences in color with enzyme or dew retting, the variables involved in enzyme retting also contribute to differences in the lightness, redness-greenness, and yellowness-blueness of the resulting fibers. Results indicate that objective color measurements and color standards can define important fiber properties in order to tailor raw materials for specific industrial applications.

Jablonský M. et al. [11] use a method of objective fiber identification using color vectors of a microscan from stained fiber digital photography. The objective micro-colorimetric method, using RGB (red, green, blue) vectors with discriminatory analysis, reduced the number of stains to 1; requires no morphological information; and the discriminatory power (dp,) of this approach is up to 95 to 100% of correctly identified unknown samples with one color vector R or B.

Using optical arrays based on chemoresponsive colorants (dyes and nanoporous pigments) probe the chemical reactivity of analytes, rather than their physical properties. Colorimetric sensor arrays have demonstrated excellent potential for complex systems analysis in real-world applications and provide a novel method for discrimination among closely similar complex mixtures (Askim J. R. et al. [12]).

Bergfjord C. and Holst B. [13] presents a simple procedure for identifying the textile bast fibers. The procedure is based on measuring the fibrillar orientation with polarised light microscopy and detecting the presence of calcium oxalate crystals (CaC2O4) in association with the fibers. To demonstrate the procedure, a series of fibre samples of flax, nettle, ramie, hemp and jute were investigated. An advantage of the procedure is that only a small amount of fiber material is needed.

Hinsch E. and Robinson S. [14] use a method of testing for colorfastness to light was developed. Additionally, the colorfastness to light testing method developed using the L-2 Blue Wool Standard and QUV Accelerated Weathering Machine is a viable alternative to current standard colorfastness to light testing methods.

It should be noted that digital image colorimetry (DIC) on smartphone is regarded as a powerful, fast and low-cost analysis method to measure target analyte with color changes of digital image obtained by the built-in camera [15].

To process the results of the study, we used the methodology of comparing means using statistical analysis is illustrated with solid examples in the textile field in the work of K. F. Choi [16].

METHODS

To describe the characteristics of color in practice use different color models, which include RGB, HSL, CIELAB, HSV and others. These models represent color indicators in the form of corresponding coordinates. The RGB model has been adopted as a standard by the International Commission on Lighting. Based on it, the color coordinates of any radiation given by its spectral composition can be calculated, and the coordinates of any color in another color system, the reference colors of which are set in the RGB system, can be calculated.

The master model for almost all color models used in technical fields is CIEXYZ. The XYZ color is set as follows:

$$X = \int_{380}^{780} I(\lambda)\bar{x}(\lambda)d\lambda$$
$$Y = \int_{380}^{780} I(\lambda)\bar{y}(\lambda)d\lambda \quad (1)$$
$$Z = \int_{380}^{780} I(\lambda)\bar{z}(\lambda)d\lambda$$

where $I(\lambda)$ is the spectral density of any energy photometric quantity, such as radiation flux, energy brightness, etc., in absolute or relative terms.

Like the CIEXYZ space it derives from, CIELAB colorspace is a device-independent, "standard observer" model. The colors it defines are not relative to any particular device such as a computer monitor or a printer, but instead relate to the CIE standard observer which is an averaging of the results of color matching experiments under laboratory conditions. The three coordinates of CIELAB represent the lightness of the color (*L** = 0 yields black and *L** = 100 indicates diffuse white; specular white may be higher), its position between red and green (*a**, where negative values indicate green and positive values indicate red) and its position between yellow and blue (*b**, where negative values indicate blue and positive values indicate yellow).

CIECAM02 is the color appearance model. The two major parts of the model are its chromatic adaptation transform, CIECAT02, and its equations for calculating mathematical correlates for the six technically defined dimensions of color appearance: brightness (luminance), lightness, colorfulness, chroma, saturation, and hue.

To describe the color coordinates of the flax fiber, the HSB model was chosen compatible with the standards of organoleptic evaluation of fiber quality. HSB (hue, saturation, brightness) are alternative representations of the RGB color model, designed in the 1970s by computer graphics.

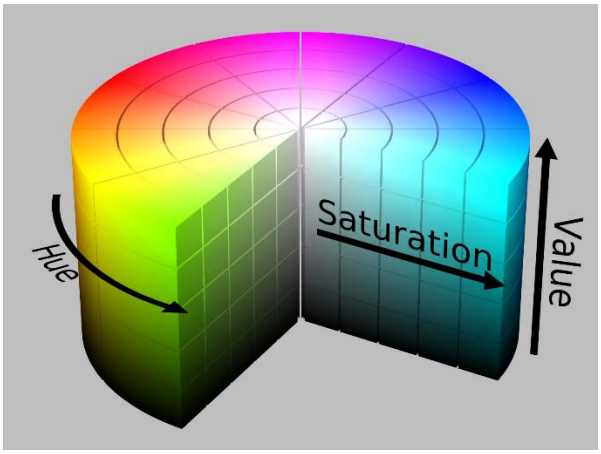

Figure 1. Color distribution scheme in the HSV model (for Hue, Saturation, Value; also known as HSB, for Hue, Saturation, Brightness).

This color model is the easiest to understand. In addition, it is equally used for both additive and subtractive colors. It agrees well with human perception, because the color tone is equivalent to the wavelength of light, the saturation is the intensity of the wave, and the brightness is the amount of light. The HSB model diagram is shown in fig. 1. It can be used for both additive and substrate colors. This model is named after the first letters of English words: Hue - color tone, Saturation - saturation, Brightness - brightness. It agrees well with human perception, because the color tone is equivalent to the wavelength of light, Saturation - the intensity of the wave, and Brightness - the amount of light.

The value of the Hue is expressed in the angle of rotation of the radius vector *N*. Red corresponds to 0°, yellow - 60°, green - 120°, blue - 180°, blue - 240°, purple - 300°. The Saturation value is described as the length of the radius vector. The less saturated the color, the closer to the center of the circle is the coordinate. The center of the circle corresponds to black. Saturation is measured as a percentage: the minimum Saturation is 0, the maximum is 100.

The HSB system is abstract. There is no direct procedure for measuring Hue and Saturation. According to any method, the red, blue and green components are first measured, which are then converted into HSB coordinates. The equation is used to convert from RGB to HSV

$$V = \max(R,G,B);\ v = \min(R,G,B);$$
$$S = \begin{cases} 0; if\ V = 0 \\ (V - v)/V \end{cases};$$
$$C_r = \frac{(V-R)}{(V-v)};\ C_g = \frac{(V-G)}{(V-v)};\ C_b = \frac{(V-B)}{(V-v)}; \quad (2)$$
$$H = \frac{\pi}{3} \cdot \begin{cases} C_b - C_g; if\ R = V \\ 2 + C_r - C_b; if\ G = V \\ 4 + C_g - C_r; if\ B = V \end{cases}$$

where $C = (c_1, c_2, c_3)$ – the sensation of radiation given by the vector of its coordinates in the physiological color system. Signals of photoreceptors c1, c2, c3 represent radiation coordinates in the physiological color system. If we denote the spectral sensitivities of the photoreceptors of the eye with maxima in the zone of long, medium and short wavelengths of the visible range by l(λ), m(λ) and s(λ), then the radiation with the spectral composition c(λ) that excites the corresponding photoreceptors and determines the color of radiation, described by the formula

$$c_1 = \int c(\lambda) \cdot l(\lambda) d\lambda$$
$$c_2 = \int c(\lambda) \cdot m(\lambda) d\lambda \quad (3)$$
$$c_3 = \int c(\lambda) \cdot s(\lambda) d\lambda$$

Based on the analysis of standard methods for determining the color properties of flax fibers and device designs to determine these properties, a digital stand-alone device was created to determine the color of the test specimen, calculate color coordinates in RGB and HSB formats, and determine color uniformity and whiteness of the test material. To determine the color of flax fiber, a device DDCIFF-1 was developed (Fig. 2). The principle of operation of the developed device is based on measuring with the help of a photo sensor the intensity of the basic components of light reflected from the surface of the test material in the RGB system.

The device consists of a plastic housing 1, inside which are the electronic circuit, digital display 4, optical unit and light source. On the reverse side is the control panel 5. On top under the protective cover 3 is the measuring chamber 2.

To determine the color index, it is necessary to tightly fill the measuring chamber 2 with a uniform layer of fiber weighing 20 g and a length of at least 85 mm, following the parallel arrangement of the fibers (Fig. 3).

The normalized mass, the length of the fiber sample and the number of repeats of measurements were determined by research results. To obtain objective measurement results, it is necessary to prepare 3 fiber samples and analyze each sample on both sides and in three zones: apical, middle, basal. The final measurement result is the average value for each color coordinate. The measuring chamber with the enclosed sample is covered with a protective cover 3. Then you need to turn on the device and using the buttons on the control panel 5, select the desired mode and perform measurements. The digital display will show the color coordinates in HSB format, and if necessary, using the control panel, you can display the digital color coordinates in RGB format (Fig. 4). The scheme of the device DDCIFF-1 for measurement of indicators of color of flax fiber (DDCIFF-1) is presented in Fig. 5.

The device is implemented on arduino-compatible systems (Arduino/Genuino Nano) (Fig. 6). The device uses special RGB LEDs with fixed spectral characteristics to illuminate the surface of the test sample.

The Arduino Nano is Arduino's classic breadboard friendly designed board with the smallest dimensions. The Arduino Nano comes with pin headers that allow for an easy attachment onto a breadboard and features a Mini-B USB connector. The ATMega328 CPU runs with 16 MHz and features 32 KB of Flash Memory (of which 2 KB used by bootloader). With a length of 45 mm and a width of 18 mm the Nano is Arduino's smallest board and weighs only 7 grams. The Nano is made for breadboard use and features soldered headers for all pins, allowing to attach the board easily on any breadboard. Built-in LED Pin - 13. Digital I/O Pins - 14. Analog input pins - 8. PWM pins - 6. I/O Voltage 5V. Input voltage (nominal) 7-12V. DC Current per I/O Pin 20 mA.

Character display LCD0802A has 2 lines of 8 characters; it is possible to display a total of 16 letters, numbers or symbols. Dimensions 58mm x 32mm x 13mm. Weight: 25g. Based on SPLC78D controller with 14 pins.

The device uses 5050 RGB BIN1 LEDs. For red diode LZ-5054BIN1Red TOP LED (5050) absolute Maximum Ratings (T_a=25 °C). Power Dissipation *PD* = 80 mW. Forward Current (DC) I_F =30 mA. Peak Forward Current I_{FP} =100 mA. Operation Temperature T_{opr} = -40~ +95 °C. Storage Temperature T_{stg} = -40 ~ +100 °C. The electrical and thermal characteristics of the green and blue diodes are similar. Some optical characteristics are shown in Figure 7.

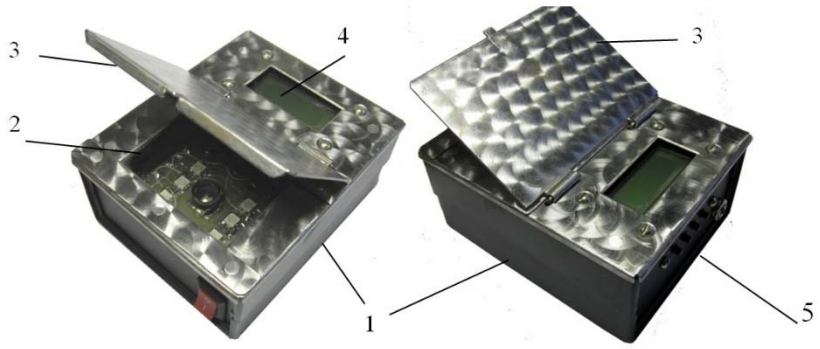

Figure 2. The device DDCIFF-1: 1 - the case; 2 - measuring chamber; 3 - protective cover; 4 - digital display; 5 - control panel.

Figure 3. Placement of the sample in the measuring chamber of the device DDCIFF-1.

Figure 4. The digital display will show the color coordinates in HSB format, and if necessary, using the control panel, you can display the digital color coordinates in RGB format.

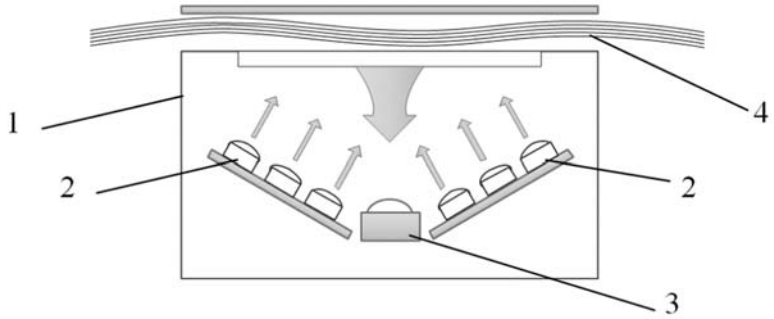

Figure 5. Scheme of the device DDCIFF-1: 1 - the case; 2 - RGB LEDs; 3 - photo sensor (photoresistor); 4 - research material.

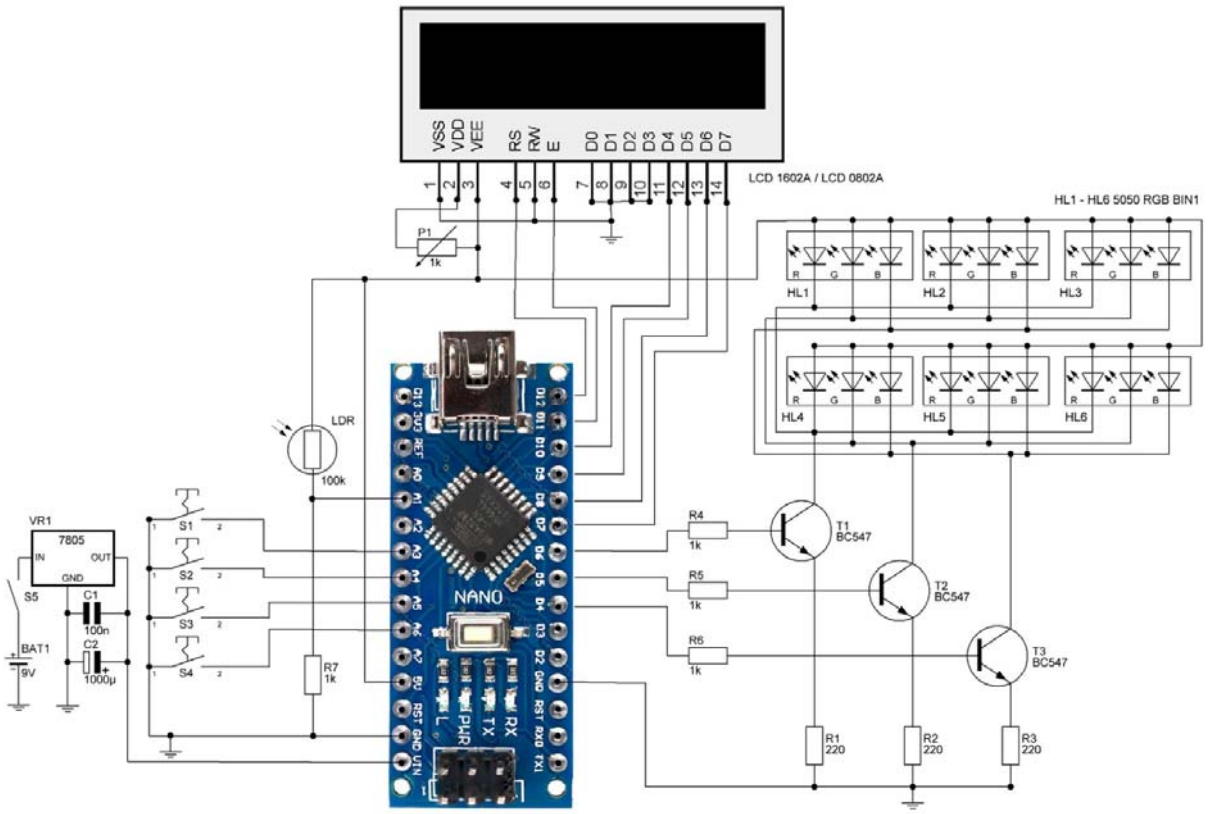

Figure 6. Electrical schematic diagram of DDCIFF-1.

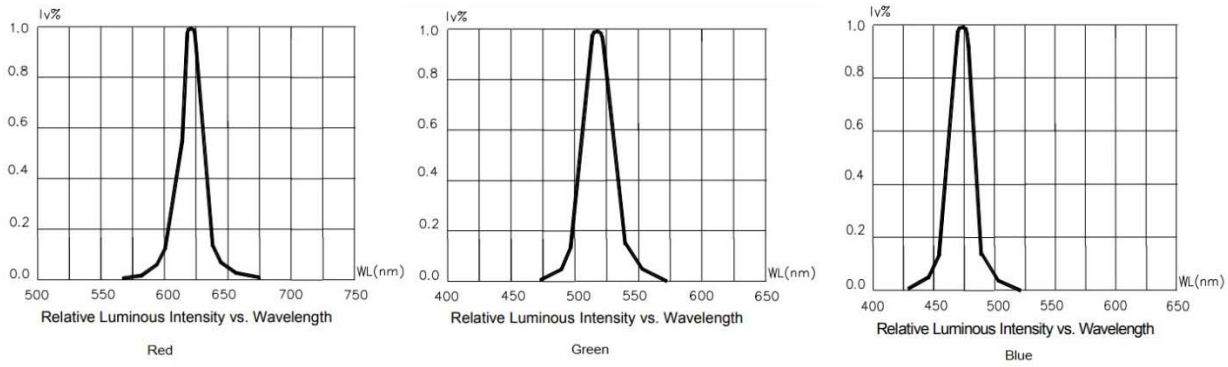

Figure 7. Optical Characteristics Curves – Relative Luminous Intensity vs. Wavelength (Ta=25°C).

The signal of the photoresistor, which sequentially measures the intensity of red, green and blue light reflected from the test material, is fed to the ADC input of the microcontroller, where it is processed according to the developed algorithm and output to a digital indicator. Buttons S1 - S4 are used to select the operating modes of the device.

Special RGB LEDs with fixed spectral characteristics are used in the device to illuminate the surface of the sample under study. Enabling one or another color to illuminate the sample and analyzing the illumination of the photosensor is performed by the microcontroller. Light fluxes of red, green and blue colors, having reflected from the surface of the sample, alternately fall on the photoresistor, which changes its resistance depending on the intensity of the light flux. For the convenience of calculations, the results of measuring the intensity of basic colors are reduced to a single-byte value with limits of 0-255, using the equations

$$R = R'\frac{255}{k};\ G = G'\frac{255}{k};\ B = B'\frac{255}{k} \qquad (4)$$

where R' – red light intensity, G' – green light intensity, B' – blue light intensity, R – single-byte value of red light intensity, G – single-byte value of green light intensity, B – single-byte value of blue light

intensity, *k* is the maximum digital value obtained after analog-digital conversion.

When working in RGB mode, the indicator displays the values of the intensities of red, green and blue colors, as well as calculated for (4) the intensity of reflected light, taking into account the relationship between the intensity of base colors according to television standards

$$Y = 0{,}299 \cdot R + 0{,}587 \cdot G + 0{,}112 \cdot B \qquad (5)$$

where *Y* represents its luminance signal, *R* – red light intensity, *G* – green light intensity, *B* – blue light intensity.

A standard algorithm is used to convert the obtained color coordinates from RGB to HSB in the developed device [17]. In the HSB mode, the value of Hue H, Saturation S and Brightness B is displayed on the indicator. In accordance with DSTU 4015-2001, the color of the fiber is divided into four groups. For convenience, color groups that contain multiple colors in their description have been divided into subgroups. The result is a table. 1, on the basis of which the list of colors used in the evaluation of flax fiber is determined.

Analysis of table. 1 show that the cylinder, which represents the color model HSB, for our purpose can be divided into parts (Fig. 1). There are zones in which the color saturation varies from minimum to maximum value, ie from zone S0 to S3, as well as three zones of Brightness - respectively B0, B1, B2. A similar assessment of visual parameters is used in zonal spectroscopy methods. These methods provide the possibility of differentiation of the studied samples and automation of the processing of the obtained data, based on the spectral information obtained from the object of study.

The developed device uses three spectral zones in which the study of the studied material is carried out. These spectral bands of radiation are: red with a wavelength of λ_r = 700 nm, green with a wavelength of λ_g = 546 nm and blue with a wavelength of λ_b = 436 nm.

Zonal spectroscopy methods can be attributed to the so-called computer qualimetry, because they are characterized by high speed and efficiency of information. As a result of zonal spectroscopy of flax fiber, you can get spectral prints of the test material formed in the N-dimensional space, where N is the number of spectral zones in which the sample is studied. To describe such data, petal diagrams are used, with which you can visually compare the samples with each other or find a degree of similarity of these samples, using (6)

$$M = \sqrt{(R_v - R_r)^2 + (G_v - G_r)^2 + (B_v - B_r)^2}$$
$$P = 100 - \frac{M}{K} \cdot 100, \qquad (6)$$

where *M* is the degree of similarity of the samples; *K* is the reading of the instrument that characterizes the maximum value of the difference between the samples, *P* – similarity of samples in %, R_r, G_r, B_r – calculated values of color coordinates, R_v, G_v, B_v - measured values of color coordinates.

To determine the sensitivity of the developed device, standards from the color catalog were used, where different shades of basic colors were selected, as well as standards of shades of gray (Fig. 8) with predefined coordinates (Table 1). Since a ten-bit analog-to-digital converter is used in the proposed device, the maximum value of voltage conversion to digital form will be equal to 1024. It is known that monochromatic colors in the RGB system are calculated for a maximum value of 255, therefore, for the convenience of further calculations and presentation of measurement results, automatic conversion is provided in the device values according to the formula

$$R_r, G_r, B_r = R_v, G_v, B_v \cdot \frac{255}{1024}, \qquad (7)$$

where R_r, G_r, B_r – calculated values of color coordinates, R_v, G_v, B_v - measured values of color coordinates.

After measuring of the reference samples, a summary table of results was obtained (Table 2). Equation (7) is used to analyze the intensity of reflected light. You can make sure that the device captures different intensities of reflected light and clearly distinguishes the shades of the selected standards.

According to the description, the color of the fourth standard corresponds to gray, the color of standards 1-3 according to the description can be attributed to light gray, 5 and 6 to dark gray, and the seventh to black. The results of analysis of measurements of selected standards using the developed DDCIFF-1 device in HSB format are shown in the Table 3.

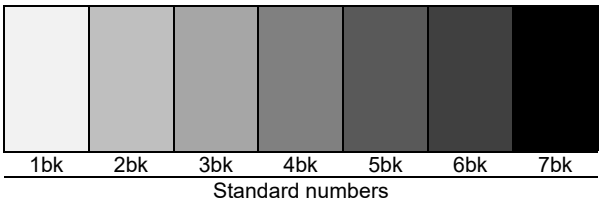

Figure 8. The palette of shades of gray of seven experimental standards for determining the parameters of the device.

Table 1. Color coordinates of selected standards.

Base color	Designation of color standards	Color coordinates of standards		
		X	*Y*	*Z*
Light gray	1bk	73,08	74,55	84,41
	2bk	68,05	69,36	80,47
Gray	3bk	49,02	49,85	58,25
	4bk	34,95	35,72	41,68
	5bk	22,51	22,81	26,78
Dark gray	6bk	8,29	8,46	10,08
	7bk	2,14	2,17	2,75

Table 2. Measurement results of selected standards.

The results of the experiment	Designation of color standards						
	1bk	**2bk**	**3bk**	**4bk**	**5bk**	**6bk**	**7bk**
Average value *R*	221,6	215,5	166,6	126,5	86,4	32,6	43,3
Average value *G*	222,0	216,0	178,6	140,0	100,4	37,9	28,4
Average value *B*	217,9	207,8	163,0	118,1	73,8	6,3	0
The average square deviation, σ_R	0,49	0,50	0,49	0,50	0,49	0,49	0,65
The average square deviation, σ_G	0,59	0,59	0,60	0,59	0,60	0,60	0,59
Standard deviation, σ_B	0,65	0,70	0,65	0,56	0,69	0,70	0,02
$\pm m_R$	0,30	0,31	0,30	0,31	0,30	0,30	0,34
$\pm m_G$	0,37	0,37	0,37	0,37	0,37	0,37	0,37
$\pm m_B$	0,40	0,44	0,40	0,35	0,43	0,44	0,10
C (coefficient of variation) *R*	0,23	0,24	0,31	0,42	0,60	1,58	1,57
C (coefficient of variation) *G*	0,28	0,29	0,35	0,44	0,63	1,67	2,19
C (coefficient of variation) *B*	0,26	0,30	0,33	0,37	0,62	1,48	2,07

Table 3. Results of analysis of measurements using the developed DDCIFF-1 instrument in HSB format.

The results of the experiment	Designation of color standards						
	1bk	**2bk**	**3bk**	**4bk**	**5bk**	**6bk**	**7bk**
Average value *H*	66,5	64,8	105,3	97,0	91,7	69,7	39,6
Average value *S*	2,0	4,1	8,8	16,0	26,7	82,9	100,0
Average value *B*	87,0	84,9	71,0	55,0	39,5	16,7	15,0
σ_H	10,05	9,31	2,05	1,61	1,79	1,10	1,11
σ_S	0,63	0,54	0,40	0,00	1,10	1,14	0,00
σ_B	0,00	0,30	0,00	0,00	0,50	0,00	0,46
$\pm m_H$	6,23	5,77	1,27	1,00	1,11	0,68	0,69
$\pm m_S$	0,39	0,33	0,25	0,00	0,68	0,70	0,00
$\pm m_B$	0,00	0,19	0,00	0,00	0,31	0,00	0,28

From the obtained results (Table 3), it is possible to preliminarily determine the limits corresponding to the brightness zones B_0, B_1, B_2, which include the numerical ranges describing black and dark gray color, when B_0 = 0-50, gray color - B_1 = 51 -70 and light gray – B_2 = 71-100.

In order to determine the sensitivity of the device to colors, 3 groups of standards with 7 shades of the base color in each group were selected. For convenience, they were labeled R_1–R_7, G_1–G_7, B_1–B_7, respectively. As a result of research with color standards, the average values of the color coordinates in the *RGB* format and the *HSB* format were determined, which made it possible to place the standards in the *SB*-space without taking into account the H coordinate, which is responsible for the color.

The point diagram (Fig. 10) shows how the standards were located, taking into account the brightness and color saturation. If this space is conditionally divided into four parts, then you can imagine the color and describe it. For example, if we take light standards R_1, G_1, B_1, and then they are in the upper left part of the SB space, and dark R_7, G_7, B_7 - in the lower right part. Based on the obtained data, the intensity of light reflected from the surface of the standards was calculated.

The summary results of the calculations are graphically displayed in Fig. 11. Analysis of Fig. 11 shows that in cases where it is not necessary to take into account the color components of the sample, the degree of whiteness can be determined with the help of the developed device.

When analyzing the data, it should also be taken into account that the standards have a uniform color and glossy coating, and the investigated samples of the flax fiber are a set of parallel fibers, so the light falling on their surface will be reflected randomly. As a result, the intensity of reflected light in basic colors will be much lower compared to standards. In addition, the color of the fibers may differ along the entire length, or may be approximately the same, which will characterize the degree of heterogeneity of the sample in terms of color.

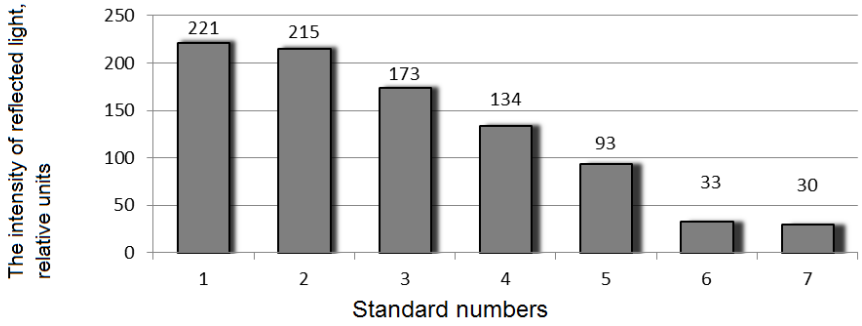

Figure 9. Shade diagram of seven experimental standards for evaluating the sensitivity of the developed device.

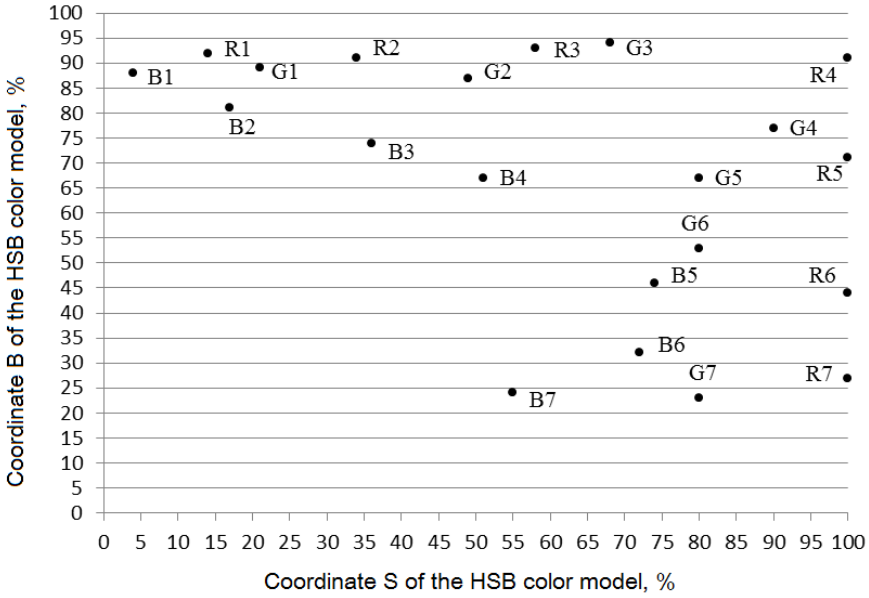

Figure 10. Distribution of selected standards in the SB-space.

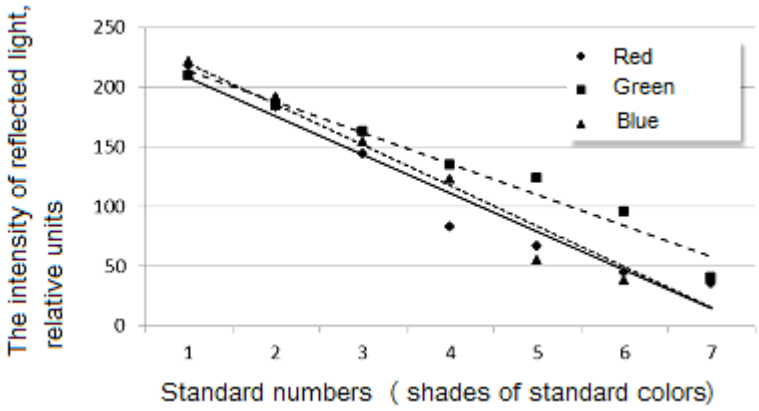

Figure 11. Dependence of the intensity of the reflected light on the brightness of the shade of the selected standard.

Thus, as a result of the conducted experiments, it was established that the developed DDCIFF-1 device is sensitive to the color, shades of color, and the degree of whiteness of the samples under study.

To study the color indicators using the developed device, it is necessary to determine the mass of the sample. For this, a homogeneous in color sample No. 6 was chosen. The length of the staple was equal to 85 mm, and the mass of the formed weights was 0.5-3.0 g, with an increase in mass by 0.5 g. The obtained result (Fig. 12) indicates that an increase in the mass of the sample to 1.5 g or more contributes to the stabilization of the obtained data according to the basic green color.

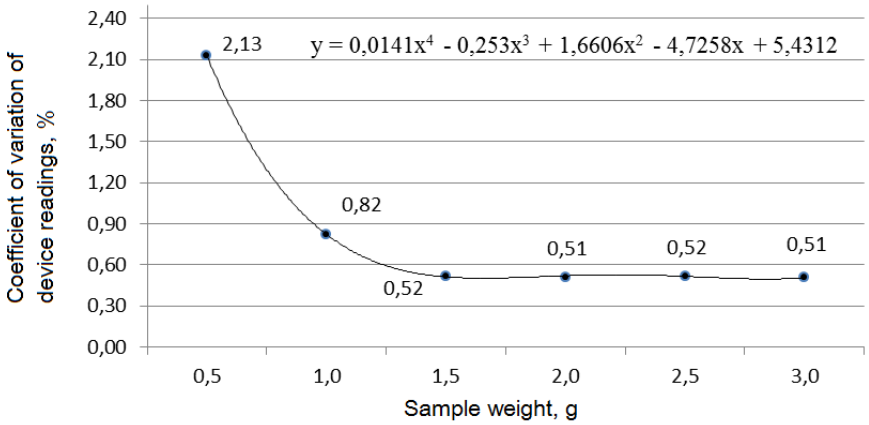

Figure 12. Dependence of the intensity of the reflected light on the brightness of the shade of the selected standard.

Table 4. Determination of the minimum number of repetitions during the measuring the color indicators of flax fiber.

The results of the experiment	Fiber sample number		
	1	2	3
Average value R	125,40	116,20	121,50
Average value G	119,56	108,50	113,31
Average value B	100,32	90,21	87,81
σ^2_R	0,49	0,87	2,16
σ^2_G	0,59	0,72	3,52
σ^2_B	0,96	1,20	2,64
Student's criterion	2,26		
Permissible relative error, %	5		
Coefficient of variation C_R, %	0,41	0,79	1,87
Coefficient of variation C_G, %	0,52	0,70	3,27
Coefficient of variation C_B, %	1,01	1,41	3,16
Number of experiments, R	1,03	1,13	1,74
Number of experiments, G	1,05	1,10	3,00
Number of experiments, B	1,20	1,40	2,91
Total number of experiments	3		

Proof of this is the low coefficient of variation, which is 0.51-0.52%.

The analysis of the research results shows that an increase in the mass of the sample from 0.5 to 1.5 g ensures a decrease in the coefficient of variation of the measurement result from 2.13% to 0.52%. A further increase in the mass of the tested sample from 1.5 to 3.0 g does not affect the coefficient of variation; it remains at the level of 0.51-0.52%.

This is explained by the fact that when the mass of the sample is less than 1.5 g, the window of the measuring chamber is incompletely filled. This leads to partial reflection of radiation from the sample and the surface of the protective cover of the camera. This circumstance causes an increase in the coefficient of variation of the measurement results and significant inaccuracies of the obtained result. A sample with a minimum mass of 1.5 g and a length of 85 mm completely and evenly fills the window of the measuring chamber. However, to obtain stable measurement results, it is recommended to prepare a sample of 2.0 g.

In order to objectively assess the fiber color indicator during work with the developed device, it is necessary to determine the number of repetitions. Using the methods of mathematical statistics and a known relative error, it is possible to calculate the number of experiments according to the existing methodology by formula (8):

$$n = \frac{t^2\sigma^2}{\varepsilon^2} + 1. \quad (8)$$

A series of studies was conducted to determine the required number of experiments *n*. For this, 3 fiber samples were prepared with a tenfold repeatability. In each repetition, color coordinates were determined in RGB format for the apical, middle, and basal parts. The color coordinates were first determined on one side, and then the sample was turned to the other side relative to the longitudinal axis of rotation and the coordinates were again determined in three places. The obtained experimental material was mathematically processed and with a given relative error of the experiment of 5%, the required number of repetitions was calculated (Table 4).

The obtained results (Table 5) show that the calculated values of the number of measurements of the intensity of each of the basic components of light are different and are in the range of 1.03-3.00, therefore, to ensure the accuracy of the

measurements with an error of no more than 5%, we choose the maximum value from by rounding it to a whole number.

Thus, to determine the color coordinates using the developed DDCIFF-1 device, it is necessary to prepare at least three fiber samples weighing more than 20 g, each sample should be analyzed from both sides and in three zones: apical, middle, basal. The average value for each coordinate is taken as the measurement result.

The use of the developed device DDCIFF-1 for the purpose of analysis and quality control of raw materials fits well into the concept of qualimetry and its modern directions.

To determine the sensitivity of the developed device, standards from the color catalog were used, where different shades of base colors were selected, as well as standards of shades of gray with predefined coordinates. Since the proposed device uses a ten-bit analog-to-digital converter, the maximum value of voltage conversion to digital form will be 1024. It is known that monochromatic colors in the RGB system are designed for a maximum value of 255, so for convenience of further calculations values.

Table 5. Color groups and their division into subgroups.

Color group	Color subgroup	Color description
1	a	Brown
	b	Green
2	a	Yellow
	b	Yellow with hints
	c	Gray with hints
	d	Dark gray with hints
3	a	Gray
	b	Dark grey
4	a	Light gray

The methods outlined in DSTU 4015-2001 are used to determine the parameters of felted flax fiber. This standard applies to long staple fiber intended for the textile industry and obtained in factory and non-factory conditions. The quality of beaten flax of each number must correspond to standard samples compiled and approved according to the established procedure. Standard samples are checked by the method of instrumental evaluation of the quality of beaten flax depending on the color group. Samples for research are selected according to the method described in the standard. If the actual moisture content of the beaten flax is lower than 9%, the lot is accepted by the actual weight, taking into account the content of pith. Acceptance of beaten flax in terms of quality is carried out by organoleptic comparison of it with standard samples. For this, 5% packs are selected and unpacked from each batch of beaten flax, but not less than three packs. In case of inconsistency of the quality of the beaten flax with the standard sample and when resolving the issue of complaints, an instrumental assessment is used and the number of the flax is set in accordance with Tables 1 and 4 of DSTU 4015-2001 [1].

For this, 15 balls are taken from those selected under this point. In the case of acceptance of beaten flax unpressed, 15 balls are taken from a batch weighing up to one ton, and from a batch of larger weight - another 15 balls for each new ton started. Then 30 handfuls are selected from 15 balls - 2 from each ball. To determine the color group of beaten flax, it is necessary to assign the number of the group to which it is closest in color to each of the 30 handfuls prepared earlier (Table 1). The result of the test is taken as the average arithmetic value of the color group number from thirty determinations, calculated to the second decimal place with subsequent rounding to the first decimal place.

As mentioned above, when measuring color indicators and determining the color group of a fiber, it is necessary to determine the limit values of the S and B coordinates of the HSB color model, since the fiber reflects less light than the previously studied color standards. During the DDCIFF-1 tests, the S and B coordinate values of the HSB color model were determined because the fiber reflects less light than the color standards previously studied. During the research, standard samples (standards) of long typed fiber were analyzed, which correspond to the State Standard of Ukraine 4149: 2003 “Flax stock. Specifications”.

For our purpose, the cylinder that represents the HSB color model can be conditionally divided into parts (Fig. 13).

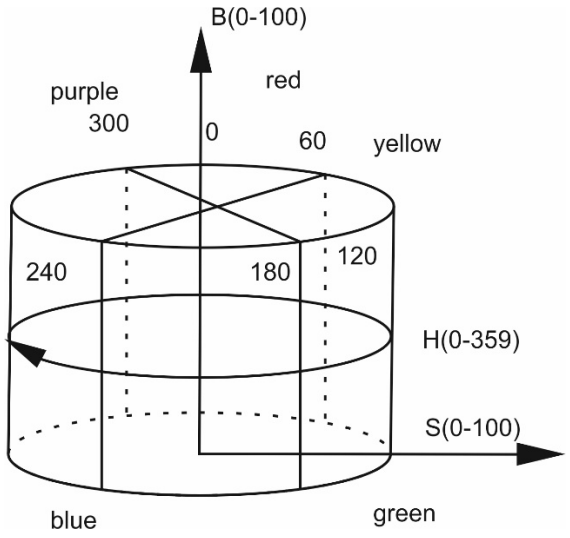

Figure 13. Division of the HSB color model into conventional parts by saturation and brightness.

There you can distinguish zones in which the color saturation varies from the minimum to the maximum value, that is, from the S_0 to S_3 zone, as well as three brightness zones - B_0, B_1, B_2, respectively.

Based on this, we get four conditional cylinders S_0, S_1, S_2, S_3, divided into three parts B_0, B_1, B_2. The color of the inner cylinder S_0 changes from black to white. Conditionally dividing it into three parts by brightness, we will get the following ranges: B_0 – color range that

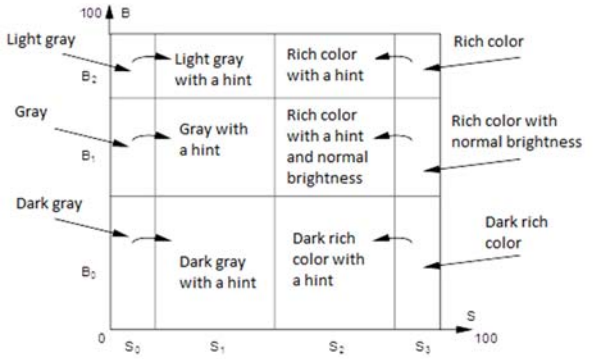

Figure 14. Distribution of shades and colors in the HSB color model.

includes black, dark and dark gray colors; B_1 – layer of colors with normal brightness; B_2 – a layer of bright colors and hints. According to these parts, the inner cylinder of the S_0 model can be divided by color into black and dark gray, gray and light gray zones.

Conventional cylindrical parts S_0, S_1, S_2, S_3 allow you to determine the saturation of the obtained color, that is, part S_0 is responsible for the color with its minimum saturation - gray color, S_1 - for gray with hints, S_2 - for color with hints, S_3 - for pure color. The H parameter is responsible for the color tone, which shows the angle relative to which the color is determined (Fig. 13).

Based on this, knowing the color coordinates of the sample under study in the HSB system, one can easily imagine which part of the cylinder these coordinates belong to and thereby objectively determine the color group.

If you take a section of a cylinder, you can fix groups of colors in certain places. Using the table 5, place the color group on the section of the color model according to DSTU 4015-2001 (Fig. 14).

A similar assessment of visual parameters is used in zonal spectroscopy methods. These methods provide the possibility of differentiating the studied samples and automating the processing of the received data, based on the spectral information obtained from the research object.

When measuring color indicators and determining the color group of a fiber, it is necessary to determine the limit values of the S and B coordinates of the HSB color model, since the fiber reflects less light than the previously studied color standards. During the research, samples of long woven fiber that correspond to GOST 2975-73 "Flax stock. Specifications" and DSTU 4149:2003 "Flax stock. Specifications".

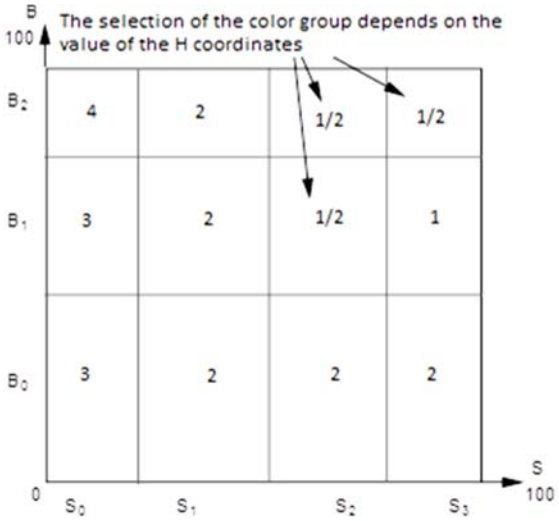

Figure 15. Distribution of color groups according to DSTU 4015-2001 in the *HSB* color model.

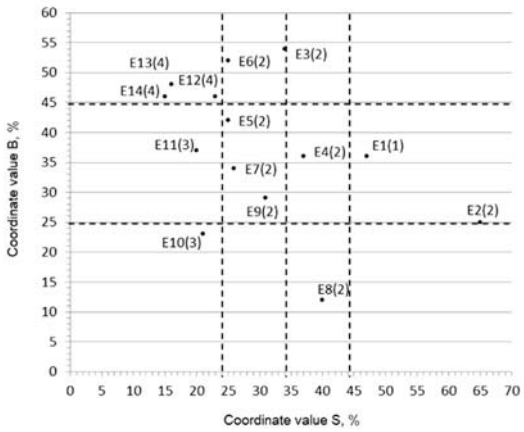

Figure 16. Distribution of standards in the SB color space (color group is indicated in parentheses).

As a result, we obtained the average values of the color coordinates and color group of those standards that are described as meeting the above standards. To identify the standards, they were designated as E_1-E_{14} (Table 6 and Table 7).

According to the obtained data, a scatter plot was constructed (Fig. 16), which shows the distribution of fiber samples by color groups and determined the boundaries of the distribution of the proposed color model space. The obtained limits have numerical values: S_0 = 0-24, S_1 = 24-34, S_2 = 34-44, S_3 = 44-100, B_0 = 0-25, B_1 = 25-45, B_2 = 45-100. The degree of reproducibility and precision of the proposed device was assessed according to current methods. The stability of the color measurement results was assessed using Schuhart maps.

Table 6. Description of color indicators of fiber standards.

Number of a standard	Defined color indicators						
	average values of color coordinates in RGB format			*average values of color coordinates in HSB format*			*color group*
	$\overline{X}_R$	$\overline{X}_G$	$\overline{X}_B$	$\overline{X}_H$	$\overline{X}_S$	$\overline{X}_B$	
E_1	91	76	48	39	47	36	1
E_2	63	40	22	26	65	25	2
E_3	137	116	90	33	34	54	2
E_4	91	81	57	41	37	36	2
E_5	106	96	79	44	25	42	2
E_6	133	125	100	45	25	52	2
E_7	87	82	64	47	26	34	2
E_8	30	26	18	40	40	12	2
E_9	74	69	51	47	31	29	2
E_{10}	58	58	46	60	21	23	3
E_{11}	95	91	76	47	20	37	3
E_{12}	117	109	90	41	23	46	4
E_{13}	122	122	103	60	16	48	4
E_{14}	118	117	100	57	15	46	4

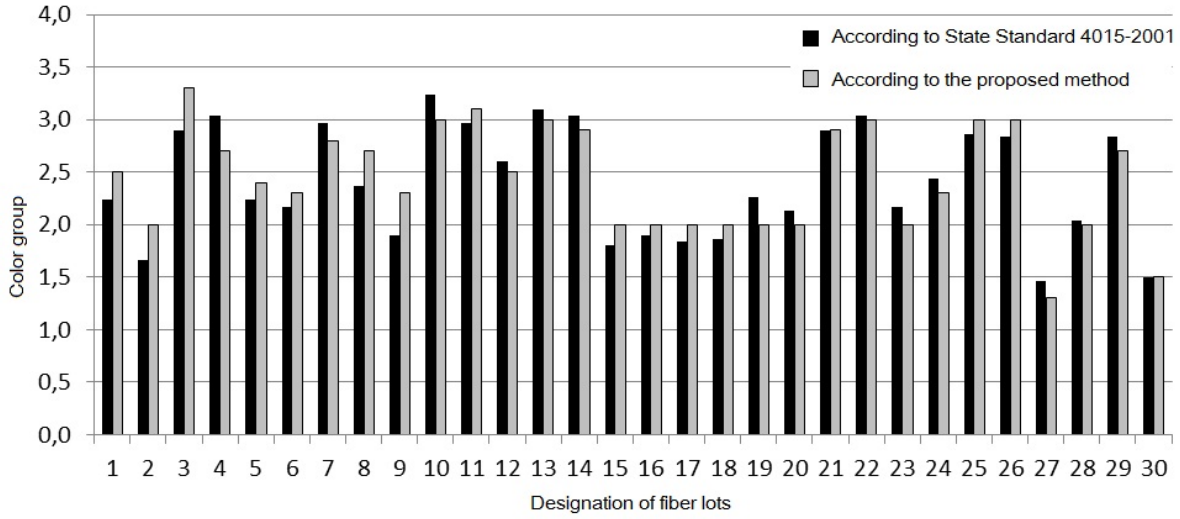

Figure 17. Color groups obtained by two methods.

When analyzing the data, it should also be borne in mind that the standards have a uniform color and glossy coating, and the studied samples of flax fiber are a set of parallel fibers, so the light falling on their surface will be reflected chaotically. As a result, the intensity of the reflected light in the base colors will be much lower compared to the standards. In addition, the color of the fibers may differ along the entire length, and may be approximately the same, which will characterize the degree of heterogeneity of the sample in color.

To determine the color coordinates using the developed device DDCIFF-1 it is necessary to prepare at least three samples of fiber weighing more than 20 g, each sample to be analyzed on both sides and in three zones: apical, middle, basal. The measurement result is the average value for each coordinate.

30 different batches were selected to determine the color heterogeneity of the fiber. From each batch took 10 samples of 20 g. Given that the average length of a handful of different batches of fibers ranges from 48.2 cm to 93.0 cm, each sample was conventionally divided into 10 parts and in each part measured by the developed device DDCIFF-1. Analyzing the obtained measurement results, we can conclude that the characteristic of color unevenness in length can be described by the coefficient of variation. The high value of the coefficient of variation indicates that the fiber was obtained from trusts, which was cured unevenly, which indicates the heterogeneity of physical and mechanical quality of the fiber.

Thus, as a result of the conducted experiments it was established that the developed device DDCIFF-1 is sensitive to color, color shades and the degree of whiteness of the studied samples. In order to verify the conformity of the boundaries defined for each color group, a comparative analysis was performed.

Table 7. Color coordinates of the selected samples, which were determined using the DDCIFF-1 device.

Batch number	Color	The results of the experiment												
		$\overline{X}_1$	$\overline{X}_2$	$\overline{X}_3$	$\overline{X}_4$	$\overline{X}_5$	$\overline{X}_6$	$\overline{X}_7$	$\overline{X}_8$	$\overline{X}_9$	$\overline{X}_{10}$	σ	$\pm m$	Coefficient of variation, c
1	2	3	4	5	6	7	8	9	10	11	12	13	14	15
1	R	111	111	103	111	112	108	107	110	111	112	2,69	1,67	2,59
	G	114	112	101	110	112	108	109	113	114	113	3,75	2,32	3,57
	B	90	88	81	83	85	86	84	83	84	83	2,53	1,57	3,15
2	R	97	99	93	97	96	95	94	92	93	98	2,24	1,39	2,48
	G	88	89	84	83	87	86	86	88	84	88	1,95	1,21	2,38
	B	67	69	65	70	66	69	65	68	65	67	1,76	1,09	2,76
3	R	117	106	111	109	107	114	114	116	118	114	3,95	2,45	3,70
	G	117	110	113	118	117	110	110	115	117	110	3,29	2,04	3,05
	B	97	90	93	89	95	97	96	90	90	90	3,10	1,92	3,53
4	R	94	105	98	99	100	93	98	99	95	105	3,88	2,40	4,15
	G	99	106	97	102	99	107	101	97	98	106	3,68	2,28	3,84
	B	77	85	76	77	75	79	81	85	77	84	3,67	2,27	4,85
5	R	118	115	112	118	118	114	113	115	114	111	2,40	1,49	2,20
	G	112	108	107	107	112	111	106	112	109	108	2,23	1,38	2,15
	B	88	85	84	84	84	83	85	89	88	87	2,00	1,24	2,46
6	R	97	103	94	101	98	103	98	103	98	93	3,46	2,14	3,69
	G	101	99	94	93	97	95	97	97	99	100	2,48	1,54	2,69
	B	78	77	71	75	74	76	70	70	76	75	2,75	1,70	3,91
7	R	94	93	100	95	97	94	101	95	98	92	2,84	1,76	3,13
	G	94	91	100	95	97	94	98	91	94	96	2,72	1,69	3,02
	B	75	71	78	78	74	72	71	77	74	78	2,71	1,68	3,82
8	R	115	104	107	107	110	113	116	113	106	105	4,15	2,57	3,99
	G	116	106	107	114	110	107	108	107	105	117	4,15	2,57	3,99
	B	94	83	84	85	94	94	85	92	95	86	4,71	2,92	5,56
9	R	102	104	101	100	104	104	100	101	104	104	1,69	1,04	1,73
	G	100	99	95	94	98	97	97	98	97	101	2,01	1,25	2,17
	B	78	75	71	75	74	78	77	79	74	79	2,49	1,54	3,45
10	R	101	102	101	102	102	101	100	103	102	101	0,81	0,50	0,84
	G	101	100	100	102	99	100	99	101	100	102	1,02	0,63	1,07
	B	81	79	77	80	80	79	82	82	82	80	1,54	0,95	2,02
11	R	112	109	110	108	109	110	113	108	113	108	1,90	1,18	1,82
	G	117	112	112	113	114	111	114	111	111	112	1,79	1,11	1,68
	B	96	89	90	96	92	92	94	95	88	91	2,72	1,69	3,11
12	R	58	56	63	57	64	65	58	61	59	59	2,93	1,82	5,15
	G	59	54	60	54	60	60	54	55	58	58	2,52	1,56	4,65
	B	45	41	48	41	41	45	48	48	45	41	2,93	1,82	6,98
13	R	77	89	79	80	78	82	82	88	78	77	4,12	2,56	5,37
	G	89	99	88	88	89	89	88	95	98	98	4,53	2,81	5,18
	B	76	85	76	76	80	85	80	76	77	85	3,83	2,37	5,07
14	R	95	103	95	100	98	96	95	95	101	95	2,87	1,78	3,10
	G	95	103	97	102	103	98	100	95	95	96	3,17	1,96	3,39
	B	76	85	82	82	82	85	76	76	75	85	3,98	2,47	5,22
15	R	91	90	85	84	90	89	90	86	85	91	2,62	1,63	3,14
	G	84	81	73	75	75	84	81	82	75	84	4,18	2,59	5,54
	B	66	60	54	55	60	64	66	58	55	62	4,27	2,64	7,49
16	R	127	120	123	122	120	125	124	124	125	125	2,16	1,34	1,84
	G	128	124	108	127	125	125	109	108	107	108	8,97	5,56	8,09
	B	89	84	72	75	80	74	75	72	73	75	5,37	3,33	7,37
17	R	112	98	107	100	98	103	100	108	105	99	4,58	2,84	4,69
	G	95	87	87	85	88	87	84	88	90	86	2,90	1,80	3,49
	B	71	61	60	65	63	62	65	62	61	62	3,03	1,88	5,05
18	R	166	164	166	164	165	162	168	164	169	164	1,99	1,23	1,27
	G	142	140	138	141	140	140	142	140	140	144	1,55	0,96	1,16
	B	117	118	119	118	116	120	115	120	119	115	1,81	1,12	1,62
19	R	127	126	126	127	124	129	127	125	130	127	1,66	1,03	1,38
	G	117	116	114	117	119	118	116	115	119	118	1,58	0,98	1,42
	B	89	90	88	93	89	87	93	91	91	89	1,90	1,18	2,22
20	R	102	100	104	101	104	102	103	102	103	102	1,19	0,74	1,22
	G	89	89	90	89	90	89	87	91	90	89	1,00	0,62	1,19
	B	66	66	65	65	68	64	67	65	65	63	1,36	0,84	2,19
21	R	79	80	81	79	80	80	80	79	78	79	0,79	0,49	1,05
	G	77	78	77	79	76	78	77	77	78	78	0,79	0,49	1,08
	B	63	63	61	62	61	62	62	64	63	62	0,88	0,55	1,49

22	**R**	58	56	60	58	58	56	60	58	58	56	1,40	0,87	2,55
	G	59	58	60	61	61	61	58	61	58	58	1,35	0,84	2,39
	B	49	49	47	50	49	49	50	49	47	48	1,00	0,62	2,17
23	**R**	87	95	91	85	81	85	90	86	93	95	4,49	2,78	5,33
	G	85	90	87	82	78	83	87	84	89	90	3,67	2,27	4,52
	B	61	66	65	55	54	59	64	63	66	67	4,40	2,73	7,49
24	**R**	81	57	62	65	88	69	90	96	96	99	14,95	9,27	19,63
	G	79	55	60	63	84	64	91	95	94	96	15,33	9,50	20,69
	B	55	32	39	40	63	43	70	73	72	78	16,01	9,92	29,86
25	**R**	44	34	28	39	47	42	26	39	53	54	8,99	5,57	23,34
	G	47	36	29	43	52	43	26	43	53	54	9,22	5,72	22,82
	B	37	29	24	35	42	36	22	35	45	43	7,37	4,57	22,33
26	**R**	63	71	77	64	65	69	65	65	66	64	4,09	2,53	6,44
	G	64	73	77	64	66	72	69	66	66	65	4,19	2,60	6,48
	B	53	57	65	49	54	59	57	52	53	52	4,32	2,68	8,27
27	**R**	110	101	103	103	103	98	96	82	82	86	9,29	5,76	10,15
	G	91	78	77	76	77	72	71	59	67	70	7,93	4,92	11,33
	B	65	53	51	47	52	46	48	36	46	47	6,93	4,30	14,89
28	**R**	99	94	95	89	105	95	92	89	83	84	6,33	3,92	7,21
	G	82	78	82	78	96	84	82	78	70	72	6,78	4,20	8,91
	B	58	55	59	57	71	65	60	59	49	51	6,02	3,73	10,87
29	**R**	91	85	85	78	89	96	98	115	110	99	10,91	6,76	12,16
	G	93	85	85	77	88	95	96	117	110	105	11,78	7,30	13,05
	B	71	63	63	55	66	73	76	95	89	88	12,42	7,70	17,72
30	**R**	104	95	109	101	102	99	108	113	125	125	9,77	6,06	9,53
	G	84	75	89	77	78	79	90	87	99	98	8,10	5,02	9,98
	B	58	48	60	51	51	52	64	59	69	70	7,35	4,55	13,30

To do this, organoleptically determined the color group of the selected fiber samples according to the method described in the above standard, and also determined the color coordinates of each sample using the device DDCIFF-1.

Statistical processing of experimental data based on the determination of the correlation coefficient ($r = 0.98$, $t_p = 1.1 < t_m = 2.05$), confirmed the presence of a strong direct relationship between the results and high predictive power of the proposed method (Fig. 17).

30 different batches were selected to determine the heterogeneity of the fiber in terms of color. From each batch, 10 samples of 20 g were taken. Taking into account that the average length of a handful of different batches of fiber ranges from 48.2 cm to 93.0 cm, each sample was conditionally divided into 10 parts, and in each part, measurements were made with the developed device DDCIFF-1. Analyzing the obtained measurement results (Table 7), we can conclude that the characteristic of color unevenness along the length can be described by the coefficient of variation. A high value of the coefficient of variation indicates that the fiber was obtained from the stock, which was laid unevenly, and this indicates the heterogeneity of the physical and mechanical indicators of the quality of the fiber, as well as the unsatisfactory quality of the products made from it.

The results of research have shown that this method is suitable for determining the color characteristics of flax fiber. The proposed technique allows to automate the process of analysis of color characteristics of flax fiber and to sort flax materials by groups. The objectivity of the assessment is increased by increasing the number of measurements and the use of sensory analysis based on modern electronic equipment. Automation of the evaluation process eliminates subjectivity and at the same time accelerates the process of obtaining color characteristics of the fiber.

Design and research work and testing of devices were performed on the basis of the Institute of Bast Crops of the National Academy of Agrarian Sciences of Ukraine. In the process of approbation (testing) of the equipment it is established:

a) the proposed *HSB* (Tone-Saturation-Brightness) color model is suitable for describing the color coordinates of flax fiber. This allows you to clearly determine the color group of the test sample by the calculated coordinates;
b) the correlation between the readings of the device and the physical and mechanical quality of flax fiber is established, which allows to use the obtained mathematical dependences to predict the physical and mechanical properties of flax fiber;
c) experimentally determined the main parameters of the prototypes of the device DDCIFF-1, and developed recommendations for its practical application, in particular, the mass of the measured fiber sample should be 20 g, and measurements should be performed in triplicate in three places on both sides of the sample;
d) studies have confirmed the feasibility of using the developed device DDCIFF-1 in the process of assessing the quality of flax fibers according to the developed method, the relevance of the development is confirmed by the obtained patent of Ukraine № 83772.

CONCLUSION

The proposed color model HSB (Tone-Saturation-Brightness) is suitable for describing the color coordinates of flax fiber. This allows you to clearly determine the color group of the prototype by the obtained coordinates.

Experimental studies have confirmed the feasibility of using the device DDCIFF-1 in the process of assessing the quality of flax fibers according to the developed methods. The novelty of technical solutions proposed during the development of the device DDCIFF-1 is confirmed by the patent of Ukraine and testing in production.

To use the DDCIFF-1 device in production, it is necessary to improve its performance characteristics - to ensure the display of the fiber color group defined by the standard, rather than RGB or HSB color coordinates

REFERENCES

1. State standard of Ukraine 4015:2001. Scutched flax. Specifications, Kyiv, Derzhspozhivstandard of Ukraine, 2001, 16 p. (in Ukrainian)
2. Akin D. E.: Developing standards to judge flax fibre quality, 28th International Cotton Conference (Bremen Germany), 2006, pp. 177-187. Available from: https://www.ars.usda.gov/research/publications/publication/?seqNo115=191791
3. Akin D. E., Gamble G. R., Morrison III W. H., et al.: Chemical and structural analysis of fibre and core tissues from flax, Journal of the Science of Food and Agriculture, 72(2), 1996, pp. 155-165. https://doi.org/10.1002/(SICI)1097-0010(199610)72:2<155::AID-JSFA636>3.0.CO;2-X
4. Kandi S. G.: The effect of spectrophotometer geometry on the measured colors for textile samples with different textures, Journal of Engineered Fibers and Fabrics, 6(4), 2011, pp. 71-78. https://doi.org/10.1177/155892501100600410
5. Raluca B. R. A. D.: A review of color measurements in the textile industry, Annals of the Oradea University, Fascicle of Textiles, 2016, pp. 19-24.
6. Epps H. H., Akin D. E.: The color gamut of undyed flax fiber, AATCC review, 3, 2003, pp. 37-40.
7. Sarkar A. K., Seal C. M.: Color strength and colorfastness of flax fabrics dyed with natural colorants, Clothing and Textiles Research Journal, 21(4), 2003, pp. 162-166. https://doi.org/10.1177/0887302X0402100402
8. Akin D.E., Epps H.H., Archibald D.D., et al.: Color measurement of flax retted by various means, Textile Research Journal, 70(10), 2000, pp. 852-858. https://doi.org/10.1177/004051750007001002
9. Weisnerova D., Weisner I.: Computer image analysis of seed shape and seed color for flax cultivar description, Computers and Electronics in Agriculture, 61(2), 2008, pp. 126-135. https://doi.org/10.1016/j.compag.2007.10.001
10. Epps H.H., Akin D.E., Foulk, J.A., et al.: Color of enzyme-retted flax fibers affected by processing, cleaning, and cottonizing, Textile Research Journal, 71(10), 2001, pp. 916-921. https://doi.org/10.1177/004051750107101011
11. Jablonský M., Dubinyová L., Varga Š., et al.: Cellulose fibre identification through color vectors of stained fibre, BioResources, 10(3), 2015, pp. 5845-5862. https://doi.org/10.15 376/biores. 10.3.5845-5 862
12. Askim J. R., Mahmoudi M., Suslick K. S.: Optical sensor arrays for chemical sensing: the optoelectronic nose, Chemical Society Reviews, 42(22), 2013, pp. 8649-8682. https://doi.org/10.1039/C3CS60179J
13. Bergfjord C., Holst B.: A procedure for identifying textile bast fibres using microscopy: flax, nettle/ramie, hemp and jute, Ultramicroscopy, 110(9), 2010, pp. 1192-1197. https://doi.org/10.1016/j.ultramic.2010.04.014
14. Hinsch E. M., Robinson S. C.: Comparing colorfastness to light of wood-staining fungal pigments and commercial dyes: an alternative light test method for color fastness, Coatings, 8(5), 2018, pp. 189-200. https://doi.org/10.3390/coatings8050189
15. Fan Y., Li J., Guo Y., et al. Digital image colorimetry on smartphone for chemical analysis: A review, Measurement, 171, 2021. https://doi.org/10.1016/j.measurement.2020.108829
16. Choi K. F.: Sampling and statistical analysis in textile testing, Fabric Testing, Woodhead Publishing, 2008, pp. 27-47. https://doi.org/10.1533/9781845695064.27
17. Fairchild, Mark D.: Color appearance models, John Wiley & Sons, 2013, Chichester, UK, 472 p.

AIMS AND SCOPES

“Vlakna a Textil” is a peer-reviewed scientific journal serving the fields of fibers, textile structures and fiber-based products including research, production, processing, and applications.

The birth of this journal is connected with three institutions, Research Institute for Man-Made Fibers, Svit (VÚCHV), Research Institute of Chemistry of Textiles (VÚTCH) in Žilina and Department of Fibers and Textiles at the Faculty of Chemical Technology, Slovak Technical University in Bratislava, having a joint intention to provide, utilize and deposit results obtained through the research, development and production activities dealing with the aforementioned scopes. „Vlákna a Textil“ journal has been launched as a consequence of a joing of existing magazines „Chemické vládkna“ (VÚCHV) and „Textil a chémia“ (VÚTCH). Their tradition should provide a good framework for the new journal with the main aim to create a closer link between the basic element of the product - fibre and its fabric - textile.

Since its founding in 1994, the journal introduces new concepts, innovative technologies and better understanding of textile materials (physics and chemistry of fiber forming polymers), processes (technological, chemical and finishing), garment technology and its evaluation (analysis, testing and quality control) including non-traditional applications, such as technical textiles, composites, smart textiles or garment, and nano applications among others. The journal publishes original research papers and reviews. Original papers should present a significant advance in the understanding or application of materials and/or textile structures made of them.

VLÁKNA A TEXTIL
Volume 29, Issue 4, December 2022

CONTENT